CHARACTERIZATION OF A NOVEL IN-GROUND HEAT EXCHANGER FOR APPLICATIONS IN SUSTAINABLE BUILDING ENERGY AND MAINTAINING PERMAFROST

by

Sarah R. Nicholson

Bachelor of Engineering, Ryerson University, 2018

A thesis presented to Ryerson University

in partial fulfillment of the

requirements for the degree of

Master of Applied Science

in the program of

Mechanical and Industrial Engineering

Toronto, Ontario, Canada, 2020

AUTHOR'S DECLARATION FOR ELECTRONIC SUBMISSION OF A THESIS

I hereby declare that I am the sole author of this thesis. This is a true copy of the thesis, including any required final revisions, as accepted by my examiners. I authorize Ryerson University to lend this thesis to other institutions or individuals for the purpose of scholarly research. I further authorize Ryerson University to reproduce this thesis by photocopying or by other means, in total or in part, at the request of other institutions or individuals for the purpose of scholarly research. I understand that my thesis may be made electronically available to the public.

CHARACTERIZATION OF A NOVEL IN-GROUND HEAT EXCHANGER FOR APPLICATIONS IN SUSTAINABLE BUILDING ENERGY AND MAINTAINING PERMAFROST

by

Sarah R. Nicholson

Master of Applied Science, Mechanical and Industrial Engineering

Ryerson University, 2020

Abstract

This thesis investigates the use of a Helical Steel Pile (HSP), as an in-ground heat exchanger for a Ground-Source Heat Pump (GSHP) system. A multi-layered soil conductivity dataset was created to quantify thermal performance across a variety of climate and soil conditions. Geometric features of the HSP were optimized using parametric sweeps, and the capacity of the pile to supply a building load was characterized for a variety of inlet fluid temperatures, seasons, and locations. Transient simulations of the pile characterized its ability to supply three different types of building load sets across a year. Finally, 40-year simulations showed the potential for the HSP to provide heating to buildings in a northern region while also mitigating the thawing of permafrost from climate change. The results indicate a potential to provide sustainable thermal energy to remote communities while delaying the predicted thawing of permafrost locally by up to 75 years.

Acknowledgements

The author would like to acknowledge the Anishinaabe, Mississaugas and Haudenosaunee groups who are a part of the Dish With One Spoon treaty. It is because of this invitation onto the land in the “spirit of peace, friendship and respect,” that this research was able to be conducted at Ryerson University. This work hopes to honour and uphold the spirit of this treaty by recognizing the one spoon from which we all draw from this place, and by working towards measures that greater protect the land and share its resources fairly with all.

As well, this research has been strengthened by the tireless efforts of Leya Kober, a hardworking mechanical engineering undergraduate student who worked as a research assistant on this research to develop climate and soil zones. Further, the experience and knowledge of all experts in this field have been incredibly valuable throughout this research. For their teaching of numerical simulation, technical communication, and everything required to do research Dr. Aggrey Mwesigye, and Prof. Seth Dworkin (graduate supervisor) are gratefully acknowledged.

For financial and project support, Andrew Lee and Jim Ilkay at Innovia GEO Corp. have been valuable industry partners in this research, and their experience and desire for innovation were a great aid. Thank you also to NSERC CGS-M program for their funding contribution.

Dedication

_____

To Mom, Esther, Sheldon, and Rony.

For the family of friends who have given me love, meaning, and encouragement.

And for those who know struggle, but continue, nonetheless.

“Le vent se lève!... Il faut tenter de vivre!”

-Paul Valéry

Table of Contents

List of Figures

List of Tables

List of Appendices

List of Terms & Abbreviations

GSHP	Ground-Source Heat Pump
GHE	Ground Heat Exchanger
GHG	Greenhouse Gas
BH	Borehole
GCM	General Circulation Models
EIP	Energy Innovation Program
REACHE	Responsible Energy Approach for Community Heat and Electricity
HVAC	Heating Ventilation and Air Conditioning
ASHP	Air-Source Heat Pump
COP	Coefficient of Performance
HSP	Helical Steel Pile
CFD	Computational Fluid Dynamics
FEA	Finite Element Analysis
TRT	Thermal Response Test
GTI	Ground Thermal Imbalance
BGTI	Beneficial Ground Thermal Imbalance
Q_{GHE}	Ground Heat Exchange Across the Pile [W]
ρ	Density [kg/m^3]
c_p	Specific Heat Capacity [K/kg·K]
k	Thermal Conductivity [W/m·K]
T_{in}	Inlet Fluid Temperature (to the pile) [°C]
T_{soil}	Soil Temperature [°C]
PARDISO	Parallel Sparse Direct and Multi-Recursive Iterative Linear Solver
T_{air}	Ambient Air Temperature [°C]
d_o	Outer Diameter [m]
d_i	Inner Diameter [m]
L	Length [m]
T_{out}	Outlet Fluid Temperature (from the pile) [°C]

$Q_{building}$	Thermal Energy Supplied to a Building [W]
$\dot{V}_f$	Volumetric Flow Rate of Incoming Fluid [m^3/s]
$T_{air,CC}$	Climate Changed Ambient Air Temperature [°C]
Θ	Volume Fraction of Non-Mineral Soil Components (water, air, ice, void) [%]
f	Volume Fraction of Mineral Soil Components [%]
F	Weighting Factor of Soil Components [-]
BD	Bulk Density [g/cm^3]
ρ_{pd}	Particle Density [g/cm^3]
NSDB	National Soil Database
T_M	Mean annual air temperature [°C]
A_s	Air temperature amplitude [-]
t_0	Day of maximum annual temperature [day]
t	Time [hr],[yr]
z	Depth below surface [m]
$\bar{Q}$	Heat Exchange Rate by Depth [W/m]
$\dot{m}$	Mass Flowrate of Fluid Entering Pile [kg/s]
GF	Geometric Factor [m^3]
V_w	Total Volume of Water in the Pile [m^3]
ΔT	Inlet Fluid Temperature Minus Outlet Fluid Temperature [°C]
DHW	Domestic Hot Water
ΔT_{soil}	Change in Ground Temperature at a Point Over Time [°C]

Material Subscripts

st	Steel
pl	Plastic
f	Fluid

1. Introduction & Literature Review

The purpose of this research was to understand a wide range of energy needs – and how Ground-Source Heat Pump (GSHP) technology can be applied to meet these demands. To explore the sustainability of this renewable energy system further, this work focused on climate change effects on ground and ambient air temperature which might interact with the Ground Heat Exchanger (GHE) – especially in permafrost regions. Furthermore, this research aimed to provide a foundational starting point for the use of shallow helical steel piles as in-ground heat exchangers. To create a catalogue of potential performance of these piles, numerical modelling was utilized to simulate their performance across a range of soil, climate, geometric, and optimization conditions. The author aims to add to literature on this technology for the purpose of improving the feasibility of thermal energy systems across a range of regions and applications.

1.1 Heating & Cooling Demands in Canada

Canada is located on a large landmass in the northern hemisphere, and it experiences extreme cold weather conditions across its dispersed population - leading to high electricity demand [1]. Specifically, the energy demand for space heating and water heating in the residential sector is 80% of the total energy used by this sector [1], and accounts for 63% of the energy use by commercial and institutional buildings [1]. In most cases this space conditioning is supplied by either electrical or combustion energy - with natural gas being the predominant fuel for space heating accounting for 47% of these energy sources [1]. The burning of fuel for energy is known to cause Greenhouse Gas (GHG) emissions, and other environmental issues. However, when electricity is used, its generation is generally low in GHG emissions in Canada. In 2017, only 19% of the energy generated in Canada came from emitting sources - with the remaining demand supplied by nuclear (15%), non-hydro renewables (7%), and hydro energy (60%) [1].

Renewable energy solutions in Canada are a source of significant government and industry spending with $250 million and $509 million respectively spent on renewable and clean energy in 2017/18 [1]. However, these renewable systems are not yet widely used in Canada – especially for thermal energy. While sustainable energy generation is a growing industry, there is still a need to focus on reducing energy use - especially in the significant space and water heating portions. While

there are global commitments to reducing emissions, currently over 81% of emissions from Canada came from the production and consumption of energy [1]. The residential sector accounts for 11% of the total energy use leading to these GHG emissions, and 80% of this residential energy is consumed for space and water heating [1]. As such, Canada has the possibility to reduce its emissions by focusing on reducing energy demand and begin to transition into completely non-emitting sources of energy.

1.2 Status of these Demands in Northern Communities

The general information about Canada's energy generation and use often does not capture the full picture of this country. As a large area of land, with a relatively small population, many Canadians live in one of 292 remote communities [2]. These permanent communities are characterized by being disconnected from North-American electrical grids and pipelines, and are made up of approximately 67,420 non-Aboriginal people, and 126,861 individuals from First Nations, Innu, Inuit and Métis groups [2]. These communities are an important part of the Canadian demographic, and face unique energy challenges which have environmental, economic, and social impacts.

1.2.1 Current issues

The primary energy issue facing these communities is their independence from the traditional utilities used by other more densely populated areas in Canada. Figure 1.1 shows the location of each remote and Northern community, in contrast to the locations of natural gas and electricity grid sources. Aboriginal (First Nations, Innu, Inuit and Métis) and Non-Aboriginal communities are differentiated by green and yellow boxes respectively.

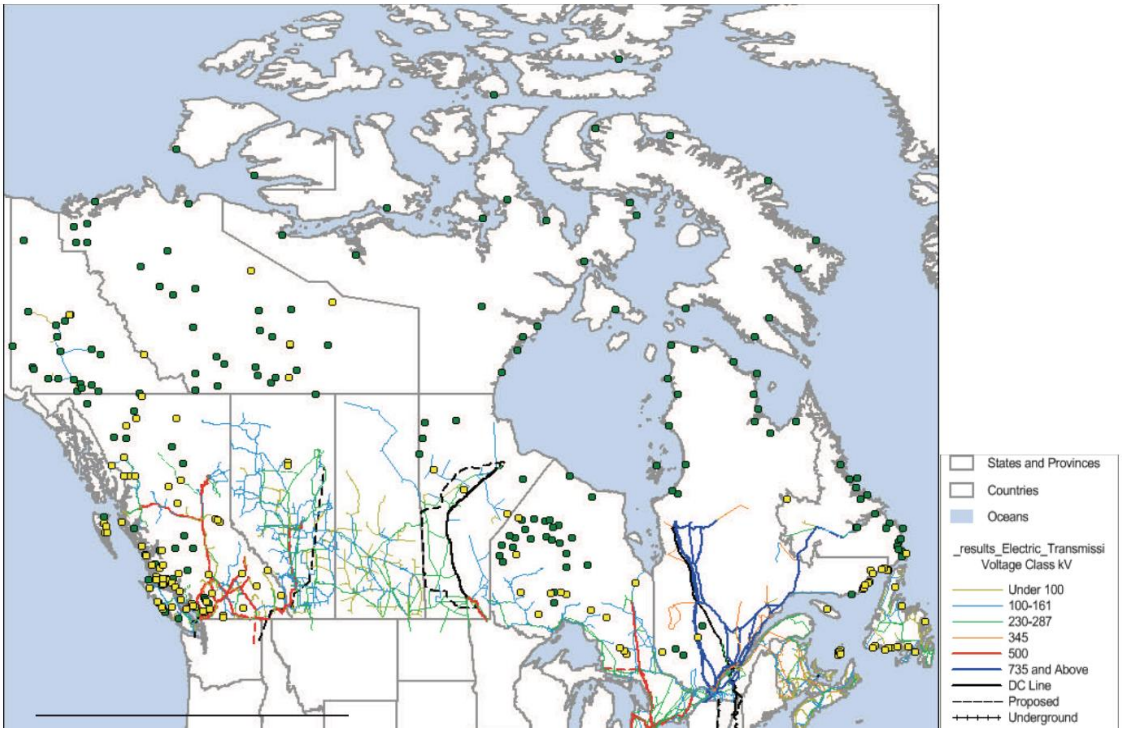

Figure 1.1. Location of remote communities and energy grids in Canada [2].

Without the convenience of energy supply as reliable as the southern half of Canada has access to, most of these communities must rely on local generation sites. Most of these power plants are powered by the burning of fuel with 176 communities relying on diesel energy (and a suspected 73 more), and only two are powered by natural gas [2]. Across these communities, diesel fuel is also the primary source for space and water heating [2]–[5]. This energy source results in a dependency on importing fuel - and the high cost of such fuel [2].

The challenges facing these communities are similar to those faced by diesel-dependent groups worldwide. There are significant environmental costs to the burning of diesel fuel, accrued along its life-cycle [2]. These costs extend to the social well-being of these communities by impacting health, animals, plants, and the climate within these locations as well as globally [6]. Furthermore, these generators are noisy – and require maintenance, and transportation to deliver their fuel, which can result in increased emissions by vehicles, increased risks of fuel spills, and groundwater/soil contamination [2]. Furthermore, these generators are vulnerable to “black-outs” wherein communities may be forced to face harsh winter conditions without heating or electricity for extended periods of time until a solution can be reached [2].

Beyond these challenges, the economic costs of these generators create significant barriers to individuals, and economic development in these areas. Prices for energy depend on the location of these communities but can cost up to $1.3/kWh [7]. When compared to a residential mid-peak winter rate in Toronto, ON ($0.14/kWh) [8], individuals in these communities pay a rate 9 times greater than the average Toronto resident. Higher energy costs have rippling effects for a community, and can lead to less investment in these communities, less access to services and employment, and perpetuate a cycle of poverty.

To compound these energy issues, housing in these communities is often inadequate, and in need of major repairs [9]. These housing issues disproportionately affect the security, and well-being of Indigenous women [9], a group historically underserved in Canada. Furthermore, the majority of existing energy generation equipment are beyond their design age of expiration, meaning the conditions, and reliability of energy will continue to decay [10].

There exists a need for renewable, reliable, and cheaper thermal energy in Canada's nearly 300 remote communities. Meeting these demands in spite of a lack of infrastructure, access to grids, unique geographic conditions and high costs is a difficult challenge - but one that must be met by energy experts in order to ensure an equitable quality of life for all Canadians.

1.2.2 Climate Change Effects

Climate change effects compound energy concerns in Canada's remote communities [5]. Temperature increases due to climate change in higher latitudes enhance the negative side-effects and feedback loop [11]. Complex factors are involved in the study of climate change in these regions - one of the most significant being a lack of wide-spread historical data [11] [12]. Furthermore, the connection between multiple environmental systems can sometimes have competing results when predicting effects of climate change. Snow cover, groundwater movement, elevation, forestation, and ambient air temperature are all interlinked in their seasonal, and long-term effects on each other. Regardless, many studies have shown that there is climate change occurring in northern regions [5], [11]–[20]. One study, which investigated climate conditions at two locations in the Northwest Territories over decades showed significant increases in ambient

air temperatures [11]. This trend is shown with mean annual air temperatures at Table Mountain, Northwest Territories from the years 1964-2007 in Figure 1.2.

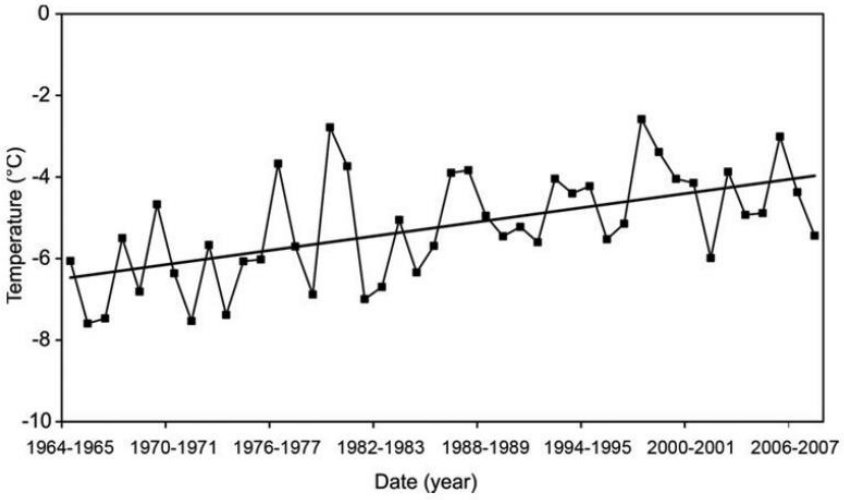

Figure 1.2. Measured increase in mean annual air temperature over time [11].

Figure 1.3 shows that this temperature rise was most significant in the winter months from data recorded from 1950-2006, along with data measured in the study from 2000-2008 ("on-site" values) [11].

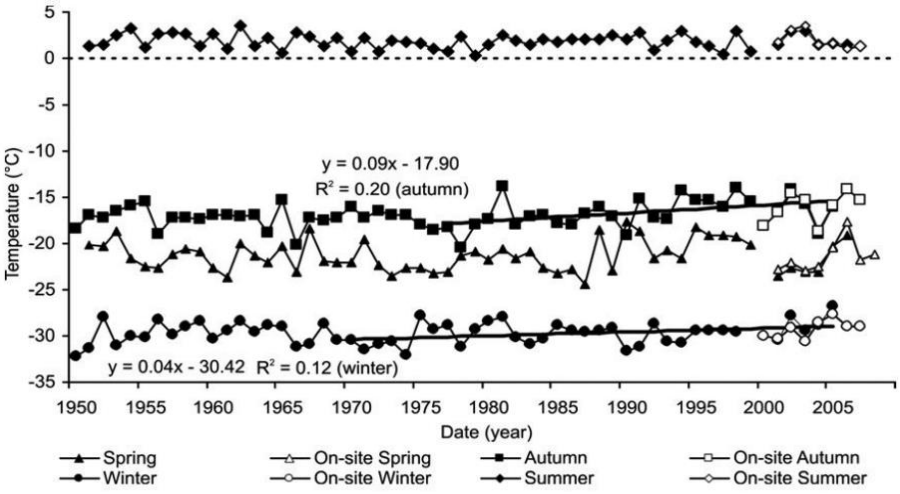

Figure 1.3. Trends of seasonal air temperature increases [11].

These increases in mean ambient air temperature of approximately 2°C across the past 40 years, are complemented by models which predict future climate change in Northern Regions. Figure 1.4 shows the expected temperature rise and changes to snow cover until the year 2060[18].

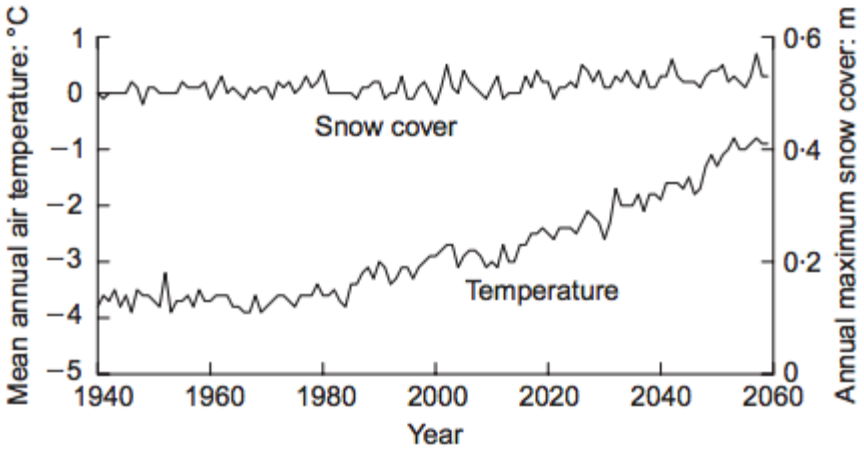

Figure 1.4. Predicted temperature and snow cover changes over the next 40 years [18].

The effects of climate change on Canada's northern and remote communities may be severe. From a change in energy demand due to changing climate conditions, to a need for infrastructure to withstand potential flooding, and ground changes, energy solutions in these regions must plan for a rapidly changing climate.

1.2.3 Permafrost Considerations

The most significant effect of climate change in Canada's northern regions are the changes to permafrost layers which may occur as a result of warming. Many of the communities in this study are built on continuous or discontinuous permafrost regions. These regions are characterized by an active layer (which freezes and thaws seasonally) above a layer of permafrost (ground which remains at or below 0°C year-round). It should be noted here, that although warming of permafrost is called "thawing" there may not always be ice in this layer - nor is the ice constant throughout, rather "thawing" here refers to the warming of these soil zones above the freezing point of water. Changes to the permafrost layer can have significant ecological and structural impacts [11][12][13][14][15][16][17][18][19][20][21][22][23][24]. Permafrost is a complex system which is affected by snow cover, seasonal temperatures, ground conditions, and proximity to non-permafrost areas, however, it has been shown that the increase in ambient air temperature can lead to thawing of permafrost zones [11] [12] [13] [19] [20].

Studies have shown that permafrost, and ground temperatures have already been rising [11], with some reporting annual ground mean temperature increases of 0.2 to 0.6°C/decade from 1978-2008

[11]. Figure 1.5 shows the measured ground temperature changes by depth from five boreholes (BH1-BH5) from 1979-1980 to 2007-2008 in Northwest Territories [11].

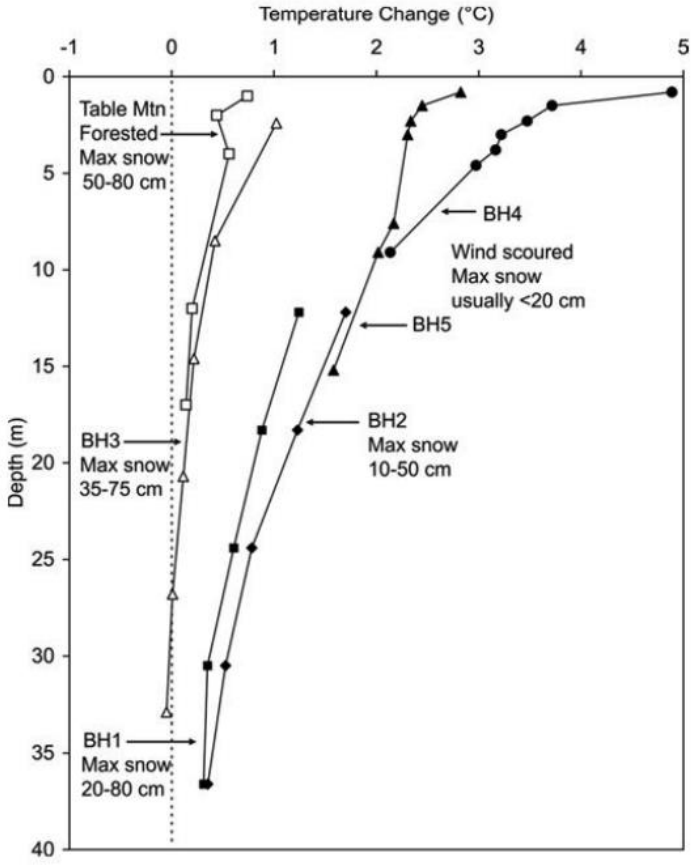

Figure 1.5. Measured ground temperature changes by depth across 28 years in the Northwest Territories [11].

This figure highlights that temperature changes near the surface of the ground are most extreme, but even up to depths of 35 meters there was a measured warming of the soil. It also indicates that this warming is non-uniform and depends on depth and location, a preface for the importance of detailed soil models which account for the variation in thermal properties by location and depth.

Several numerical and analytical models have been generated to predict permafrost thawing, which utilize the thermodynamic equations governing heat transfer to and from these regions of permafrost [13][18][24]. One such numerical model shows the predicted changes to annual ground temperature as a result of climate change in Figure 1.6 [18].

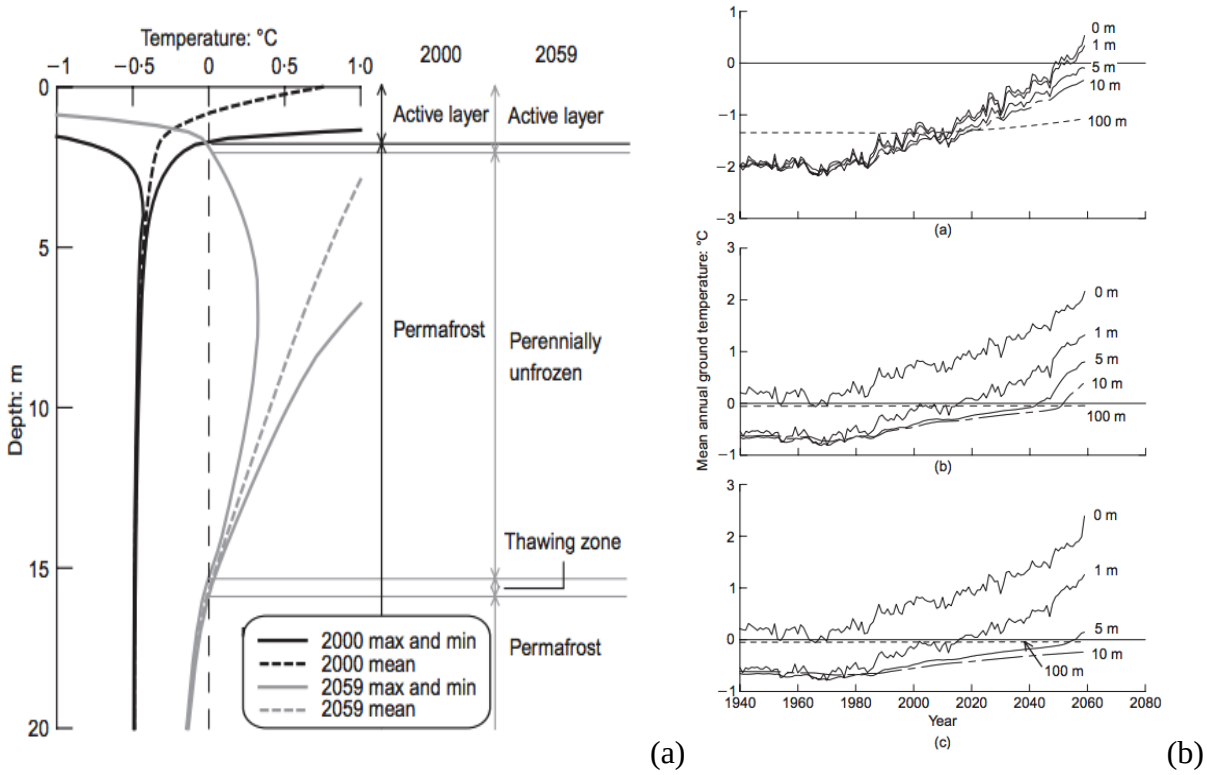

Figure 1.6. (a) Changes to the permafrost layer, and (b) simulated temperature changes by depth for three different climate models [18].

This model highlights the decreasing height of the permafrost layer of soil with increasing ambient air temperature. In Figure 1.6 (a), this results in a change of permafrost height of almost 10 m, Figure 1.6 (b) shows that within 40 years, this model predicts mean ground temperatures will rise to at or above 0°C even 5 m deep in the soil [18].

Yet another predictive simulation utilized six common climate change General Circulation Models (GCM) developed by the Canada Institute for Climate Studies at the University of Victoria [25] to predict transient changes to permafrost in Canada across 100 years [13].

Figure 1.7 shows the predicted changes to permafrost area from this study.

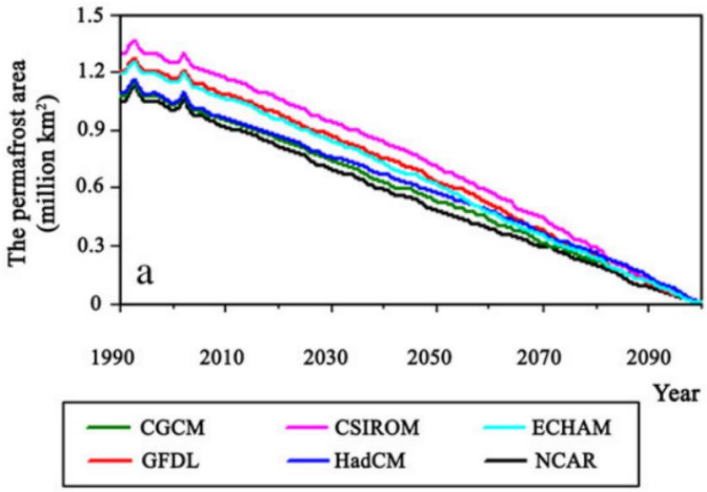

Figure 1.7. Predicted change in permafrost in Canada [13]].

This prediction shows that the total area of permafrost in Canada will be nearly halved over the next 40 years (2020-2040). Furthermore, the areas at risk of melting in Canada coincide with many of the same locations of residence for northern and remote communities. Figure 1.8 shows the regions that are most sensitive to warming – mainly northern Ontario, Alberta and Manitoba.

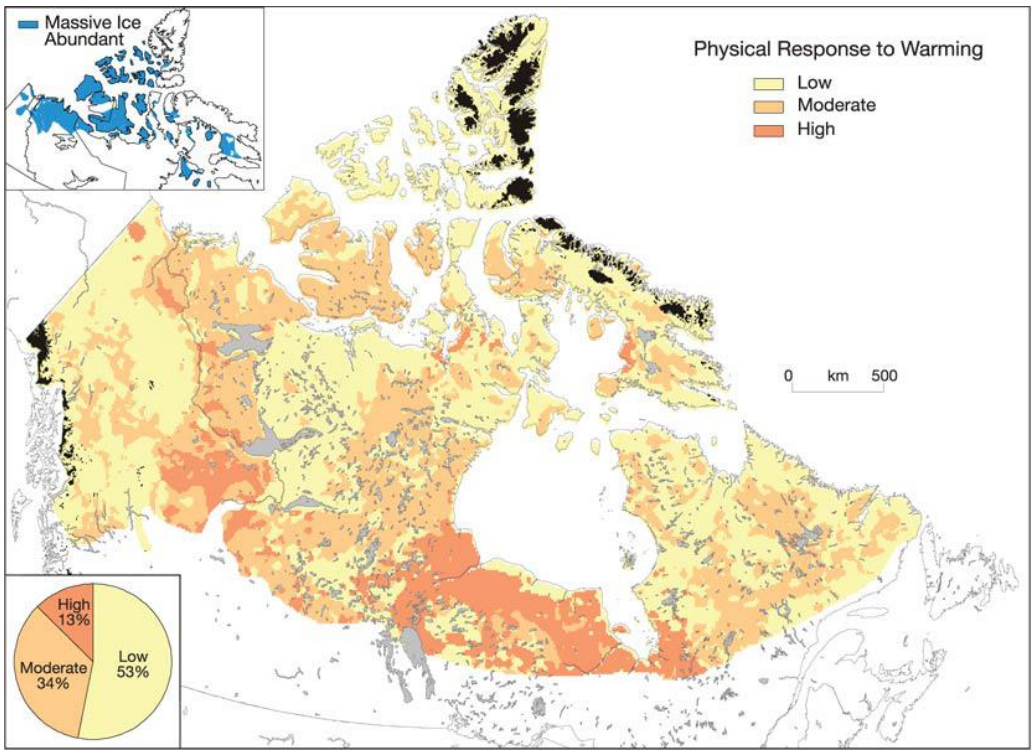

Figure 1.8. Locations at risk for melting [19].

As permafrost melts, there is an increase in groundwater flow [16] [17], which can act as a thermal transport that exacerbates the thawing of permafrost [24]. Furthermore, conductive thawing can

occur in permafrost layers that are in contact on one or all sides with non-permafrost soil - as areas of permafrost thaw, surrounding layers are at risk for thawing as well [24]. Generally, the melting of permafrost - and the absence of its layers can increase the rate at which heat is transferred to these regions from all sides within the ground.

Environmental consequences of permafrost thawing are: net forest loss (up to 11.6% already measured in 40 years) [20], release of carbon [22] and methane [15] into the atmosphere, increased water streamflow [16], changes to water chemistry [14], and the creation of sinking zones known as thermokarsts [16]. These effects threaten the stability of communities in these areas, and there has already been an increase in thermokarst activity, as shown in thaw slumps from melted permafrost under lakes in the Mackenzie Delta of Northwest Territories in Figure 1.9 [14].

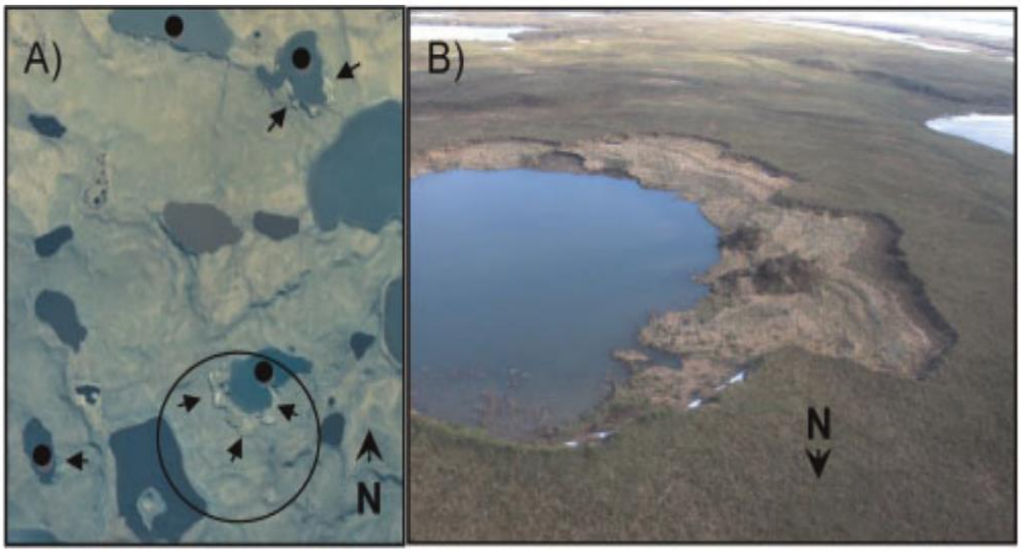

Figure 1.9. Permafrost sinking at lakes [14].

The foundation of a building built on permafrost relies on the stability of that permafrost year-round, and instability would cause significant sinking, flooding, and damage to the construction [18]. Figure 1.10 shows such damage inflicted on a store in Nain, Newfoundland [26].

Figure 1.10. Sinking of a building due to thawing of permafrost [26].

Furthermore, buildings which are space conditioned can warm the surrounding soil by conduction with the above 0°C building material [27]. This building heat loss results in a directly "man-made" permafrost thawing effect from infrastructure. Research into such effects in Canada show that there is particular risk of heat and moisture transfer from new building constructions, and leaks caused by utility lines [23]. In Iqaluit, a new arena began sinking shortly after opening, and closed for 7 years (2003-2010) while a $2.2 million repair was performed on the building [21]. Ultimately, the maintenance of the permafrost zones in northern communities is essential to maintain buildings.

1.2.4 Current Solutions & Opportunities

All arctic land masses are characterized by similar issues faced in Canada, and so global governments, industries, and researchers are looking into solutions for these communities' energy needs [4]. This interest has led to international proposals for various renewable energy plants - mostly focused in Russia, North America, Iceland, and Norway [4] [28]. These sources investigate using hydrogen, solar power, wind, biofuel, nuclear, and hybrid systems.

In the 1980s, Canada saw a push for wind turbines in remote locations, however none of these projects are currently operational due to a mix of installation and operational issues [7].

Nevertheless, feasibility studies for wind power are continuing to be reported, and there remains potential for diesel-wind hybrid energy generation systems [4]. Northern solar energy is abundant in summer months due to seasonal-light variation which leads to higher solar availability than more southern Canadian locations. Figure 1.11 highlights the difference in average monthly hours of sunlight between four Canadian locations [29], proving that solar energy is a potential source of renewable generation in remote and northern locations [4].

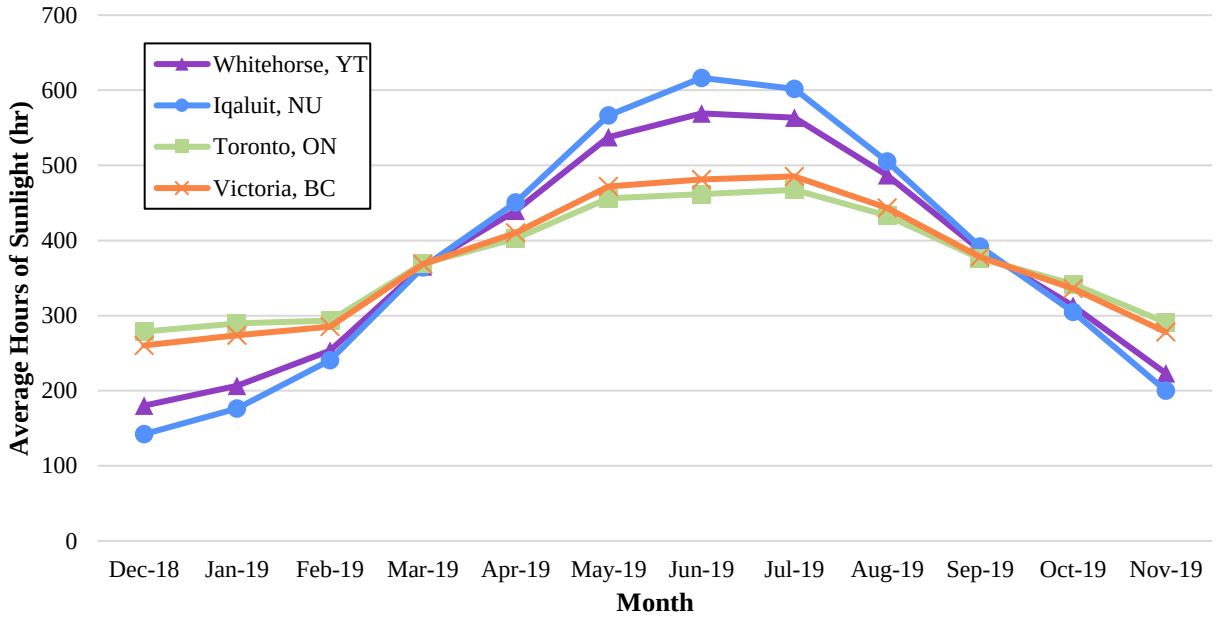

Figure 1.11. Average monthly hours of recorded sunlight [29].

Biomass as a fuel source is also heavily investigated to offset diesel fuel for heating [4] [30]. While this energy source still produces emissions, it is generally well received by local governments as a more cost-effective source of energy [4]. Other renewable energy sources are explored in research (such as geothermal, and tidal energy) [10], though they are often disqualified due to a lack of infrastructure, and the high capital cost of installation [31].

The potential for these sources of energy is of interest to government bodies in Canada, and has led to various programs specifically focused on developing these projects. The federal government of Canada has renewable energy funding sources specifically for use in Northern and remote communities, such as the Energy Innovation Program (EIP) [32]. Table 1.1 is a summary of four currently active demonstration sites in the category of “Clean Energy for Rural and Remote Communities,” receiving EIP funding.

Table 1.1. EIP projects started in 2018 for clean energy in rural and remote communities [32].

Project	GI Contribution	Location	Technology Proposed	Expected Benefits
Hybrid smart-grid solar PV and battery demonstration project [33]	$2,299,000.00	Gwa'yasdams, BC	Smart-grid solar PV, battery energy storage, integrated diesel power plant	Use 50,000 L less diesel fuel annually, 72-hours energy storage
Destruction Bay Renewable Hybrid-Diesel Project [34]	$2,000,000.00	Destruction Bay, YK	Wind turbines, battery and energy management system	Economic, social and environmental benefits
Gull Bay First Nation Diesel Offset Micro Grid Project [35]	$2,000,000.00	Gull Bay, ON	Solar PV, battery storage, diesel generators	Use 130,000 L less diesel fuel annually
Mary's Harbour Renewables [36]	$2,543,815.00	Mary's Harbour, NL	Hydro, solar PV, lithium-ion battery storage	Use 400,000 L less diesel fuel annually - reduction of 30%

Furthermore, in their Reconciliation plan, the federal government details their "support for distinctions-based housing strategies," a funding strategy that aims to address the housing needs of Indigenous people in Canada [9]. This project promises $600 million to support housing on reserves, $400 million for housing plans in Nunavik, Nunatsiavut and Inuvialuit - communities in the Inuit region [9]. As well as $500 million given towards a Métis Nation's housing strategy [9]. Finally, the Northern Responsible Energy Approach for Community Heat and Electricity (REACHE) Program funds projects that replace off-grid diesel energy and heat generation with renewable energy systems [37]. In 2017, the federal government promised $53.5 million to this project, to be implemented in 2018-2019 [37]. Applications for this funding are required to focus on "proven technologies" used by solar, wind, storage, hydro, biomass, and heat recovery systems [37].

These projects are mostly focused on the generation of electricity - an important piece for improving the lives of inhabitants. Reductions of electricity demand in industries in the north are being explored [38], however, there is also a potential to improve the heating and cooling equipment of buildings - in order to reduce the electricity demand devoted to space conditioning. The two strategies of renewable generation and sustainable use can be implemented as complementary solutions.

Improving the space conditioning of buildings in the North is something that is being researched by some building scientists, architects, and engineers worldwide. From passive house building design which optimize solar heat gain in the northern city of Yekaterinberg, Russia [39], to high performance building strategies for cold climates [40] [41], new building development can be optimized to help reduce the demand for high cost heating energy.

However, retrofitting the existing buildings in remote and northern communities provides another opportunity, and the Heating Ventilation and Air Conditioning (HVAC) equipment used to generate space conditioning may be the most effective place to start. Can thermal energy be supplied to these communities in a way that reduces the environment, economic, and social costs currently affecting them? Is there a way to use renewable HVAC sources to reduce the dependence on imported fuel? Could the combination of sustainable energy generation projects with efficient-use energy equipment lead to these off-grid communities being sufficiently powered by less costly means?

Figure 1.12 shows an elevated house in Nunavut, which has been built on pile stilts to reduce the ground warming effects of direct soil contact - to maintain permafrost stability. Further methods to address the permafrost melting issues include heat pipes [42], thermosyphons [43], thermopiles [44], and frost foundations [27] are currently being employed.

Figure 1.12. House in Clyde River, Nunavut raised on piles to avoid contact with frozen ground [45].

These systems utilize innovative heat exchange methods (often involving two-phase flow which employs latent heat of vaporization and capillary action to transport thermal energy to a desired location), however, they are currently not utilizing the heat removed from the ground for another purpose. Could this waste heat meet building demands while stabilizing the ground? Are the current methods enough to keep up with climate change?

1.3 GSHPs for Heating & Cooling

1.3.1 In General

A Ground-Source Heat Pump (GSHP) is a renewable thermal energy system which utilizes the near-constant ground temperatures to exchange heat to and from the conditioned space and the soil for space conditioning [46] [47] [48]. These systems are gaining international popularity due to their ability to reduce costs, energy use, and emissions [49], and are growing rapidly in Canada with an estimated 10,000 units installed annually [49]. However, their implementation has been limited by the high initial costs, space requirements, and lack of popularity/reputation among end-users and industry professionals [49].

While these systems utilize electricity to operate the pump equipment, the GSHP can produce 3-6 times the energy that it uses [48]. Furthermore, these systems are buried - meaning they are less intrusive than other renewable energy systems, and their heat exchange within the ground reduces urban heat island effect [50], which is not the case for Air-Source Heat Pumps (ASHPs) or other conventional refrigeration systems. Finally, these systems operate efficiently in cold climates as their heat source/sink is not in direct contact with extreme seasonal air temperatures [47].

This technology can lower building conditioning electricity demand to only that which is needed to power the refrigerant pump of the GSHP system [51]. With their coefficients of performance closely linked to their ability to draw and expel heat with the ground, GSHPs have great potential in seasonal climates where ground temperatures are constant at a certain depth in comparison to the extreme seasonal changes of air temperatures [52]. In winter, heat is extracted from the ground and transferred to a refrigerant, which then transfers the heat to the air inside the building with the help of a compressor. In the summer, the reverse process occurs so that heat is transferred to the refrigerant from the indoor air, and then from the refrigerant to the ground. The reduced electricity

demand attributed by GSHPs results in lower electrical costs, making them more economical than conventional heating and cooling systems over a long period of time [53].

GSHPs are a sustainable technology, as they undergo a natural thermal recharging or natural thermal recovery process [54]. Through the influence of building loads, inlet temperatures to the GSHP change with season, which determine whether heat is transferred to or from the ground. When building loads switch from heating to cooling mode, the heat extracted from the ground during the cold season will replenish when heat from the air in the building is deposited back into the ground. This operation can be thought of as natural thermal recharging and works best in climates and building types that have balanced heating and cooling loads over the year so that the ground has a chance to recover after each season [55]. GSHPs are also sustainable because they last a long period of time, and require very little maintenance [56] – but their most significant contribution to environmental sustainability is their ability to provide thermal energy without the burning of fossil fuels. Furthermore, the reduced electricity demand with the use of GSHPs results in the production of less GHG emissions than would be with conventional heating systems.

Currently, the widespread implementation of GSHPs is limited by high installation costs and the size of the boreholes [57]. GSHPs have higher capital costs than conventional heating systems, which can be a deterrent when their installation is considered. Borefields – the collection of Ground Heat Exchangers (GHEs) – are normally in a grid configuration due to space limitations, but studies have shown that this arrangement can result in thermal imbalances within the ground if heating and cooling loads are not balanced [58]. Furthermore, optimizing the borefield length for costs depends on the building loads and geographical location of the system [59]. Thermal imbalance over time causes a gradual increase or decrease to ground temperature, depending on whether the building is heating or cooling dominant. As the change in ground temperature increases, heat transfer decreases, and so does the coefficient of performance (COP) of the GSHP [60].

To meet some of the challenges presented with GSHPs, helical steel piles (HSPs) have been proposed for use as GHEs – replacing conventional boreholes. HSPs, which are commonly used for building foundation anchoring and stability in the construction industry, are piles that have a

screw head which can be drilled into various ground materials, including bedrock and ice. They do not need to be drilled as deep as boreholes, and do not require as specialized drilling equipment and expertise, which reduces installation costs. Boreholes are typically installed to a depth of about 300 m below ground level, while piles tend to be installed to a depth between 10-25 m [54]. Since drilling is roughly priced by depth [61], boreholes may be much more expensive to drill than piles – when the thermal capacities are comparable. HSPs are dual-purpose, since they can also be used for foundational support for buildings. This way, they take up even less space than boreholes, and create very little environmental disturbance by providing dual function from one installation and component.

Jalaluddin and coworkers [62][63] studied the thermodynamic properties of three types of shallow GHEs with an experimental setup in Japan [62]. Similarly, researchers in Seoul measured higher COPs for GSHPs that utilized energy foundations – steel piles and concrete structural elements performed more efficiently as GHEs than the standard COPs for conventional GSHPs [64]. These works provide useful data for validation of future shallow piles, however they do not yet check the effects of a novel two tube system presented in this research and within the environmental conditions of Canada (a colder climate with implications for other northern regions). Similarly, a parametric study on the geometric features of a spiral-coil heat exchanger performed by Min-Jun Kim *et al*. [65] utilized an optimization process and simulation methodology that can inform the optimization of the piles presented in this research. The borehole radius and pipe diameter were shown to be key features in heat exchange optimization due to their effects on thermal resistance as shown in [66]. Furthermore, many long-term numerical simulations have been performed on conventional borehole heat exchangers to check for their optimal spacing [58], and to compare performance within air source heat pumps and hybrid systems. The present research will provide novel geometric optimization for shallow GHEs by studying the effects of key parameters on thermal performance – while also using a novel pipe offset design. The offset of the inlet and outlet pipes in this two pipe GHE creates an asymmetrical heat exchange profile radially around the pile – which may be used as an advantage for designers of pile arrays, wherein the spacing between piles may be reduced by clustering the lower heat exchange sides together.

While there are possibilities for performance enhancement by geometric changes, the soil thermal properties were deemed the most important factors for heat exchange performance in a simulation of horizontal spiral heat exchangers [67]. Despite this finding, soil thermal conductivity has most commonly been represented by a constant value, not considering the varying soil properties by depth found in actual operation. Therefore, the present research aims to add further insight into the thermal performance of a pile in a varying soil domain, with the thermal conductivity of the soil calculated to reflect borehole data from a test site location and a national database. Performance effects of the addition of this variable are analyzed, with an aim to closer approximate realistic ground conditions with the simulation model – and investigate whether a multilayered soil approach affects the geometric optimization results, and thermal capacity.

Finally, conventional GHEs are used almost exclusively with turbulent and transitional flow rates – a strategy to increase heat transfer by taking advantage of mixing and convection found in high flow rates. The use of laminar flow is not common in GHEs, and there has not been research on the thermal performance potential of low flowrate piles. However, for shallow heat exchangers such as the HSP in the present study, a laminar flow rate allows the fluid to equilibrate with the ground temperature by increasing residence time of working fluid in the pile. This results in greater heat exchange potential with the soil, while reducing the pumping requirements of the fluid.

1.3.2 In context of northern communities

In Canada's Northern and remote communities, there is a significant need and possibility for the use of renewable energy systems to provide heating and cooling to the building. This possibility is coupled with complex environmental concerns, and a requirement to maintain permafrost integrity in these areas. Fortunately, the problems facing these communities are ones that may be well addressed by the use of GSHPs.

Firstly, because a GSHP requires less energy input than the thermal energy it outputs [46], the high energy costs currently faced by residents may be lowered – which also improves the payback period for such systems in these areas. Furthermore, GSHP equipment simplifies infrastructure, has high reliability, and low maintenance costs due to a lack of servicing needs – all of which

provide significant benefits to remote areas where technicians and parts may not always be available [61].

Environmentally, the GSHPs would reduce local pollution due to the lack of combustion gasses as well as minimizing noise pollution [61]. These systems can be coupled with other renewable energy generation technology and may be installed alongside some of the existing projects underway in Canada's off-grid communities.

The novel design presented in this research utilizes existing structural steel piles (already used in these areas to lift buildings off the ground or reduce their sinking), as the in-ground heat exchanger. With this component there exists a potential to not only provide more reliable, and sustainable heating – but to also provide structural support for buildings.

The third potential impact of these new GSHPs in Canada's remote areas is the possibility to use the ground thermal imbalance to counteract climate change effects on permafrost. Current GSHP systems are traditionally designed to balance their thermal loads annually, so that the heat which is removed during the heating season is returned in the cooling season. This balance maintains the integrity or capacity of the surrounding soil to continue to exchange heat across years. However, given the climate change-induced temperature increase in permafrost soils over time, this thermal imbalance consideration may change. Given that each year (mainly in the winter) the soil will be gaining more heat than it would without climate change, the GSHPs could be designed to extract this added heat in such a way that it may maintain the ground temperature required for freezing – in spite of climate change effects. This "beneficial ground thermal imbalance," has not yet been investigated in this function, and so this research will aim to present a foundational case for this potential – to be optimized and adapted in many future iterations.

1.3.3 Key Components' Limitations & Possibilities

1.3.3.1 The Ground Heat Exchanger

The ability of the GSHP to deliver space condition relies on the Ground Heat Exchanger (GHE) component. This component delivers heat exchange with the soil which allows the heat pump to then exchange heat with the indoor circulating equipment. The GHEs are differentiated by their

arrangement within the soil (vertical, or horizontal), and their supply of working fluid (open-loop, or closed-loop systems) [47]. Within these differentiations, various layouts of the piping that transports the heat exchanging fluid also exist. Most commonly, there are U-loop, double tube, and multi-tube pipe configurations [62], and there also exist helical pipe configurations [68]. Increasing the performance of GHEs depends on their function, which generally falls into two categories: to increase heat exchange capability, or (less commonly) to store thermal energy. Depending on the aim of the GHE system, the choice of geometric features (even internal fins [69]), flow rates, and additional modifications can be made to optimize this function [66].

GHEs are the focus of much innovation in the field – specifically to find ways to reduce the high costs (for deep drilling vertical boreholes), and large space requirements (for drilling horizontal borehole fields). These costs and specialized drilling equipment have often limited GSHPs to larger scale commercial, multi-unit residential, or industrial building developments – and these challenges are likely one of the reasons they are not yet widespread in residential and rural applications in Canada.

To address these concerns, researchers have begun work adapting existing in-ground structural equipment to serve the potential dual purpose of being a GHE and a building foundation [70] [71]. This innovation could greatly reduce the cost of a project [72] by reducing the depth of drilling and having the potential to share installation with another building component. Much of this work has focused on incorporating GHEs in shallow cement piles, as their thermal mass is favorable for thermal storage capabilities [73], and some research also utilizes tunnels and sewers to house the GHE equipment [74]. The focus of this study, however, is on the use of helical steel piles to replace conventional boreholes in a GSHP system. These steel piles have some mention in the literature [62] [63] [75], but are still relatively unexplored in their potential in Canada. The benefits of these piles in the context of this investigation into Northern and remote communities, are that they are able to be drilled with relative ease into many ground conditions, including ice and permafrost [70]. Furthermore, these piles are currently used to elevate and support some buildings in these communities – meaning that there already exists experience and technology to implement these GHEs in Canada's northern and remote areas.

1.3.3.2 The Soil Component

While it is a natural resource, the soil domain should be considered a highly important component due to its impact on the thermodynamic performance of GSHPs [61] [71] [76]. The ability for a GHE to perform its function is directly tied to the capacity of the surrounding soil, and the system is vulnerable to the long-term changes that soil might experience.

Soils are non-homogenous mediums that vary in composition and characteristics across regions and by depth. These changes can affect their thermal properties, and thereby the performance of the GSHP. Specifically, the water and ice content of the soil has a significant effect on the GSHP performance as wet soil has higher thermal conductivity, and can reduce the length of GHE required to achieve the design heat exchange [61].

Finally, the soil temperature imposes design limitations on a GSHP system – whether the intention is to maintain a frozen soil, or to mimic natural ecosystems in the surrounding area, the system must be designed to operate in a way that meets these requirements. While the biological impacts of the soil are rarely studied in this field, there are some indications that decreasing the temperature of groundwater in the soil below 10°C creates an environment within which some bacteria-consuming microorganisms cannot survive [73]. Future studies should investigate this further and increase the intersection of research performed by climate scientists, microbiologists, geographers, and geotechnical engineers.

1.3.3.3 Helical Steel Pile Configuration

A helical steel pile is a hollow casing with a welded screw and tip which allow for drilling installation into the ground. They are shorter than conventional vertical boreholes, with the proposed system being a height of 20 m compared to the hundreds of meters of boreholes. Within the steel casing, a working fluid is pumped through inlet and outlet plastic pipes – attached to the surface of the pile. This working fluid allows for heat exchange with the surrounding steel wall and soil domains in order to achieve the change in temperature required for the heat pump operation. The offset of the pipes create novel flow conditions which can allow for specialized pile array configurations, and directional ground temperature imbalances (with the highest heat exchange rates observed along the length of the pile beside the inlet pipe. Within the cooling

season, warm fluid (transporting heat from the building) is reduced in temperature after travelling through the pile in order to bring cooling to the space. Similarly, the winter season requires an increase in fluid temperature across the pile in order to draw heat from the soil into the supplied area. Figure 1.13 is a representation of the key differences between conventional boreholes (a u-tube is shown here) and a helical pile heat exchanger – where there is a difference in length, and the potential for dual purpose rather than just one.

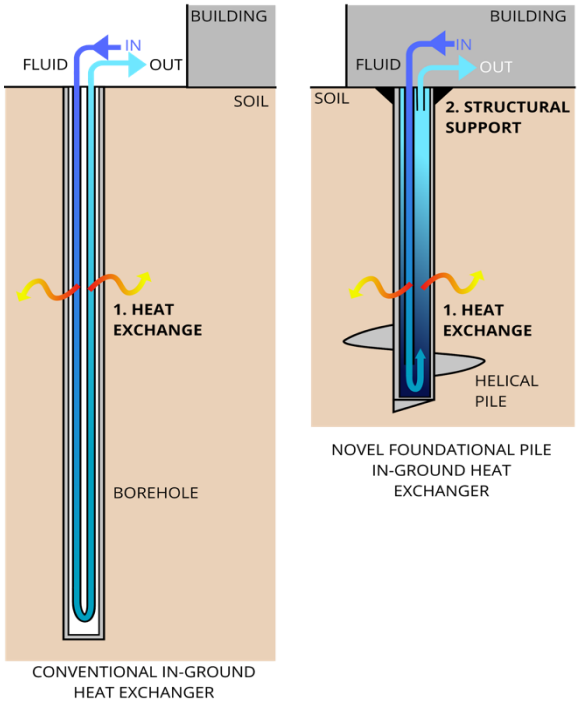

Figure 1.13. Comparison of a conventional u-tube in-ground heat exchanger (left) with a pipe-offset structural pile heat exchanger (right). Both provide working fluid heat exchange with the soil, but the pile has the potential to also anchor the building as a structural support.

The proposed system will operate with similar surface equipment (heat pump and distribution system within the building) to conventional GSHPs, however, the novelty of this HSP design lies in the shallower depths and unique pipe offset positions. Typically, the inner pipes are arranged in U-tube, concentric double tube, or multi tube configurations. However, the present system will utilize two offset plastic pipes which are disconnected within the larger volume of water in the steel casing. Essentially, the water will be funneled into the pile through a long plastic inlet pipe, flow back up through the cavity, and then out through an offset outlet pipe. The potential performance effects of this pile geometry are explored in this research, and optimizations for pipe diameters, and lengths are performed using parametric sweeps in Section 4.

1.3.3.4 Evaluating GSHP Performance

1.3.4 Basic Thermodynamics of a Ground-Source Heat Pump

This section presents a simplified description of the thermodynamics of a GSHP, it is meant to broadly explain its basic functions to create a foundational understanding for all potential readers of this thesis. Further details are well presented by researchers in this field and may be found in the texts referenced throughout this work.

A heat pump delivers heating and cooling to a space by transferring energy to or from that space. Unlike other forms of heating which require the *generation* of heat (such as a natural gas combustion furnace), a heat pump provides heat by *exchanging* it with an outside source. Another important feature of a heat pump is that the direction heat travels can be reversed – so that the same equipment that provides heating in the winter can provide cooling in the summer.

To achieve this energy movement, a heat pump uses internal pipes filled with refrigerant to carry heat. This refrigerant is chosen for its ability to change phase at chosen temperatures and pressures. As these temperatures, flows, and pressures are controlled (by mechanical equipment in the heat pump), the refrigerant becomes more gaseous (in the evaporator) and more liquified (in the condenser). Each time the refrigerant changes phase, it either *releases* (when it condenses to liquid) or *absorbs* heat (when it evaporates). It is by this process that heat can be moved from one place to another (such as inside a too-warm summer building, to an outside location).

The connection between the heat pump's refrigerant loop, the environment, and the building it services occurs via heat exchangers. The source of heat for a heat pump is the environmental domain from which it extracts or expels heat from the refrigerant fluid. In a Ground-Source Heat Pump (GSHP), this environmental area is a volume of nearby earth. This section of the ground is connected to the GSHP by pipes carrying fluid (typically water mixed with antifreeze). This component is called the Ground Heat Exchanger (GHE) because the fluid in its pipes carry heat to and from the ground. A similar heat exchange occurs in the building by the building's distribution system throughout the space (through forced air in ducts for example).

A schematic of these heat exchanges is shown in Figure 1.14 for both the summer (left) and winter (right) operating seasons. The ground heat exchanger, ground-source heat pump, and building distribution system are the main components, and each has their own fluid flowing network through pipes (in the GHE, and GSHP) or with ducts or pipes (to distribute heat through the space). Heat exchange occurs across these fluid lines to move the heat from or into the building depending on the temperature inside that space.

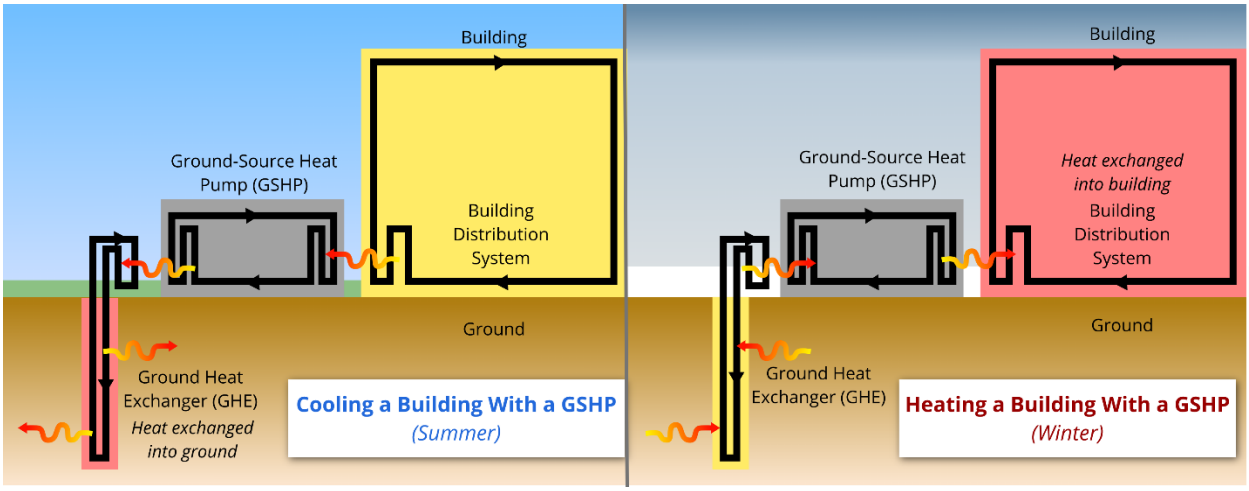

Figure 1.14. Overview of the heat exchange occurring across the building, heat pump, and ground heat exchanger to deliver heating and cooling.

Heat naturally travels from spaces of higher temperature to spaces of lower temperature. Generally, it is hotter above ground in the summer than below it, and it is colder above ground in the winter than below it (though this depends greatly on the location and climate, as explored in Section 3). The existence of a nearly constant ground temperature is the source of energy that a GSHP utilizes. Designing efficient, cost effective, and practical GHEs improves the performance of the GSHP system overall, and this component is the focus of this thesis work.

To attain the usable heat exchange required by the GSHP, the GHE undergoes energy transfer with the surrounding soil. This heat exchange is complex – involving conduction, convection, phase change, ion exchange, and some radiation effects within the soil [73]. While analytical methods are possible to calculate heat exchange and temperature distributions, due to the inclusion of the soil domain (and the environment surrounding it), exact analytical representations of a full in-ground heat exchanger for a GSHP are not commonly possible [73]. More details about ways

designers and researchers have been able to simplify, solve and study these GHE despite their complexity are presented in Section 1.3.5 and Section 2.1.2.

1.3.5 Modelling of GSHP

Analytical solutions exist to predict the performance of GSHPs [50], however, due to the complexity and size of GSHP operation researchers often utilize Computational Fluid Dynamics (CFD) and Finite Element Analysis (FEA) to solve governing equations in a numerical simulation. In these models, the accuracy of simulation depends on imposed boundary conditions, grid size and spacing, detailed material properties, and the correct choice of computational solver and convergence criteria. Even still, computational models can converge and output results when their conditions were input incorrectly, and for this reason it is important to complement numerical modelling with experimental data for validation whenever possible.

The computational requirements to run the software used in these models can sometimes limit the ability to create full-scale models of systems - especially those which use large domains, turbulent fluid flow, and the coupling of multiple physics modules. This is the case with modelling of GHEs, and so previous literature have used various methods to simplify these models. The most common case is to approximate fluid flow - rather than simulating it. This technique is applied with a line source heat model [77] (which takes the place of the fluid filled pipe), which represents conduction from a borehole along a line.

This method is useful for conventional vertical boreholes, but shallow piles have a ratio of diameter to length that is much larger [78], and so potential radial effects cannot be assumed to be negligible in their simulation. As such, a solid cylindrical model may be used to capture these radial heat transfer effects from the GHE [78].

However, a model which assumes constant heat flux across the pile (radially or along the length) is still limited by its ability to realistically replicate physical systems [76]. Due to advances in computational technology, researchers can now model the full fluid domain coupled with the heat transfer domain – thereby capturing the variability of heat transfer phenomena across the geometry of the GHE [63] [69]. These models are able to couple the heat transfer through the working fluid,

its surrounding walls, and the soil utilizing Multiphysics coupling. This setup communicates key variables between the fluid and solid governing equations until convergence is reached for both transmissions.

The model presented in this study utilizes the coupled method of modelling the GHE, modelling the full fluid flow and heat exchange within the soil domain. The GSHP is "fed" into this model via boundary conditions on the fluid inlet of the GHE which mimic the fluid exiting the GSHP. Similarly, the outlet fluid of the GHE model can be assumed to be the inlet fluid to the GSHP – in order to calculate its thermal performance in simulation that more closely mimics actual operation.

1.3.6 Limitations & Possibilities

While these models generally have good predictive performance, most GHE numerical simulations simplify the soil to a homogeneous medium – ignoring the effects of layering by depth, water content, and porosity – to average the thermal capacity and conductivity across the whole domain. In reality, soil is a highly complex porous medium - with material properties that vary by depth, season, and temperature [24] [79]. Due to this complexity, geotechnical engineers have developed several methods for determining the characteristics of the soil. A Thermal Response Test (TRT) may be performed on a soil sample to measure its thermal properties, however, this test requires lab equipment, and soil samples. Therefore, analytical models have also been developed to approximate these values based on soil type and distribution [80] [81].

In spite of these methods to determine soil properties, it is still most common in this field to assume average and constant values – broadly applied to regions. A few studies [50] [72] [82] [83] have introduced multiple soil layers, but these often rely on experimental data and do not yet provide information for designers in Canada across varying regions. The effect of this limitation is found in over and under sizing of borefields – and the potential to cause damage to soils if improperly sized. Temperature distribution in the soil is a key result of numerical simulation of GHEs, yet measuring the temperature rises outside of the pile was found to have inaccuracies as a result of the homogeneous thermal property assumptions for the soil [84].

Furthermore, there currently does not exist experimental data for the short helical steel pile GHEs with the geometry proposed in this study. While this data is being collected in future work, the validation of a shallow pile of similar geometry was performed for an experimental study by Jalaluddin *et. al.* for laminar flow [62]. More details about the validation of this study are presented in Section 1.6.4.2.

Modelling of GSHPs and GHEs improves as the technology, software, access to data, and knowledge of them improves. As such, there is great potential for future models to accurately predict fluid flow, heat transfer, porous media, freezing/thawing, phase-change materials, and other heat exchanger modifications. The understandings gained from modelling an increased complexity of systems will lead to a more informed industry - with the potential to customize GSHP systems depending on a wide range of variables. Ultimately, modelling is an effective way to predict system performance and employ modifications before building prototypes or demonstration sites - saving material cost and waste and reducing the potential for over or under sizing of equipment.

1.4 Existing Knowledge Gaps in the Literature

While the field of renewable energy using GSHPs has ever growing research and insights from all over the world, there remains some opportunities for reviewing assumptions or filling gaps within this research.

Firstly, the details of the soil domain can be expanded within modelling from the assumption of constant material properties to a more realistic variable representation of soil layers across regions and conditions. Updating this domain to accurately reflect its complex features may be difficult within the field of GSHPs because some of the detailed knowledge of the ground is located within other fields of study – such as geography, chemistry, and geotechnical engineering – this requires much interdisciplinary coordination and research. Furthermore, since conventional vertical GHEs reach such deep depths, measuring the variable properties across such a large volume of soil domain has a greater experimental cost than the benefits of accuracy might be provide. The variations within the soil domain tend to be within the upper layers, and so the assumption of constant ground properties may be reasonable for systems which reach deep depths. However, as

shallow systems are employed more widely, information about the soil properties becomes more and more valuable for accuracy of prediction and design.

Borehole logs collected from various installation sites and surveys can be combined into detailed databases for use by GHE designers and modelers. This information could be synthesized into functions within regions that predict the relevant properties depending on known or easily measured values (such as climate information). As well, the effects of the porous nature of the soil domain on its heat exchange behaviour can be more broadly expanded through input conditions and equations to be used by modelers who may not have the computational ability to model the exact physics of a large volume of porous media. Detailed information about the soil domain is housed in a wide variety of fields and there exists an opportunity for this information to be shared in an interdisciplinary manner to improve the ability for GSHPs to operate sustainably within the soil.

The choice of flow rates for GHEs has most commonly been set within the turbulent flow regime, and this is the most common instruction given to designers and installers from the literature [73]. Having high flow provides many benefits for conventional deep ground GHE systems, as it is needed to ensure the fluid flows and mixes across the entire length of the piping. Convective heat transfer is most commonly the focus for these systems, with the goal to maximize heat transfer rate and capacity – therefore, a turbulent flow would understandably increase the efficacy of convective heat transfer. However, in shallow GHE systems, and those with larger volumes of fluid, the conductive thermodynamic effects of a slow flow may also provide key advantages – and may produce more effective thermal performance of a shallow GHE than a turbulent flow would. The combination of use as a thermal storage medium (which nearly equilibrates the temperature of the water volume within the underground network to the temperature of the surrounding soil), and a heat exchanger (wherein this fluid is pumped through the GSHP at a rate sufficient for delivering transient space conditioning) should be further explored. When developing a new GHE design, there is a potential that the optimization knowledge from previous GHEs may not apply – and may even be in opposition to the optimization of the new design. The overall heat exchanging ability of a GHE is the sum of its convective, and conductive heat

exchange abilities. This research investigates the potential performance of a shallow GHE with slower, laminar flow rates – optimized for the combination of conduction and convection.

Installation of GSHP systems most commonly focuses on large buildings within urban or suburban environments – but there may be potential for these systems to be used in smaller, remote communities. For example, there may be potential for district heating and/or cooling to multiple small residential buildings supplied through a GSHP. For various political, historic, and social reasons, the energy needs of First Nations, Innu, Inuit and Métis communities within Canada have often been less prioritized than the needs of the larger, urban environments. Yet, remote and off-grid communities are those which may have the greatest immediate need for new innovations in the field of renewable energy. This becomes especially relevant when considering the effects of climate change in these regions. The field of sustainable energy should focus on a wide range of building applications – beyond just the locations of the largest economic markets. As well as providing a needed, and valuable service to historically underserved communities, this may also increase the innovation and creativity of designs for the unique needs of more remote locations.

Finally, the conventional design of a GSHP stresses that the supplied building load should be balanced across the seasons. In this way, the longevity of the system will be maintained by approximately extracting and supplying equal amounts of energy in the heating season as the cooling system. This design parameter is extremely valuable for systems which assume the mean soil temperature will remain unchanged across decades – the GSHP design should aid in maintaining this ground temperature and avoid causing Ground Thermal Imbalance (GTI). A graphical representation of this effect is shown in Figure 1.15 which plots the mean ground temperature (commonly called the deep ground temperature, which is assumed to be constant regardless of seasonal changes) across time. The three curves present the expected behaviour of this value when various loads are applied, these are presented without numerical axis as the exact temperature and time for this behaviour varies for each installation. The “Overheating” curve reflects an unbalanced building load which is cooling dominant; a building which demands a greater magnitude of cooling than heating across the year. The “Overcooling” curve is the inverse, in which a building demands a greater magnitude of heating than cooling over the year. The “Balanced Cycle” can be assumed to be the soil temperature with no annual interference from the

pile – because it is installed to be almost completely balanced (the amount of energy the GSHP demands is very near the amount of energy it returns across the year).

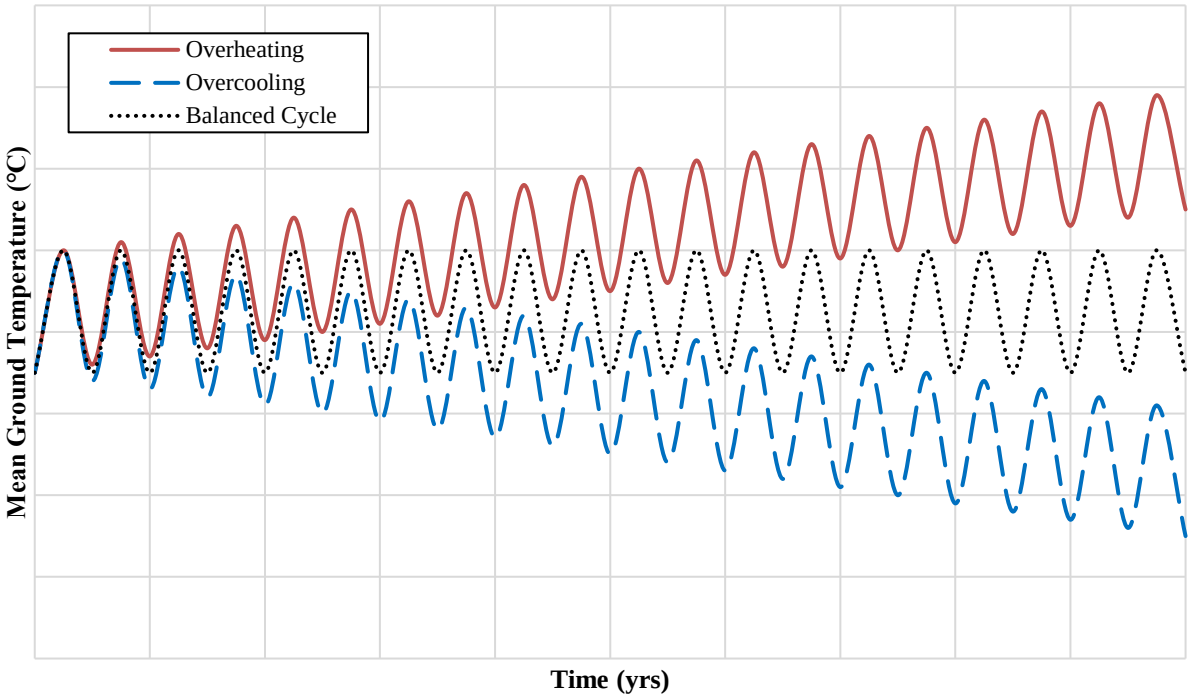

Figure 1.15. Long term effect of imbalanced loads on the mean ground temperature of the soil in the array.

With unbalanced loads, the mean ground temperature gradually diverges from the natural cycle, or perfectly balanced load curve. The cooling dominant load would eventually lead to an increase in the mean ground temperature across time, shown in the upward trend of the overheating curve. The heating dominant load would eventually lead to a decrease in mean ground temperature – as the heat which is naturally occurring within the soil is being extracted to the building at a higher rate than it can be replenished, cooling the soil. Typically, designs for a GSHP system will aim to avoid the overheating and overcooling curves across time – changing the number and spacing of GHEs as well as the load characteristics to achieve this.

However, this design process relies on the assumption that temperature migration is not already occurring within the soil across time. Such migration is investigated in this thesis (Section 3.1.2, and Section 6) through the effects of climate change (ambient air temperature increases) on the mean ground soil temperature over time. The predicted result is that the soil temperature will trend upward through seasonal overheating as shown in Figure 1.16. To prevent the thawing of

permafrost in regions where this climate change increase would warm the temperature of the ground above 0°C, there may be a potential to deliberately apply an unbalanced load through a GSHP to have a Beneficial Ground Thermal Imbalance (BGTI) effect.

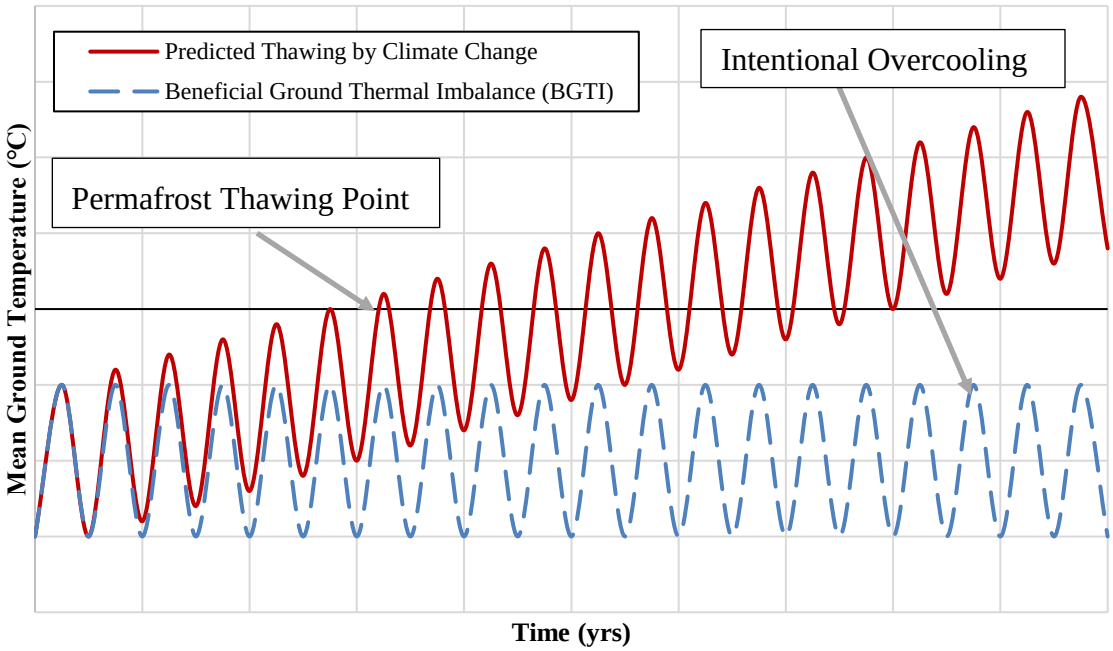

Figure 1.16. Predicted impact of climate change on mean ground temperature and the possibility for mitigating that effect with an unbalanced thermal load.

The BGTI would be achieved by overcooling the soil to a value which would mitigate the natural increase in temperature due to climate change. As the ambient air temperature heats the soil, a GSHP pile array with a heating dominant load may be able to extract this extra heat across time to maintain the current mean ground temperature and prevent thawing of permafrost.

This potential application of a GHE to act similar to thermosyphons and heat pipes already used in these regions to prevent ground thaw, but while also providing usable space heating across time (not currently possible with other permafrost cooling systems) is an exciting new opportunity within this field. Treating the overheating of the ground due to climate change as an energy source for a GSHP system is one which may address a sustainability issue within these regions – while also being capable of adapting to future climate changes. The use of unbalanced thermal loads in a GSHP system to provide certain temperature benefits is something that should be further explored within research and design of these systems to further increase their usability.

This research begins the investigation of using HSPs as GHEs, and certainly does not cover all of the possible information and optimization that can be performed on these systems. There may yet be many design iterations and insights before the system is able to provide all the benefits that it is predicted to be able to supply. Figure 1.17 shows the proposed use of these HSPs across three potential functions: 1. Structural support for buildings, 2. Operating as GHEs to supply space conditioning through a GSHP, and 3. Mitigating the thawing of permafrost by climate change by providing local BGTI through a heating dominant operating condition.

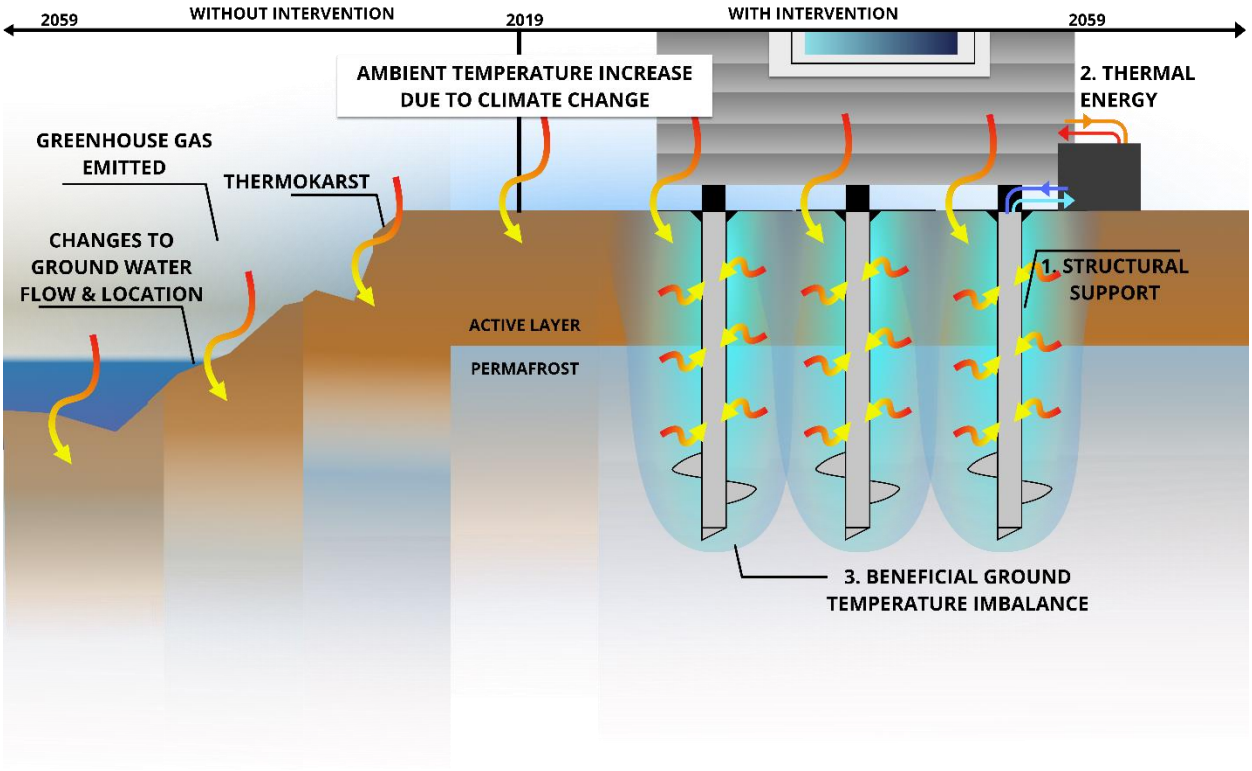

Figure 1.17. Proposed function and effect of the HSP as a GHE in Northern climates.

The literature predicts a wide variety of negative effects without such a potential intervention, wherein the thawing of permafrost by climate change will significantly impact the ground – and those living upon it. Ideally, the application of interventions which can address multiple needs of communities in these regions will provide a more sustainable and stable future in spite of increasing ambient air temperature.

1.5 Description of Papers & Contributions

Table 1.2 describes the contributions to this work by colleagues, and the location of where this information is used within this thesis (either directly, or with some modifications). Unless otherwise specified, the research performed in this work was contributed by the author.

Table 1.2. Contribution to this work by colleagues.

Colleague	**Contribution**	**Section with Information**
Dr. Aggrey Mwesigye, *Postdoctoral Fellow* Ryerson University, Toronto	Advised in the creation of COMSOL model	2.1.3
	Aided in validation methodology	2.1.4.2
	Provided equations for building load transient simulations	2.5.1
Leya R Kober, *Undergraduate Research Assistant* Ryerson University, Toronto	Contributed writing of the introduction section for a journal article	1.3.1
	Named and created the distinction between 11 Zones across Canada	3, 6.1
	Gathered soil and climate data from online databases	3
	Assisted in calculating the thermal conductivity of soil	3.1.1
	Assisted in modelling some of the geometric optimization study cases	4.3, 4.4

The research work presented in this thesis has been communicated in various forms of publications, as summarized in Table 1.3.

Table 1.3. List of publications containing information from this thesis.

Journal Articles		
Title	*Status*	*Section with Information*
Parametric investigation of the influence of geometry on the performance of a helical steel pile as an in-ground heat exchanger for ground source heat pump systems, by **Sarah R Nicholson**, Leya R Kober, Aggrey Mwesigye, & Seth B Dworkin	Submitted, under review	2.1, 2.4, 4
Impact Potential of A Novel In-Ground Heat Exchanger in Northern & Remote Communities to Mitigate Permafrost Thawing While Supplying Space Heating, by **Sarah R Nicholson**, Leya R Kober, & Seth B Dworkin	To be submitted (Spring 2020)	1, 3, 2.5.2, 6
Conference Papers & Presentations		
Title	*Status*	*Section with Information*
Modelling and optimization of helical steel piles as in-ground heat exchangers for Ground-Source Heat Pumps, by **Sarah R Nicholson**, Aggrey Mwesigye, & Seth B Dworkin	Presented & Paper Published at IQVEC 2019 in Bari, Italy	2.1, 4
Numerical modelling of helical steel piles as in-ground heat exchangers for ground-source heat pumps, by **Sarah R Nicholson**, Aggrey Mwesigye, & Seth B Dworkin	Presented & Abstract Published at CSME Congress 2019 in London, Canada	2.1, 4.3
Other Presentations		
Title	*Status*	*Section with Information*
Helical steel piles as in-ground heat exchangers for ground-source heat pumps, by **Sarah R Nicholson**, Aggrey Mwesigye, Leya R Kober, & Seth B Dworkin	Poster presented at the Clean Energy Expo 2019 through Ryerson University's Centre for Urban Energy in Toronto, Canada	1.1, 1.4
New technology in Geo-exchange, by **Sarah R Nicholson**, Pedram Hatefraad, Hiep V Nguyen, & Seth B Dworkin	Poster presented at the GRADShowcase 2019 through Ryerson University in Toronto, Canada	2.1.2

2. Methodology

The following sections outline the computational methodology utilized for this research. In order to understand and optimize the thermal performance of the HSP, a numerical model was developed and validated using experimental data from the literature. This model was then used to simulate a variety of steady state and transient cases in order to investigate the HSP's performance across a range of geometric, operational, and environmental conditions. Details of each of these studies are outlined in the Sections 2.4 and 2.5, while a general summary of the flow and purpose of these computations are presented in Figure 2.1.

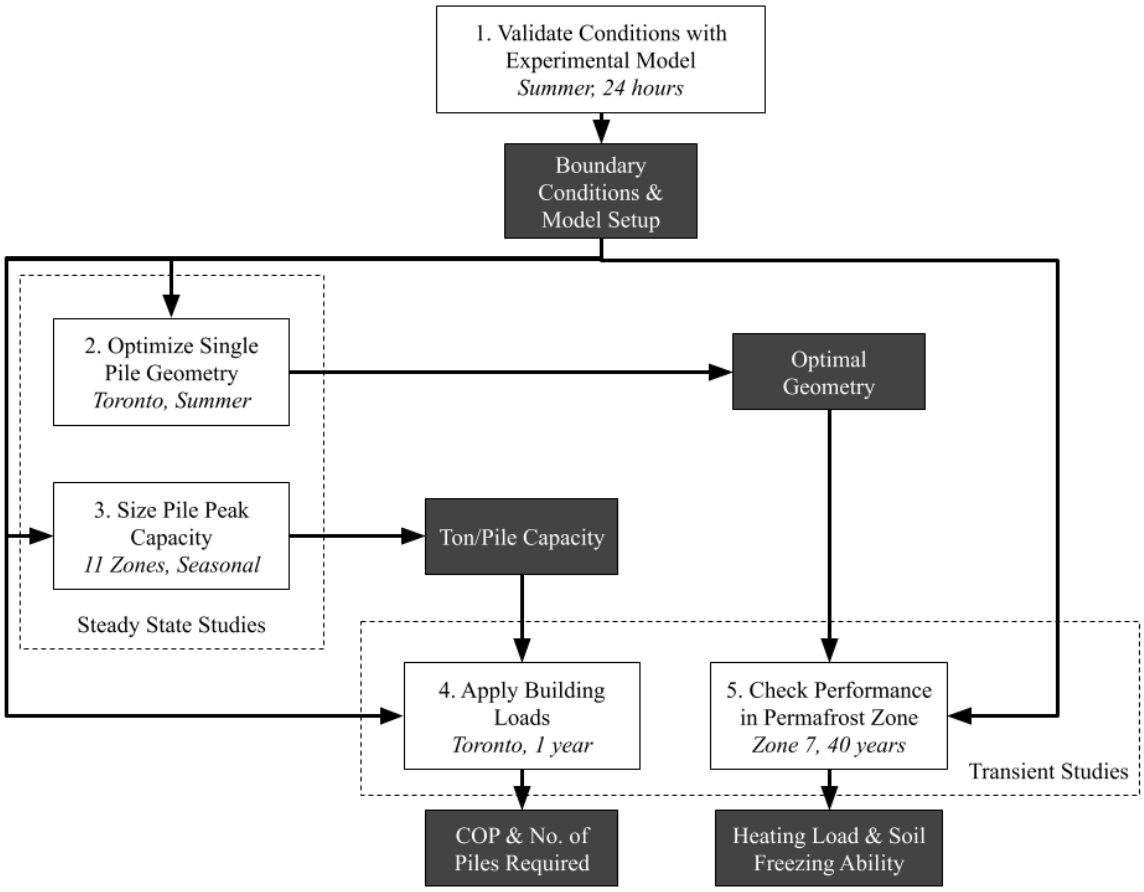

Figure 2.1. Research methodology flow and outcomes.

In the first step, the computational input and boundary conditions are validated using a model created to simulate the transient 24 hour experimental data collected by Jalaluddin and coworkers [62][63] from a similar shallow pile in Saga City, Japan. Once appropriate accuracy has been achieved, these conditions are then applied to a new computational model of the HSP investigated in this work (which is the basis for all the remaining studies). In the second step, the geometry of

this HSP is optimized for heat exchange rate using parametric sweeps through a steady state, summer operation. The capacity of the HSP is also investigated using steady state studies, for summer and winter operation across various regions and soil conditions in Step 3. The results of these steady state studies are used in Step 4 and 5, where the capacity in tons/pile is used to normalize building load data which is then simulated through a one-year transient study in the fourth step, yielding insights into the coefficient of performance and potential number of piles required to supply the demand. The optimal pile geometry from Step 2 is used in the 40-year transient study of Step 5 to compare the potential long-term influence of geometric improvements with the original pile geometry. This final step focuses on the potential usable heating energy which can be collected across 40 years in a permafrost region soil with dry and solid ice conditions. The soil temperature distribution is also investigated in this step to categorize the potential to maintain permafrost despite ambient air temperature increases.

This work aims to develop the foundation of initial data required for further research, innovation and implementation of HSPs in GSHP systems. Therefore, information about optimal geometric sizes, capacity of each pile to deliver heating and cooling loads, as well as transient performance across varying situations are investigated.

1.6 Model Development

A numerically simulated model of the pile within soil was created to optimize the system, and to explore potential use of GSHPs in northern and remote communities. The COMSOL Multiphysics® software ® [85] was utilized for this analysis. The thermodynamic effects of the system are modelled using CFD and FEA capabilities in COMSOL. This model did not consider the effects of snow cover or ground water flow. The pile depth in all cases is 20 m.

1.6.1 Preliminary Testing of Assumptions

The first model developed to simulate the HSP included the helix and tipped cap which are used to install the pile into the ground like a screw. It was initially thought that the helix of the pile might act like a heat exchanging fin (increasing the thermal performance of the pile) so initial simulations were performed with multiple helix features. A view of the bottom of this pile model

(with one helix) is shown in Figure 2.2 (a), and the rough temperature distributions resulting from multiple helixes are shown in Figure 2.2 (b).

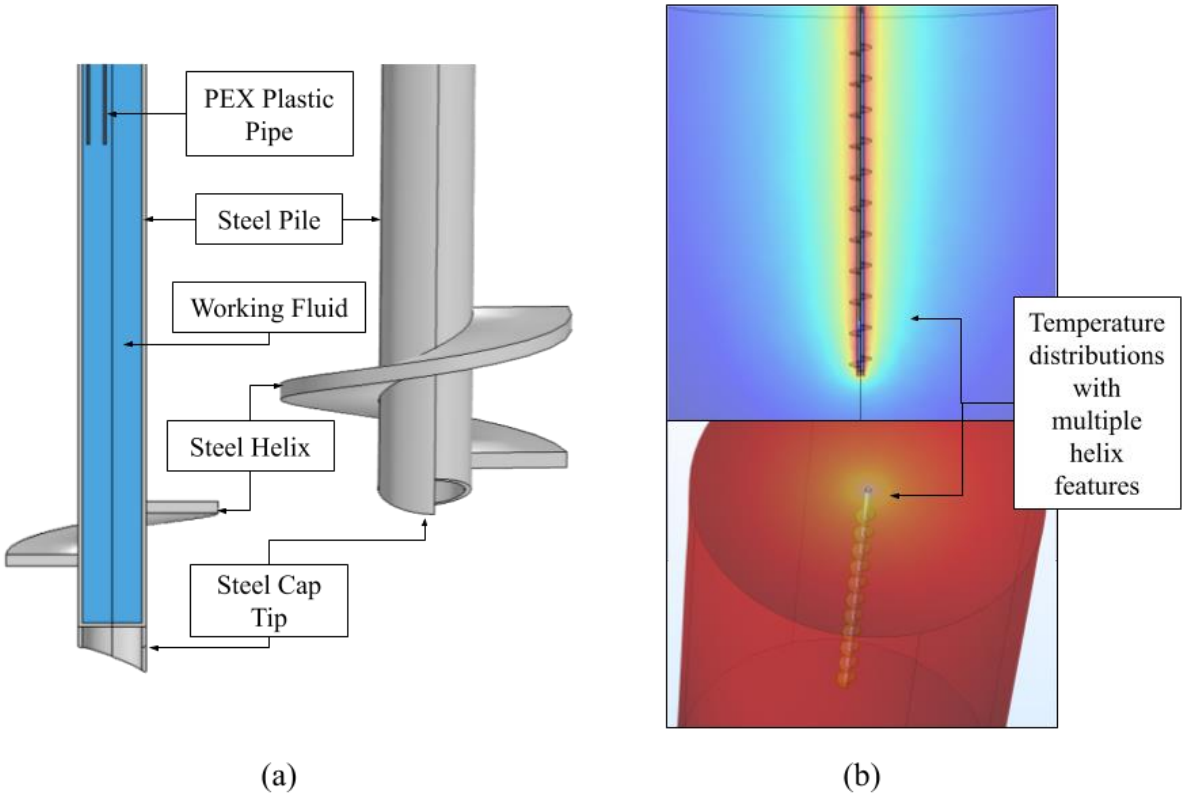

Figure 2.2. (a) View of bottom section of the helical steel pile model including helix and cap tip (section view on left), and (b) initial tests of thermal effects of helix and cap features.

After these initial simulations, the pile's helix feature was shown to have minimal impact on the heat exchange performance of the pile – with an outlet water temperature percentage difference of 0.07% when included or excluded from the model's geometry. Furthermore, modelling the helix and the cap tip resulted in an outlet water temperature percentage difference of 0.14%, when both were included or excluded. Therefore, to save computational time and greatly reduce mesh complexity, the helix and cap tip were not included in the geometry of the models. The effects of multiple helix features were not significant enough to be further explored in this work. Therefore, the assumption was made that the helical steel pile may be reasonably represented by a simpler pile model which does not include the geometry of the helix or the cap tip features. Pressure bulbs in the soil below the helix and air gaps (and the associated contact resistance) between the walls of the pile and the soil may exist, but they are not included in the model here – these should be investigated in future combined experimental/numerical studies.

The working fluid is assumed to be incompressible laminar or transitional flow, with a constant inlet temperature and flow rate. While colder climates may necessitate a water-glycol or other antifreeze mixture being used in the field, water is considered in the majority of the studies for comparison purposes (except in Section 6.2 and 6.3). The outer edges of the soil domain are assumed to be at far-field temperature conditions which reflect the ground temperature undisturbed by thermal interference by the pile. The temperature of the ground is calculated from an open boundary condition exposed to the ambient air temperature for that date of study, utilizing realistic weather data collected from the Government of Canada's historical database [86].

This analysis aims to use a mix of transient and steady state simulations to understand a variety of performance conditions. The components of the GSHP are connected to the in-ground heat exchanger via the inlet water temperature, such that the heat exchange rate of the pile – and the associated change in water temperature – can be used to understand the pile's performance across other operating conditions and HVAC equipment.

1.6.2 Physical Model

The governing equations solved by the computational model follow those used in GHE modelling research [65]. The flow is calculated as an incompressible fluid flowing within circular pipes, of no-slip wall conditions. This flow is coupled with heat transfer by considering the internal forced convection in the fluid as well as the conduction along the edges of each domain (plastic and steel pipes, volume of water, and the surrounding soil). Through this system of equations, the temperature distributions and flow fields are solved across the finite element mesh.

Utilizing the incompressible Navier-Stokes formula, the combination of these effects can be quantified, and the usable ground heat exchange across the pile (Q_{GHE}) is found. Figure 2.3 is a schematic depicting three main heat exchange functions occurring along the length of the pile in order to deliver this overall energy transfer.

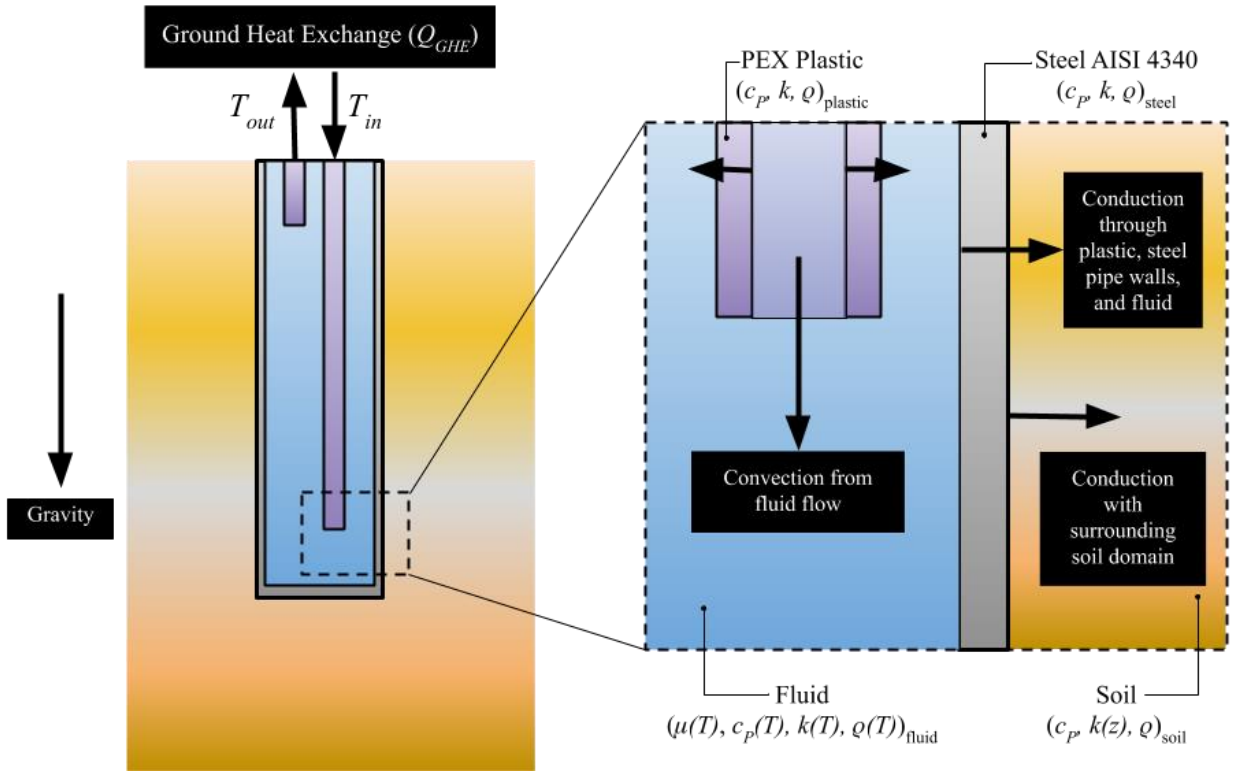

Figure 2.3. Schematic of heat exchanging phenomena within each section (close up on the right) of the entire pile (on the left) to generate usable ground heat exchange.

The temperature change across the entire pile (shown on the left of Figure 2.3) are the inputs and outputs to the control volume by which the overall ground heat exchange can be measured. This energy transfer is achieved via heat exchange across the entire 3-dimensional pile volume, details of which are shown on the right of Figure 2.3 in a rough 2-dimensional depiction of the energy transmission occurring at a section. Energy travels from and to the flowing fluid via heat conduction through the solid domains of the plastic and steel pipes, soil, and stationary fluids. Convective heat transfer also occurs via the internal forced normal flow at the inlet of the pipe, which transfers energy throughout the flow of fluid. Gravity is applied in the negative z-direction. There is assumed to be no internal energy generation, and the properties of the materials are constant unless their variability is specified (such as the fluid properties by temperature, and the soil conductivity by depth). The temperature of the fluid, plastic, steel and soil components all vary with time and location. Key material properties used are density (ρ), specific heat capacity (c_p), and thermal conductivity (k).

The magnitude and direction of ground heat exchange depends on the velocity of fluid flow, size of the system, as well as the properties and temperatures of all four components within the heat exchanger. For example, when the temperature of the incoming water (T_{in}) is lower than the surrounding soil temperature (T_{soil}), the direction of heat exchange will occur in to the pile through heat gain (a negative ground heat exchange value). This is the mechanism by which the fluid is heated by the ground in the winter to deliver space heating. If the opposite temperature conditions exist, then the energy will leave the pile in a positive heat exchange to the surrounding domains (delivering space cooling in the summer).

1.6.3 Boundary Conditions and System Parameters

Boundary conditions were imposed on the model to simulate the inflow of water at a given temperature and velocity along the entrance pipe surface. Similarly, the outflow was conditioned at the boundary of the top surface of the outlet pipe. To simulate the ambient surface above the ground, and the soil conditions below the pile, open heat flux boundary conditions were used on the top and bottom of the solid cylindrical soil domain encasing the pile. This allowed for the flow of heat across the boundaries at these surfaces, with a temperature corresponding to the outdoor ambient air temperature (simulating natural convection at the top open boundary condition), and the constant deep soil temperature (simulating the dissipation of heat within the larger surrounding soil domain at the bottom open boundary condition). Furthermore, to approximate an infinite soil domain surrounding the pile, a temperature condition was set at the outer edges of the soil domain (to imitate a far-field temperature condition). These conditions are shown in a schematic of the system in Figure 2.4.

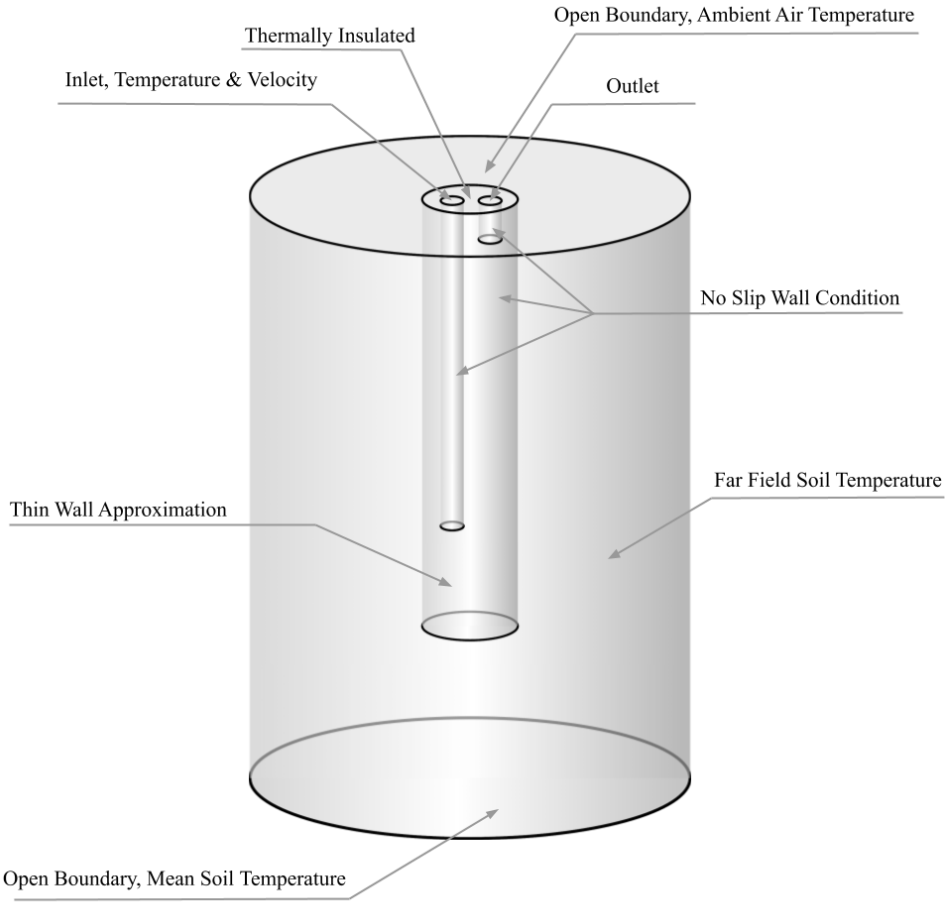

Figure 2.4. Computational domain with open boundary soil conditions at the top and bottom and constant temperature soil condition along the sides

The top surface of the pile which would be encased within the pile cap is assumed to be thermally insulated. The walls of the steel pile are modeled using a thermally thin wall approximation condition – this allows for the conductive resistance of the steel material to affect the heat exchange and temperature distribution of the simulations without having to create the physical geometry of the thickness of the pile. By utilizing this condition, the mesh was simplified, and the computational time to convergence was reduced.

1.6.4 Solution Procedure

1.6.4.1 Finite element grid & solver

A finite element grid was constructed with boundary layer gridding at the inner edges of the plastic pipes to better resolve the solid-liquid interface and more closely capture the transport phenomena at the walls of the system (with zero-slip conditions for the fluid flow). Across the larger domain

surfaces the mesh was constructed using a free tetrahedral shape. A mesh sensitivity study was performed for the variable of outlet water temperature. From a range of 49,187 mesh elements (and a steady state computation time of 2 minutes) to 3,292,542 elements (a steady state computation time of 3 hours), the outlet temperature variation was at or below 1%. An optimal mesh was chosen with 294,744 mesh elements and a computational time of approximately 10 minutes. Figure 2.5 is a sectioned top view of the mesh.

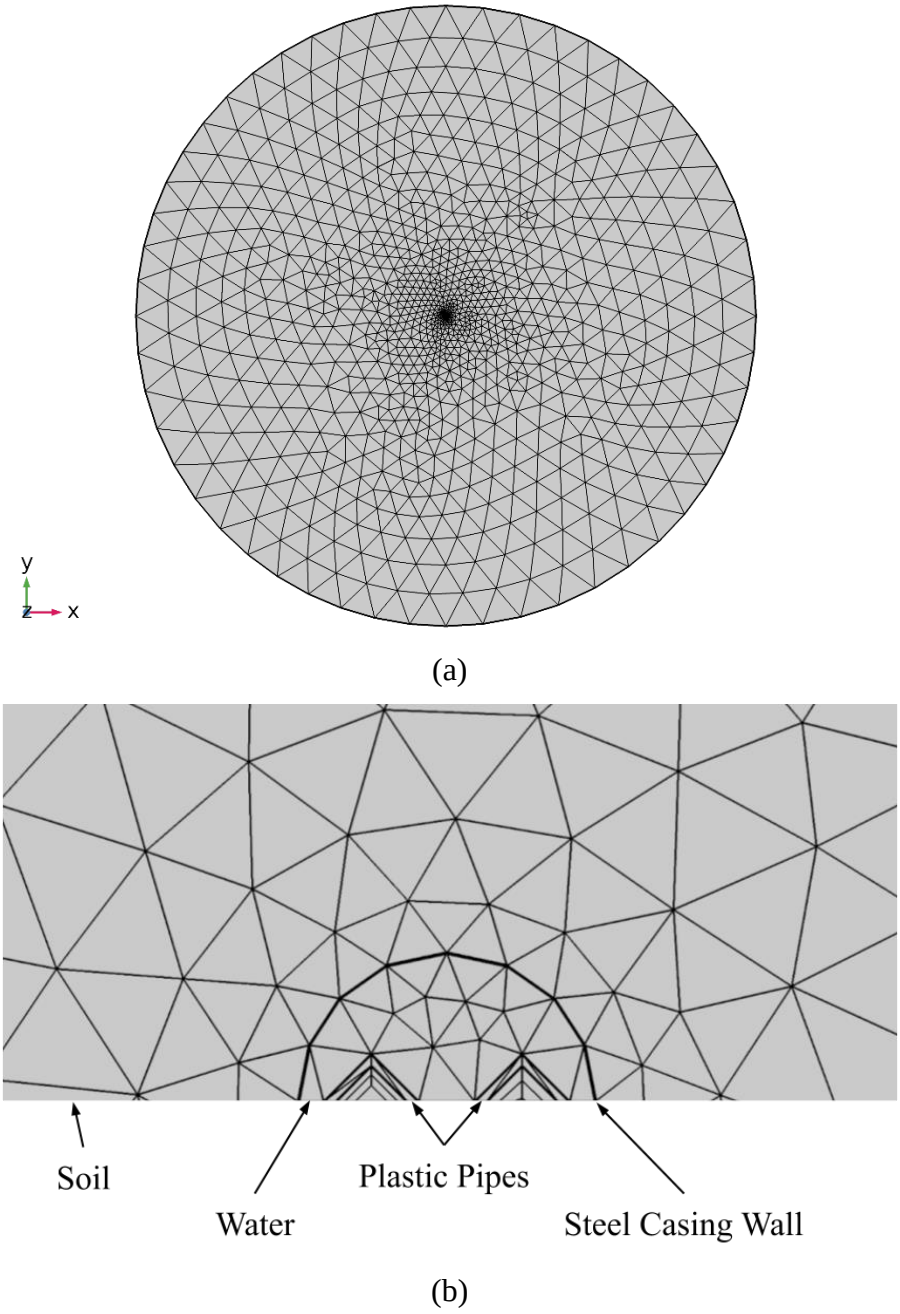

Figure 2.5. (a) Top and (b) top section view of finite element mesh utilized in solver

Further dependency testing was performed on the size of the surrounding soil domain. In order to achieve far-field temperature boundary conditions on the outer edges of the soil domain, the temperature flux at these edges should be zero. Therefore, using the above grid, the soil domain radius was simulated across a range of 3 m, 5 m, and 6 m. A radius of 5 m was deemed optimal for computational time and approximating far-field conditions.

The studies were performed using a stationary solver comprising a fully coupled Parallel Sparse Direct and Multi-Recursive Iterative Linear Solver (PARDISO) – which is a memory efficient method for solving large computational models such as the one in this present study [87]. The conjugate heat transfer (for solids and liquids) equations were coupled with the laminar fluid flow equations via a non-isothermal flow module and solver. The convergence criteria was an error per iteration less than 10^{-4}.

1.6.4.2 Model Validation

Two pile geometries are studied in the present work; Pile 1, for which experimental data exists in the literature [62][63], is used to first validate the model, and Pile 2, a newly proposed configuration using two offset internal plastic pipes. Once the boundary conditions and parameters are validated with Pile 1, the model is used for parametric optimization and further studies of Pile 2.

This procedure uses the measured outputs compared with the simulated outputs and updates the numerical model conditions until these outputs are within an acceptable range of error. Next the model conditions which yielded results with appropriate accuracy are applied to Pile 2 with the geometry of the novel pile.

The accuracy of the initial assumptions and boundary conditions were validated using an experimental pile setup from the literature. The transient response of the simulated model was compared with the measured experimental results in the studies performed by Jalaluddin and coworkers [62][63]. In their research, various pile types were modelled and experimentally tested for their heat exchange performance, where the double-tube pile type most closely represented the novel pile type proposed in this study. Figure 2.6 shows the geometry of the experimental setup

(Pile 1) and the novel system (Pile 2) – the validation model uses the larger area of the steel casing for the inlet water flow, funneled out through a long central plastic pipe. Pile 2 also has flow in the larger steel casing volume; however, the fluid is guided through an inlet plastic pipe along the length of the casing, and then out of the pile through a shorter plastic outlet pipe. These two plastic pipes are offset from the center by a distance x_{pl} in a custom cap design.

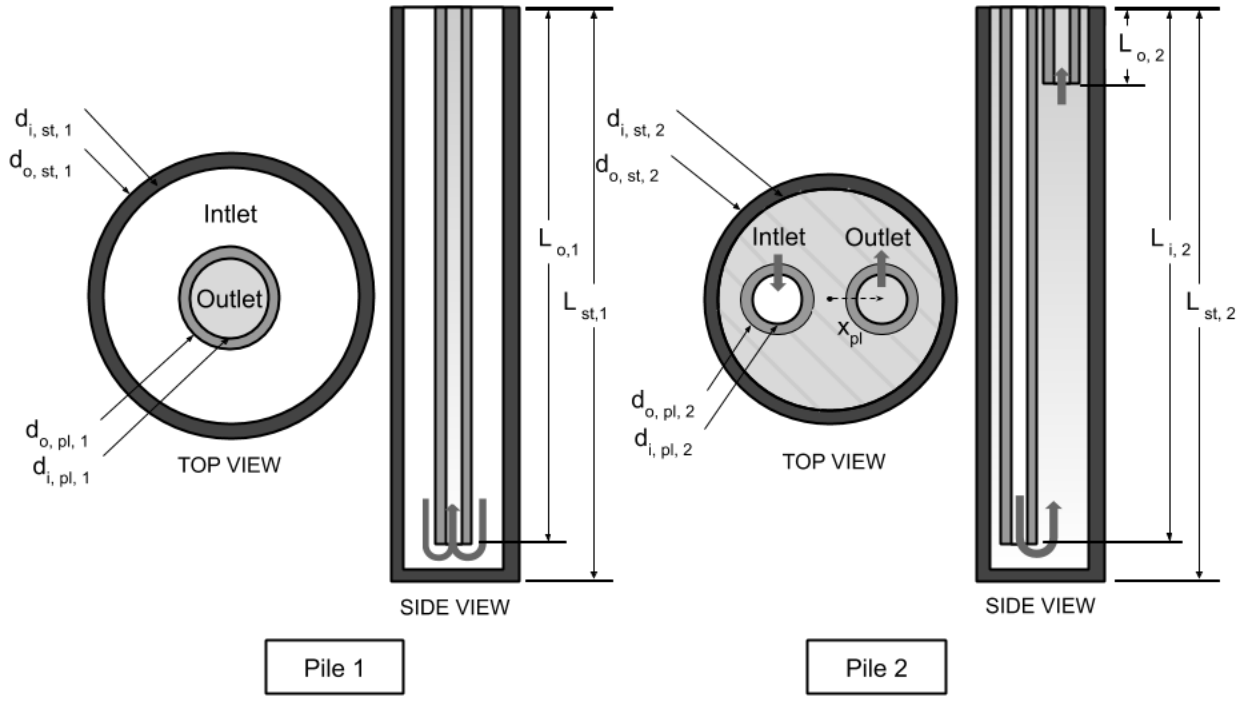

Figure 2.6. Top and side view comparison of the validation pile (Pile 1) and the novel pile (Pile 2)

The parameters of Piles 1 and 2 are defined in Table 2.1. The validation pile's temperature conditions correspond to the summer climate conditions of the experimental location in Saga City, Japan [62], whereas the ambient air temperature and soil temperature of Pile 2 are reflective of the summer temperatures in the region of this test project (Toronto, Canada).

Table 2.1. Pile configurations, parameters and properties

Parameter	**Pile 1 (Validation)** [63]	**Pile 2 (Base Case)**
Inlet water temperature (T_{in})	27°C	27°C
Soil temperature (T_{soil})	17.5°C	12°C
Ambient air temperature (T_{air})	20.3°C	26°C
Steel pipe outer diameter ($d_{o,st}$)	0.1398 m	0.1140 m
Steel pipe inner diameter ($d_{i,st}$)	0.1298 m	0.1000 m
Plastic pipe outer diameter ($d_{o,pl}$)	0.0480 m	0.0320 m
Plastic pipe inner diameter ($d_{i,pl}$)	0.0400 m	0.0240 m
Pile length (L_{st})	20 m	20 m
Pile Casing Material Properties	*Stainless Steel*	*AISI 4340 Steel*
Specific heat capacity (K/kg·K)	460	475
Density (kg/m^3)	7817	7850
Thermal conductivity (W/m·K)	13.8	44.5
Inner Pipe Material Properties	*Plastic PVC*	*Plastic PEX*
Specific heat capacity (K/kg·K)	960	1190
Density (kg/m^3)	1380	450
Thermal conductivity (W/m·K)	0.15	0.41
Soil Material Properties		
Specific heat capacity (K/kg·K)	1800	1800
Density (kg/m^3)	1700	1700
Thermal conductivity (W/m·K)	1.4	Function of depth

Given the inlet water temperature profile from the experimental data, transient studies were performed across 24 hours of cooling operation. The outlet water temperatures (T_{out}) from the pile outlet in the simulated model were then compared with the actual temperatures measured in the experimental setup (shown in Figure 2.7) to evaluate the accuracy of the model's results.

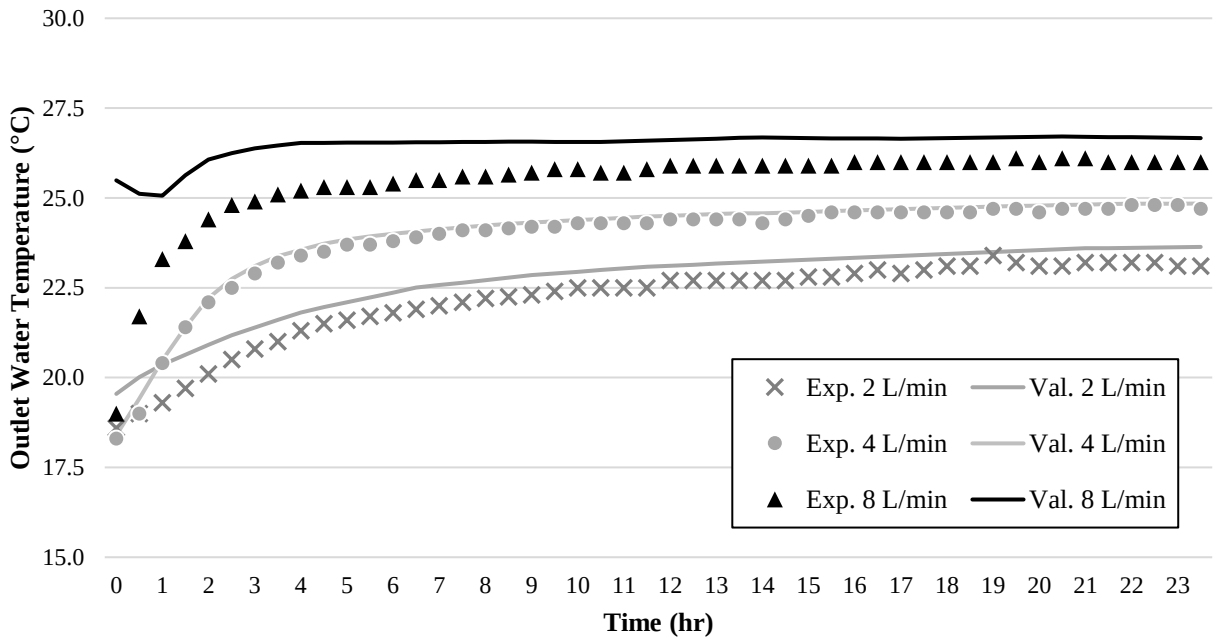

Figure 2.7. Validation of transient outlet temperature response at three flow rates

These results are compared using their values in Kelvin through a percentage error calculation, yielding average percentage errors of 0.16%, 0.04%, and 0.39% for flow rates of 2L/min, 4L/min, and 8L/min respectively. The 8 L/min validation model yielded the greatest variation between experimental and simulation temperature results due to the higher flow rate. Within the computational model, this higher flow rate yielded greater temperatures than the experimental values, due to the flow existing at higher Reynold's values than the laminar physics conditions were chosen for. The variation in these results are expected to be a result of the error associated with using laminar formulae to approximate nearly turbulent flows.

Nevertheless, these results highlight the effectiveness of the chosen boundary conditions and model setup in simulating results that closely match real life operation. However, there is also a limitation of the current model to provide accurate transient results at the higher flow rate and nearing turbulent flow. Subsequent studies are performed within a laminar range of flow, and new results will be generated after turbulent experimental data can be gathered for validation of a fully turbulent numerical model in future work.

1.7 Soil and Climate Zones

Utilizing generalized climate and soil trends across Canada, eleven zones were created as seen in Figure 2.8. These zones are contrasted with the locations of permafrost in Canada, and Figure 2.8 (b) shows that the location of permafrost ground conditions sweeps across the entire country; the Southern Limit of Permafrost touches nearly all provinces and territories [19].

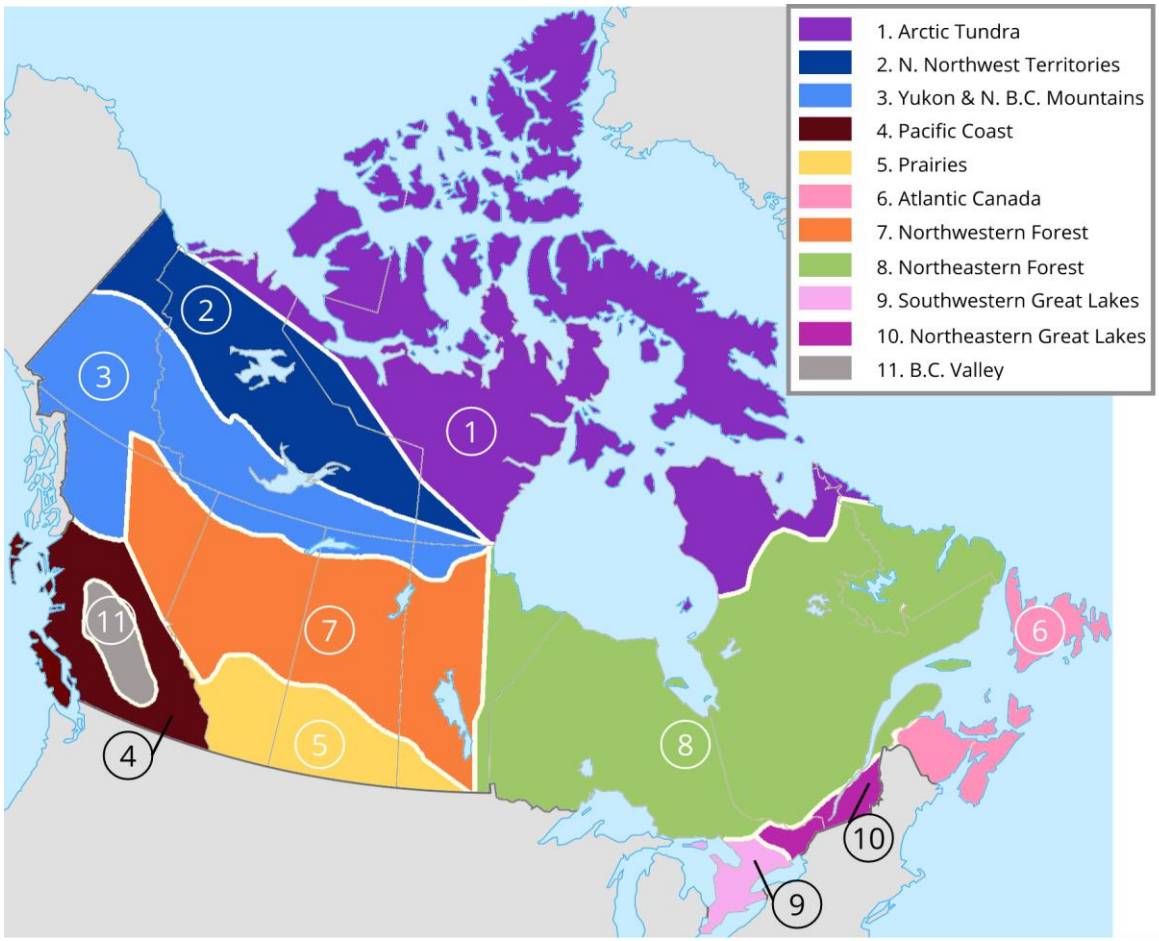

(a)

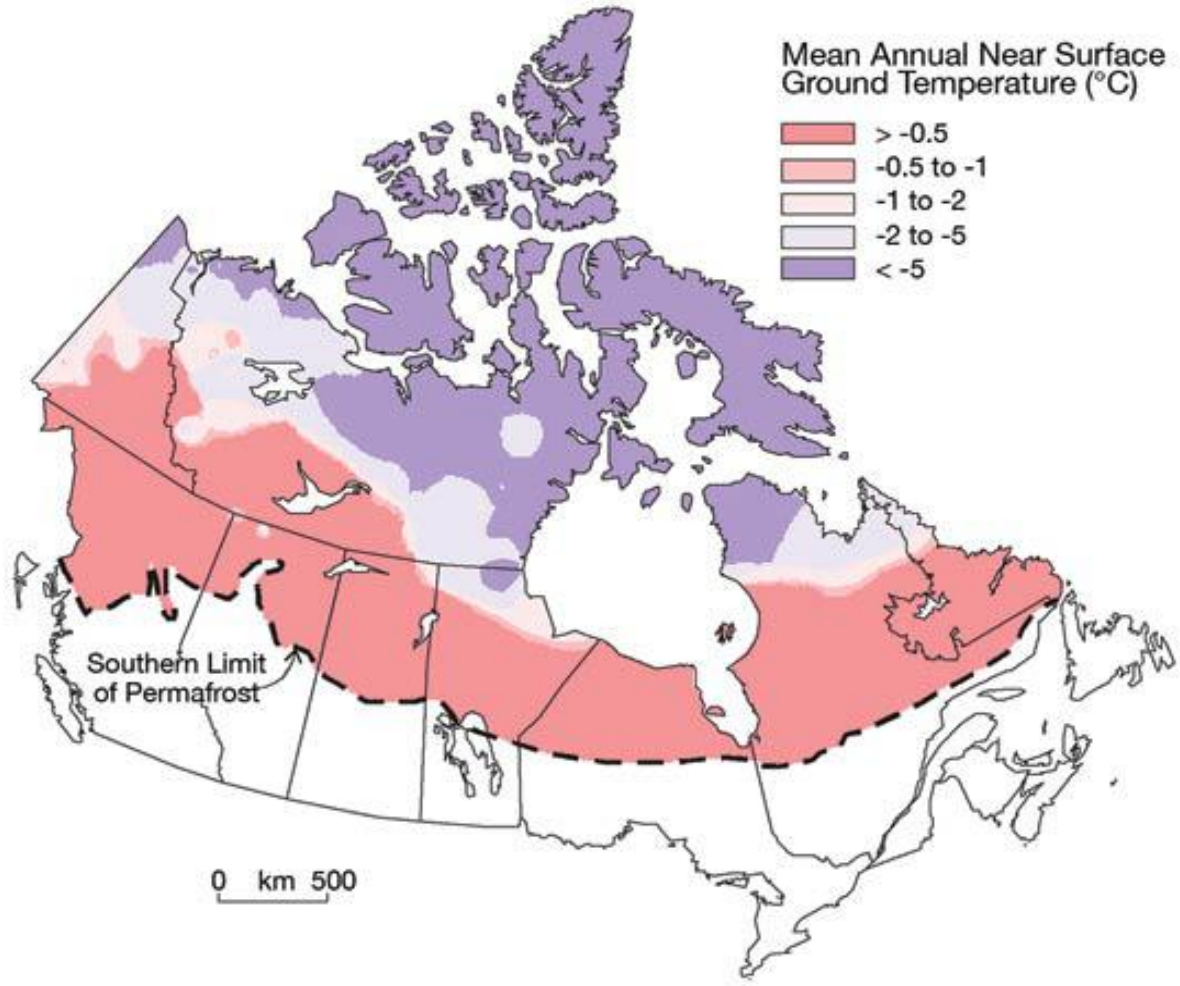

(b)

Figure 2.8. (a) Generalized zones of soil type, and (b) Canada's permafrost regions [19].

Locations of remote and northern communities are of particular interest - as well as those above the Southern Limit of Permafrost. Therefore, Zones 1, 2, 3, 7 and 8 will be the focus of the soil temperature model development for the climate change studies in Section 3.1.2. While Zone 7 is the focus of Section 6.2.

The soil conditions of all zones are investigated in Section 3.1.1, and the effect of varying thermal conductivity on the steady state performance of the GHEs is described in Section 6.1. Utilizing more detailed soil information from a location near Toronto, Ontario (in Zone 9), Sections 4 and 5 consider soil properties and saturation levels measured from a borehole test performed for this research [88].

1.8 Flow Rates

Turbulent flow rates were not the focus of this research. Rather, the performance of these piles at lower flow rates was chosen to be investigated. Therefore, to maintain Reynolds numbers below turbulent values within the pile, most of the flow rates were at 2 L/min, and 1 L/min. With these operating conditions, the functioning of slower laminar flow rates within a shallow ground heat exchanger was characterized. Advantages for these lower flow rates can be found in the longer residence time of fluid underground, allowing for greater heat exchange with the surrounding soil. Essentially, at steady state operation, the lower flow rates allow for the heat exchanger to act as a rough synthesis of a thermal storage system (with fluid near equilibration with the soil domain), and a cross flow heat exchanger (with convective heat exchange across the inner forced flow). In an attempt to bring GSHP technology to a wider range of uses, this lower flow rate may allow systems to be sized for a smaller pump, with less electricity demands required to meet the same capacity. This is a particular advantage in systems which are inhibited by the cost of mechanical equipment, and where electrical energy is of high cost or generated using unsustainable fossil fuel combustion.

In this present research, the piles are simulated and optimized as a single pile representing one part of an entire array - therein the flow losses across multiple piles in series are not simulated, and it is assumed that the defined flow rate is the exact value entering at the inlet of the pile. Future installations will need to account for flow losses across the system of pipes within the pile array, and further optimizations may be made to maintain an optimal flow rate throughout the entire array.

1.9 Steady State Studies

Initial simulations performed with the model were focused on steady state performance of the pile. These results aimed to investigate the optimal geometry of the pile in an attempt to outline potential inherent geometric relationships with heat exchange potential for this novel pipe setup. Furthermore, the steady state capacities were found to mimic the peak operating conditions and detail the limitations on fluid temperature and load capacity.

1.9.1 Parametric Sweeps of Single Pile Geometry

Before investigating the transient performance of the pile, a detailed understanding of the steady state performance and potential optimization must be established. Therefore, a set of parametric sweeps was performed for the two main geometric features of a single pile: pipe diameter, and length.

1.9.1.1 Diameter

For these studies the diameters were limited based on current available pipe sizes from manufacturers. The diameters of the outer steel pipe casing were sized from [89] and the plastic pipe sizes reflect nominal PEX plastic tubing [90]. The inlet and outlet plastic pipe sizes were assumed to be the same as each other. Also, due to space and flow limitations, not all combinations of pipe sizes were able to be simulated. More details about these sizes are included in Table 4.1 from Section 4.3.

1.9.1.2 Length

Next, the length of the inlet plastic pipes was simulated at a range of 0.5 m to a depth of 19.5 m within the 20 m steel casing. These simulations were performed using a constant soil thermal conductivity (the average value from the borehole test in Section 3.1.1), and using the borehole calculated variable soil thermal conductivity by depth. The aim is to investigate any potential variations between a homogeneous soil domain and a multi-layer soil domain, and to indicate general guidelines for plastic pipe length within the steel casing.

1.9.2 Sizing Capacity of Piles

Generalizing the capacity of a helical steel pile as an GHE is a fundamental step in the design and implementation of these systems for actual use. Therefore, a rough sizing of a pile at a potential test site is first performed. In order to generalize the steady state ability of this pile to provide thermal energy through the heat pump, the inlet water temperature to the GHE was varied through a parametric sweep. This sweep roughly reflects the changes to the water temperature that occur through the heat pump in order to meet varying capacities. This process is described in Figure 2.9

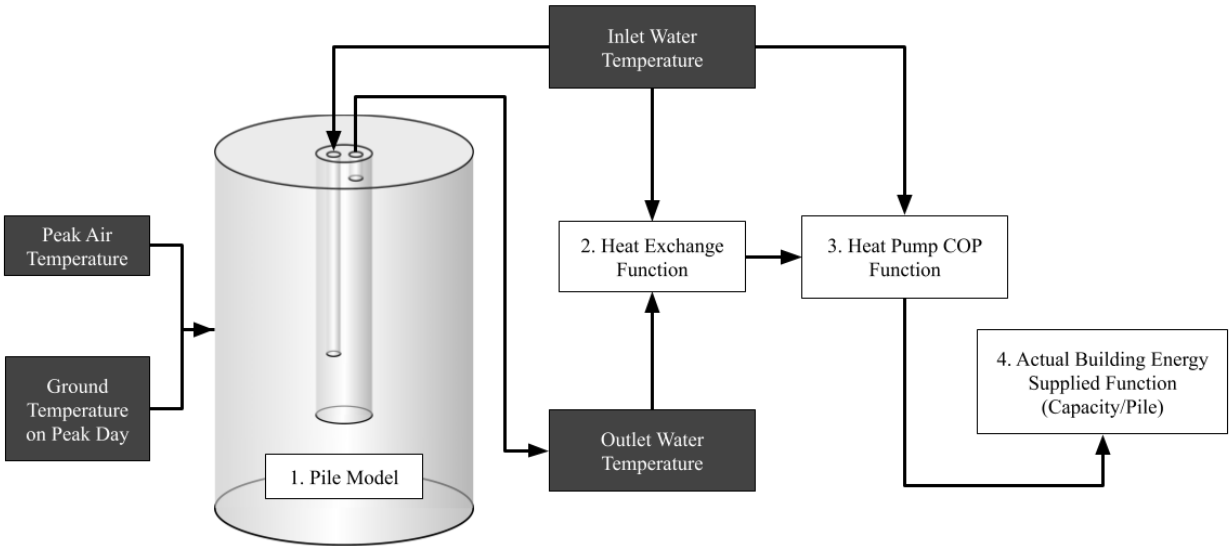

Figure 2.9. Process for steady state sizing of pile capacity.

Using the computational pile model in Step 1, temperatures were input for peak ambient air, ground and inlet water. Next, the outlet water temperature simulated through the pile model is the output which is then used in combination with the inlet water temperature in the heat exchange function at Step 2 (this step calculates the overall heat exchange achieved through the GHE). This heat exchange is then modified through a heat pump COP function in Step 3, which also takes into account the inlet water temperature to the pile. This COP function modifies the simple ground heat exchange which was first calculated in order to provide a more realistic thermal energy supply to the building (accounting for the heat pump). This actual building energy supplied is calculated in Step 4, as the pile capacity output. Through this method, the capacity of building load supplied per pile, or per unit length of pile can be found as a function of inlet temperature. This process was repeated for both summer and winter peak conditions.

1.9.3 Summer Maximum and Winter Minimum Across 11 Canadian Zones

The capacity of the piles as a function of region is investigated using the soil conductivities by zone calculated in Section 1.11. Utilizing steady state simulations, the soil conductivities in dry, wet, and iced conditions will be tested for the peak summer and winter ambient air temperature days. While the day of peak temperatures varied across regions, they were all roughly centered around the same time of year. Therefore, for comparison sake, a consistent date and time was used for all regions. The peak summer conditions are measured at 12:00 PM, noon, on August 1, and

the peak winter conditions are studied at 12:00 AM, midnight, on January 1. In this way, the instantaneous steady state thermal performance of the pile in each region is compared at the same date and time. Utilizing the collected historical ambient air temperature by hour from each location [86], the air temperatures at these times are used as the environmental inputs to the model. Furthermore, the soil temperature and conductivity by depth for each region on these two days also acts as variable inputs.

In order to prevent negative ground thermal imbalance in the soil and reflect a degree of an engineering factor of safety in the operation of these piles, the inlet water temperatures for each region varied as a function of the mean soil temperature. The difference in temperature of the inlet water to this deep ground temperature was set to not exceed 15°C in the summer, or 10°C in winter operation. Some exceptions to this rule were applied in regions of permafrost, where the winter inlet water temperature would be lower than the freezing point of a reasonable working fluid. For these cases, an inlet water temperature minimum of -6°C was applied except in the Arctic region whose inlet temperature to achieve heating operation needed to be -8°C, as seen in Table 2.2 below.

Table 2.2. Operating conditions for seasonal peaks in each zone.

	Inlet Water Temperature (°C)		Ambient Air Temperature (°C)	
Zone	**Peak Heating**	**Peak Cooling**	**Peak Heating**	**Peak Cooling**
1. Arctic	-8.00	6	-32.9	12.2
2. NNWT	-6.00	10.9	-30.2	23
3. Yukon	-6.00	15.7	-22.2	23.2
4. Pacific	0.66	25.7	-0.1	21.9
5. Prairies	-6.00	17.6	-31.5	30.6
6. Atlantic	-5.45	19.6	-11.2	28.9
7. NWF	-6.00	11.9	-23.2	24.7
8. NEF	-5.86	19.1	-27.4	24.6
9. SWGL	-2.57	22.4	-19.4	30
10. NEGL	-2.37	22.6	-25.2	28.1
11. BC	-0.88	24.1	-18.4	27.6

The goal of this work is to present a generalized case of thermal performance of an in-ground heat exchanger across the range of climate and soil conditions in Canada. Whereas previously, all geo-exchange capabilities are calculated on a per-project, site-by-site basis, creating this novel database

will aid designers in developing a generalized understanding of performance. With this knowledge, there may be predictive market movements, and a firmer link between geography and thermal performance capability of a location.

Further work can improve this database by dividing the regions into smaller zones, which also account for groundwater reservoirs, changes in elevation, and any other existing thermal interferences (either manmade or natural).

1.10 Transient Studies

To investigate the transient behaviour of the pile, two sets of studies were then performed: first to test a building load application in the Toronto climate for the duration of a year, and then to test 40 years of performance using a simple load in a permafrost area at risk for thawing.

1.10.1 Building Load Simulations

The building load simulations utilize existing hourly loads collected by Alavy *et al.* [91]. These loads are then normalized based on the capacity sizing performed in Section 2.4.2 and applied to the model utilizing transient computations of input variables. In this way, the model of a single pile approximates the performance of a pile within an array to supply the building load. While the array required to meet the various loads may need a wide range of number of piles, this simulation will allow for initial indications of COP, and temperature ranges required to meet various loads.

For all of the building loads simulated, the assumed start date of operation was on the first hour of January 1, with the assumption that no previous thermal interferences or disturbances were present in the soil. Furthermore, it is assumed that the arrangement of the pile in an array will be designed for minimal ground temperature interferences between piles. Realistically, a GSHP system may begin operating at any season in a year – and this will have an effect on the performance of the system. Supplying a heating load to a building after the cooling season has "pre-heated" the soil with higher ground temperatures will be easier than supplying this heating in the middle of the winter season when the ground temperature is lower. Nevertheless, the January 1 start date is used here to compare with a less than optimal scenario of building operation.

1.10.1.1 Description of Building Models & Data

To simulate the use of these GHEs in a realistic GSHP system, building loads were normalized and transformed through an analytical representation of the heat pump (represented by a COP correlation shown in Equation 7 below), and then applied through the transient input of water temperature to the model. In this way, the building load was assumed to be supplied at a varying value which directly meets the load required by the building. This method is different to those which use cyclic loading [58], in which the heat pump operates only in an ON/OFF function - meeting a peak heat flux requirement. While the ON/OFF method is useful for describing some heat pump systems, this present study aims to mimic those of a variable speed heat pump, which vary either the flow rate or water temperature in order to meet the transient load. Therefore, when a building load is demanded, this model assumes the heat pump is "always ON" for this hour - and that the inlet water temperature is changed to meet the load, as per the methodology presented in [68]. This procedure is shown in Figure 2.10.

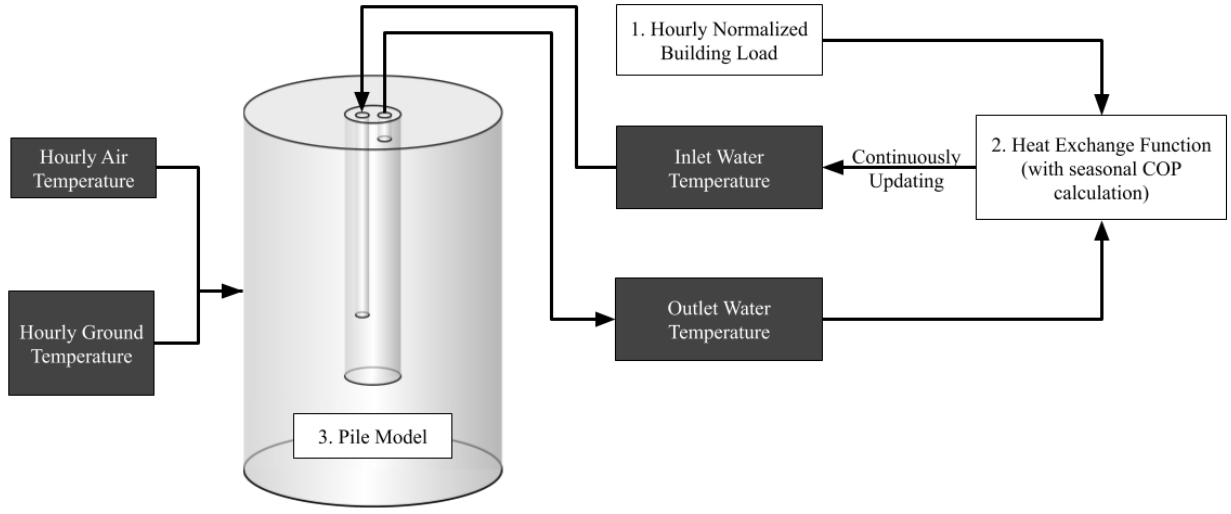

Figure 2.10. Process for simulating transient building loads through pile.

In the first step, the hourly building load from three buildings from [91] were normalized based on the capacity sized in Section 2.4.2. Then, this normalized load was input to the COMSOL model with the procedure outlined in [68]. Wherein, the heat exchange function in Step 2 yields an inlet water temperature value for simulation through the pile model in Step 3. This pile model is also modified by hourly air and ground temperature inputs to output a resulting outlet water

temperature. The temperature of the outlet water continuously updates the temperature of the inlet water via Step 2 to create a transient simulation of a building load demand.

The thermal energy supplied by the GHE (Q_{GHE}) is related to the actual thermal energy supplied to the building ($Q_{building}$) by the relationships shown in Equation 5 and 6.

$$Q_{GHE}^{heating} = Q_{building}\left(1 - \frac{1}{COP_{heating}}\right) \quad (5)$$

$$Q_{GHE}^{cooling} = Q_{building}\left(1 + \frac{1}{COP_{cooling}}\right) \quad (6)$$

The coefficient of performance (COP) for each season is defined utilizing Equation 7 which applied coefficients relating to each season, and modifies the COP depending on the inlet water temperature – in this way the performance of a general heat pump may be simulated using the coefficients for cooling and heating assumed in [68] which limit the maximum heating and cooling to conservative COP values of 3 and 6 respectively.

$$COP = aT_{fi}^2 + bT_{f,i} + c \quad (7)$$

These relations were combined within Equation 8, which is a summarized version of the inlet water temperature input used as a transient input to the numerical model in these studies.

$$T_{in} = T_{out} + \frac{Q_{building}}{\rho_f c_f \dot{V}_f}\left(\left(1 - \frac{1}{COP_{heating}}\right)A(1-B) + \left(1 + \frac{1}{COP_{cooling}}\right)B(1-A)\right) \quad (8)$$

This equation includes the volumetric flow rate of the incoming fluid ($\dot{V}_f$) measured in m^3/s. This method allows for the continuous simulation of building loads across seasons, and utilizes cycling coefficients A and B to enable the cooling or heating mode portion of the equation. These coefficients are input as a corresponding hourly value of 1 or 0 depending on whether the building load is a heating or a cooling load for that hour. The input building load does not undergo a preprocessing to filter out heating or cooling demand in off seasons, but rather reflects the entire signal across the year. The choice to include potential heating in the summer and cooling in the winter in this model was made to allow for some complexity, or noise which may exist in actual operation. Potential effects of this off season demand are included in this research.

Building load simulations were performed for a location within the area of Toronto, Canada, wherein the ambient air temperature was included from a database to reflect a year of operation. The ground temperature was calculated by the hour using Equation 4 from Section 1.12, and the outlet water temperature was probed at each time step in the simulation to update the inlet water temperature accordingly.

This method of simulation will enable the collection of water temperatures across the pile as they vary with building load, ground, and climate conditions across the year - giving further insights into the performance of these piles in a transient case for future comparison with other thermal energy systems. As well, the simulation of these building loads will further validate or invalidate the generalized sizing capacity of the system described in Section 2.4.2 - if the load is normalized for too great a capacity per pile, then the water temperatures across the year will exceed the operating range required by the heat pump.

These building load studies are limited by the assumption that operation of the pile begins on the first day of the year. For a cold climate, this means that the soil is required to provide heating energy through the pile at the beginning of the operation. However, this soil is assumed to be untouched by previous thermal loads - and so the heating energy supplied by the pile in the first winter is only that which is naturally available through the soil's collection of energy, this assumption may have a small effect on the ability of the pile to initially meet a large heating demand. During summer operation, cooling loads add heat to the soil (as it is removed from the conditioned building), which allow for more heat to be extracted during the second heating season of the year than the first. To further optimize these simulations, the building loads could be applied at a range of start dates and for a longer range of years in order to capture any potential long-term temperature effects of pile operation.

1.10.2 Permafrost Thawing Mitigation Study

The Northwestern Forest Zone (Zone 7, referring to Figure 2.8) was found to be a climate zone with a near-zero mean temperature (described in Section 3.1.2), and so it can be categorized as vulnerable to thaw in the future. For this reason, a transient study was performed at this location

simulating the years of 2020-2060. This model investigates two soil conditions from Section 3.1.1 (dry and solid ice soil) to simulate the thermal effects of different soil conductivities over these 40 years. Furthermore, the climate change effects were introduced using a simple mean ambient air temperature across time, to generate hourly annual air temperatures in this region for 40 years. This model utilizes the value of 2°C mean temperature increase, applied evenly across each year from 2020-2060 as a 0.05°C/year increase. The weather file was modified such that the current year's weather patterns are maintained with this constant magnitude increase per year. This modified weather file is labelled as the "climate changed ambient air temperature" ($T_{air,CC}$) and varies hourly.

This model is further simplified by assuming a constant inlet temperature is applied to the pile. This inlet temperature is the coupling variable between actual operation with the heat pump, and the respective building load applied. In the absence of a generalized archetype for buildings across all the regions in this study, this constant inlet temperature and flowrate are used in an aim to characterize the ground thermal effects, and heat transfer capability, so as to establish a basis for future studies with full building loads applied; this inlet temperature was -5°C (which implies the need for a water solution to avoid freezing of the working fluid). Simulations were performed with the base model described as "Pile 2" in Section 2.1.4.2 with the flow rate of 1 L/min, with a Reynold's number of 1682. Finally, the constant load was applied utilizing the geometrically optimized model from the parametric studies at a flow rate of 2 L/min. The initial model is used to investigate any potential for this system to mitigate thawing, whereas the tests utilizing the optimized pile were more detailed and aimed to investigate a potential maximum impact of the GHE on permafrost soil. This study was performed using both dry soil conductivity, and the conductivity with solid ice. As well, the working fluid was updated to roughly approximate the fluid properties of a 20% propylene glycol solution as described in [92].

1.10.2.1 Description of Ambient Temperature Rise Model

As shown in Section 1.12, the ambient air temperature increases associated with a 40-year increase of 2°C will affect the soil temperature by depth in affected regions. Modelling of these conditions were first performed assuming there was no GHE intervention – only the soil domain with a 40

year hourly ambient air temperature dataset to reflect climate change. Then, the model was updated to include the GHE.

Results from this analysis are focused on the transient ground temperature distribution across the changes in operation and ambient air temperature. The aim of this part of the study is to show whether or not a beneficial ground thermal imbalance (BGTI) can be generated from the use of the HSP heat exchanger – one which minimizes the potential ground warming by extracting excess heat through the ground loop and GSHP system. These results will be investigated at key points within the soil domain: immediately adjacent to the edge of the pile, and at varying distances radially from the centre of the pile. This focus will be on the soil region below the active layer – within the mean soil temperature depths. How much potential thawing mitigation can be achieved – and at how great a distance this effect might manifest will be investigated to guide future applications and installation.

3. Multi-Layered Soil Model Conductivity & Temperature Predictions with Climate Change

1.11 Soil Thermal Conductivity by Depth

A key variable in the thermal behaviour of the GHE is the thermal conductivity of soil. Therefore, this work aimed to utilize soil layer compositions to gauge variable conductivity by depth. In this way, the soil layers and their variations across locations can be included in the numerical model, and more closely approximate actual systems.

While the soil thermal conductivity is commonly measured using experimental testing, and is performed per site, this work relied on analytical calculation of soil thermal conductivity with data available from a borehole test, and through soil databases. Several analytical methods exist for calculating the soil thermal conductivity, including the Johansen model developed in 1975 [93], which determines an overall conductivity based on weighted dry and saturated conductivities combined with a normalized value [93][94]. Conductivity models utilizing heat transfer coefficients are also employed, which utilize partial differential equations of heat transport through the soil in order to solve for a conductivity with calculated soil temperatures and boundary conditions at three time intervals [94]. Furthermore, the de Vries [95] analytical method (also created in 1975) of soil thermal conductivity utilizes weighting factors and the conductivities of individual soil components to determine an effective soil conductivity of a given sample. These methods require the detailed sampling of soil composition, grain size and distribution, and moisture/organic content. Comparisons of the various methods have been studied in [94],[96],[97] and [81]. The simplified de Vries method [81] was chosen for this methodology due to its consistency in calculating conductivities across soil samples [94], and since the values required for this calculation are able to be found directly from the borehole test and soil database used.

For the geometric optimization of the piles, a drilled borehole test [98] was performed at a potential experimental site within the region of study for this pile. Using the soil type, water content, and grain size measured in this test, the effective thermal conductivity of the soil was calculated by soil depth – linearly interpolated across the soil region layers found in the soil profile. To expand

the studies beyond this site, soil layer information was collected and averaged from three locations within each defined zone from the Canadian Soil Information Service (CanSIS) [99], and input into the Farouki-de Vries model simplified by Z. Tian *et. Al.* [81] shown in Equation 1:

$$k_{soil} = \frac{\theta_{water} k_{water} + F_{air} f_{air} k_{air} + F_{minerals} f_{minerals} k_{minerals}}{\theta_{water} + F_{air} f_{air} + F_{minerals} f_{minerals}} \quad (1)$$

Z. Tian *et. Al.* utilize λ_n to denote thermal conductivities, however that has been changed here to k_n to avoid duplication of variable symbols within the GSHP and energy fields. Furthermore, the weighting factor has been renamed from k_n to F_n. Therefore, the terms θ_{water} and f_n are volume fractions, F_n is a weighting factor (which accounts for soil bulk densities and porosity) calculated using formulation from [81], and k_n are the thermal conductivities of each material. This equation has been modified to exclude the effects of vapour in the soil and assumes that ice would replace the water terms. These assumptions are made to approximate the lower thermal conductivity seen in unfrozen summer ground conditions. Table 3.1 lists the constant material properties assumed for each soil component, where the bulk density is only needed for the solid soil components of sand, clay, and silt.

Table 3.1. Material properties used for soil components.

	Water	**Ice**	**Air**	**Sand**	**Clay**	**Silt**
Conductivity, *k* (W/m·K)	0.57	2.28	0.025	7.7	1.93	2.74
Bulk Density, *BD* (g/cm^3)	-	-	-	1.65	1.35	1.5

Table 3.2 summarizes the result of this pre-calculation on the borehole test site, where the average soil thermal conductivity for the overall domain is 1.817 W/m·K, a reasonable value for this soil region [97]. These results were used as the soil thermal conductivity for the geometric optimization simulations in Section 2.4.

Table 3.2. Calculated soil thermal conductivity by depth below the surface

Soil Layer Depth (m)	Effective thermal conductivity (W/m·K)	Water Content (%)	Soil Type
0.2	2.156	9.3	Silt (fill)
1.8	2.035	22.0	Silt
4.6	1.804	24.0	Sandy silt
6.1	1.166	24.2	Clay
7.9	2.076	30.1	Sandy seam
26.1	1.830	28.3	Sandy silt
27.6	2.278	26.3	Sandy silt
29.0	1.193	23.2	Clay

Due to a limitation of data in the soil database, some assumptions were made to approximate soil thermal conductivity. Mainly, the available information did not include the percentage water, ice, or air present in the soil - as the volume fractions of sand, silt, and clay were from the solid volume, not including the void volume (θ_{void}). Furthermore, the bulk densities (*BD*) in the data set represented fine particles, ignoring coarse grains present in the soil. To compensate for this lack of detail, a volume average bulk density was found using proportional solid soil volume compositions from Table 3.1. Furthermore, the particle density (ρ_{pd}) was calculated using the percentage of organic content ($f_{organic}$) in a relationship defined by R. A. McBride *et. al.* from their investigation into Ontario soils [80], simplified in Equation 2:

$$\rho_{pd} = 2.646 - 2.8 * f_{organic} \tag{2}$$

Finally, the void volume (and thereby the potential content of water, air, or ice) was calculated using Equation 3:

$$\theta_{void} = 1 - \frac{BD}{\rho_{pd}} \tag{3}$$

From the void volume, several saturation conditions can be modelled: assuming the void volume is 100% air, a dry conductivity was found for each layer depth. Similarly, changing the ratio of air,

water, and ice within the void volume means various ground conditions can be calculated. These will be compared in future work.

After this calculation was performed for each of the locations, they were averaged across depth for each zone with the assumption that defined layers had constant properties between the depths defining their layer height – yielding a function of soil conductivity by depth which more closely represents actual soil properties than current homogeneous models. Table 3.3 shows the results of this calculation from the soil layer data for Whitehorse in the Yukon. This data shows the relationship between soil layer differences and the resulting conductivities. Here, the dry conductivity (k_{dry}) assumes the void volume is made up of air only, the mixed conductivity (k_{mix}) assumes the void volume is half air and half water, the wet conductivity (k_{wet}) assumes a fully (water) saturated soil, and the ice conductivity (k_{ice}) assumes that the void volume is filled with ice.

Table 3.3. Soil layer volume fractions and conductivities for Whitehorse, Yukon.

	Volume Fraction (%)				*Soil Conductivity (W/m·K)*			
Depth (m)	f_{sand}	f_{silt}	f_{clay}	f_{void}	k_{dry}	k_{mix}	k_{wet}	k_{ice}
0	66.6	16.9	5.3	11.2	3.24	3.43	3.61	4.10
-1	46.2	11.7	3.7	38.4	0.95	1.28	1.40	1.76
-10	52.3	6.1	3.1	38.5	0.98	1.32	1.45	1.86
-36	60.3	0.6	1.2	37.9	1.06	1.41	1.56	2.04
-60	60.3	0.6	1.2	37.9	1.05	1.41	1.56	2.04

As expected, these results show that increasing saturation yields increasing conductivities – and highlights that more dense and higher sand-content soils have higher conductivities than other layers. There is also a noticeable variation of conductivity across each soil layer, wherein the top layer has the highest conductivity due to the presence of organic content, and a high volume fraction of sand for the soil sample in Table 3.3. In the middle range of depths from 1 m to 10 m, the soil conductivity across saturation drops due to a higher content of lower conductivity silt and clay (rather than the highly conductive sand). Results of soil layers such as this may guide the

installation depth of a pile, wherein it is installed at a depth and length which optimizes its contact with highly conductive soil layers (for increased heat transfer) or lower conductive layers (for thermal storage). The variations by depth averaged for 11 zones are shown in Figure 3.1 for dry and saturated soils.

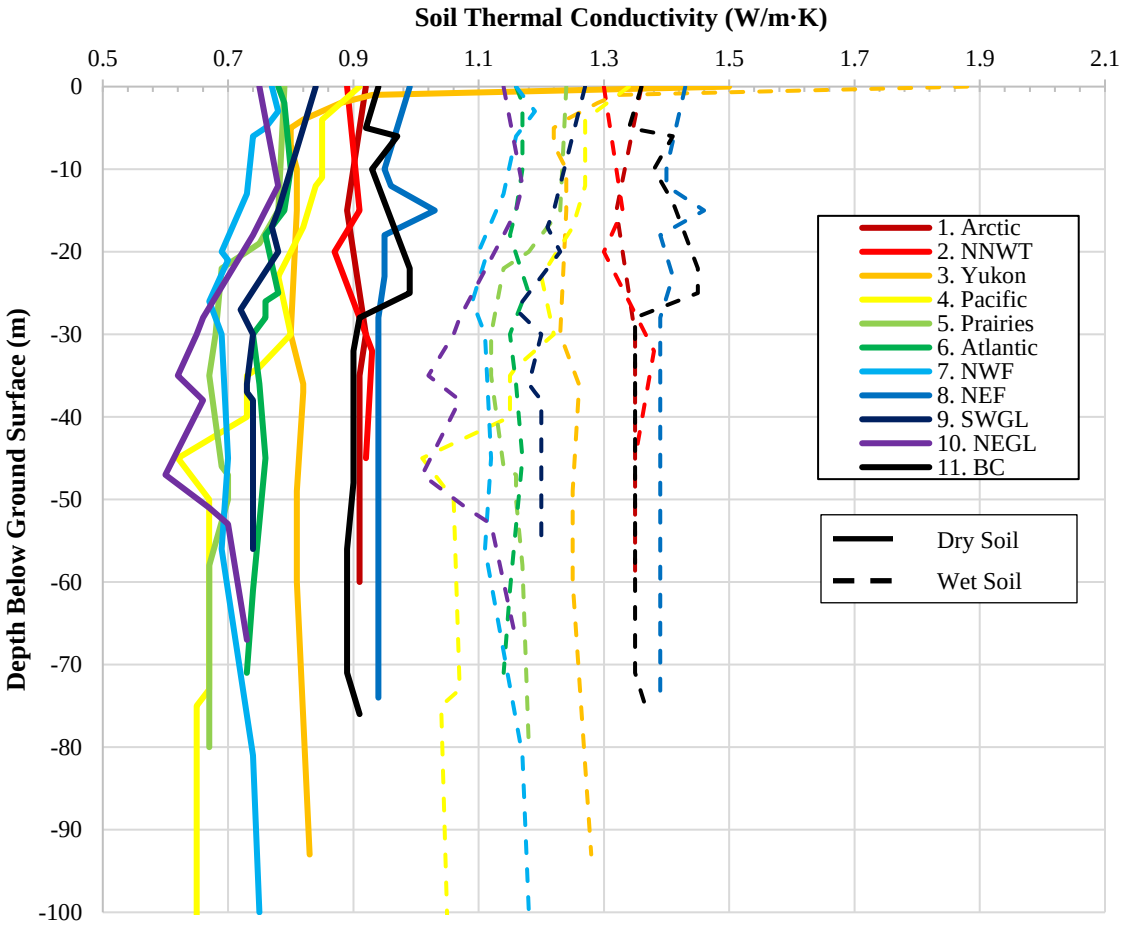

Figure 3.1. Dry (solid line) and saturated (dashed line) soil conductivity by depth per zone.

For each zone, the saturated soil conductivity is higher than the dry, and the ranges for these conductivities are from 0.60 W/m·K to 1.9 W/m·K. These values are comparable to those measured in a study on Canadian soils performed by V. R. Tarnawski and colleagues [97] who tested soil samples in a laboratory to compare the effect of dryness and saturation on conductivity. From 18 samples, they measured dry soil conductivities from 0.21-0.30 W/m·K, and saturated conductivities from 1.52-3.17 W/m·K [97]. Similarly, research into the soil conditions in areas around Wuhan city, China, to determine potential for shallow geothermal potential by J. Luo and colleagues [100] found a range of soil conductivity from 1.08-3.07 W/m·K across a variety of soil lithology with measured water content (between dry and fully saturated) [100].

The conductivities presented in Figure 3.1 highlight the non-homogeneous nature of soil – especially at depths to 35 m. For shallow GHEs, the variations in these properties may have a significant effect on performance, longevity, and optimization strategies. It should also be noted that this method of soil thermal conductivity calculation across the larger dataset resulted in moderate soil conductivity values. The borehole tested conductivities from Table 3.2 resulted in more variability in conductivity across each soil layer. This is likely due to a single dataset yielding these results – from a specific site and soil sample. In comparison, the results presented in Figure 3.1 are averaged across three locations within each zone, and these results were previously adjusted by the CanSIS when the National Soil Database (NSDB) was created in order to archive soil information across large regions. This, along with the approximations required to account for missing soil data are expected to explain the relatively low variations of soil conductivity by depth, and the low average conductivity across regions. However, these results are still valuable guides for GSHP designers and researchers, as there are variations across regions noted even within this generalized analysis. For example, the conductivity of Zones 1, 2, 3, 8, and 11 are greater than those in other regions. This result is particularly interesting in the context of permafrost response to climate change as shown in Figure 1.8 – here Zone 8 overlaps with the region of highest response to climate change. A highly conductive soil will be more responsive to the thawing effects of increased ambient air temperature, and this is reinforced by the soil conductivity model created here.

To begin to capture the effects of ice on soil conductivity, the void volume (originally modelled as air or water) was assumed to be completely filled by ice. This conductivity only considered ice to exist in the soil up to the depths at which the soil temperature on the coldest day was at or below 0°C – as calculated in Section 1.12. The depths which remained above freezing on the coldest day had soil thermal conductivities which reflected the fully saturated conditions. These results are shown in Figure 3.2.

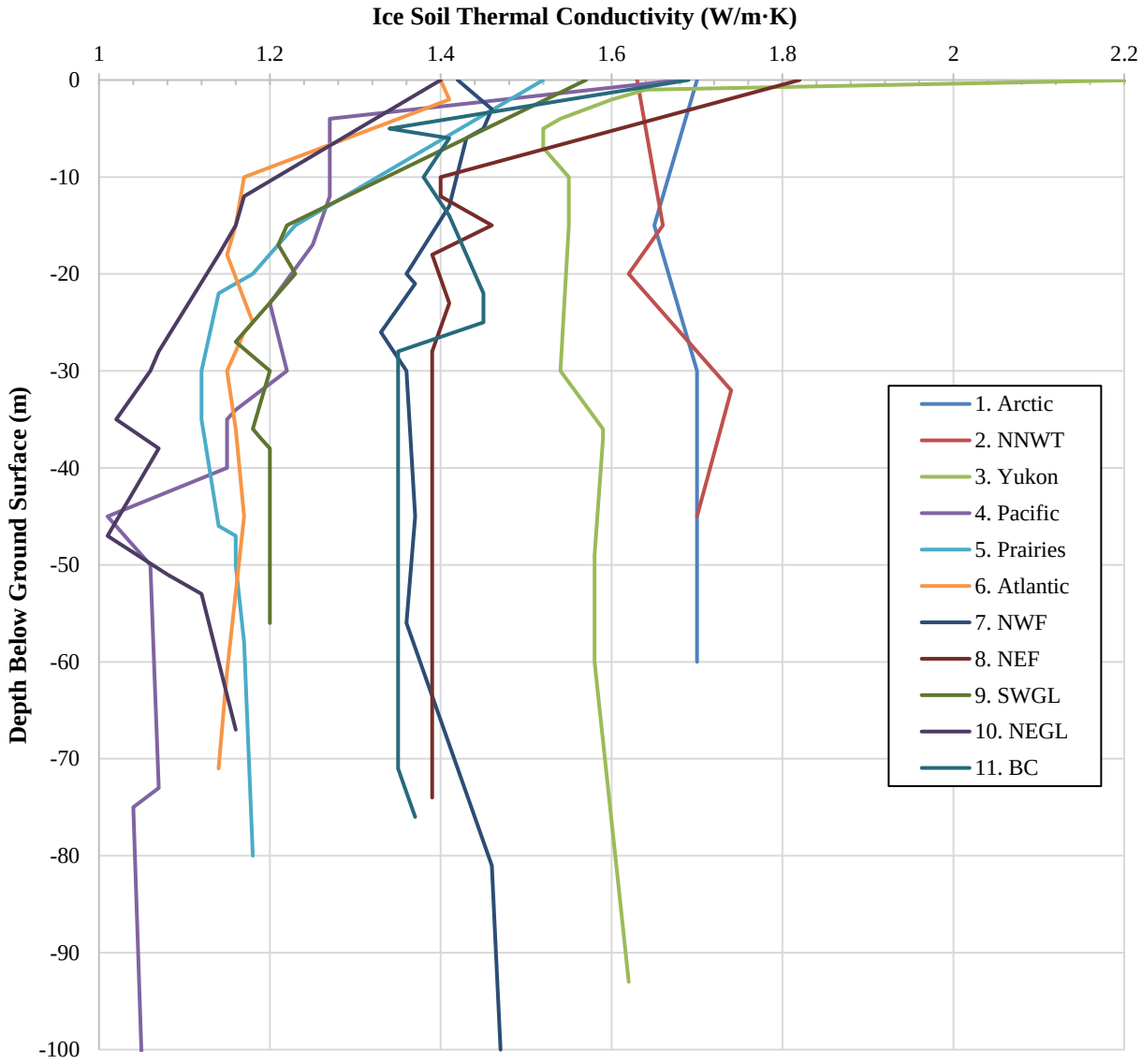

Figure 3.2. Soil conductivity by depth in each zone for soils with a void volume filled by solid ice at depths with winter ground temperatures at or below 0°C (if the ground is warmer than this freezing point, the soil condition is saturated).

These results highlight the increased thermal conductivity of ice, with an increase in soil conductivity values across zones with low ground temperatures. Measurements on soil samples from a permafrost region in Qinghai, China were performed by W. Pei and colleagues [101], who aimed to study thermal conductivity modelling of soils and rocks in these cold climates. From their 11 samples, they calculated a range of thermal conductivity for unfrozen to frozen soil of 0.794-2.081 W/m°C – with the frozen values always greater in magnitude than the unfrozen soil. The results from the ice conductivity calculations in Figure 3.2 will provide valuable winter condition properties – specifically in investigating the soil temperature distribution radially from the pile. As

the thermal conductivity of the soil increases with the presence of ice, there could be a variation in the distribution of temperature which may cause interference for pile arrays which were designed using summer soil conditions. Further improvements to this soil domain model would consider the ice as a phase change material and include an updated equation to account for thawing and melting. The present study focuses on ice in its solid state, as the aim is to prevent its thawing. Therefore, the simple, solid approximation of ice was deemed sufficient for this work.

Though this methodology supports the improvement of existing soil domain models, it still remains incomplete as it does not fully consider the heat transfer ability of groundwater flow, which can increase the heat exchange rate by depth up to 4 or 5 times in some cases [32]. Furthermore, the porosity of the soil is not modelled utilizing typical porous media heat and mass transfer equations. Initial computational models were generated to simulate a saturated porous media with the pile attached, however, the computational demands were too great for a full-scale model, and the experimental data requirements for validation could not be gathered in the scope of this study.

Therefore, although the conductivity of the soil changes to reflect varying soil layers and saturation levels, the groundwater flow is not considered - nor are the inter-particle effects of a porous medium. Finally, the thermal properties of the soil such as density and heat capacity were also maintained at constant values taken from previous studies. All thermal properties may change as temperature changes; however, this adjustment is also left to be the subject of future work.

Despite the many challenges of accurately modelling the environment within which the GHE that exist, as will be shown in subsequent chapters, the methodology presented here was able to generally categorize the variations of conductivity across large regions of permafrost soil zones in Canada – which can be useful for initial implementation strategies. Areas with higher conductivities may be more susceptible to permafrost melting, however they may also have greater GSHP performance. The methodology – and resulting data – presented in this thesis aims to provide support to future researchers and designers when building within the non-homogeneous soil domain.

1.12 Soil Temperature Model

For the geometric optimization studies presented in Section 4, a constant far-field soil temperature was used based on generalized ground conditions from the area of study. However, all other studies in the present thesis utilized a more detailed soil temperature model which changes by depth, based on the time of year and ambient air temperature conditions.

This variable soil temperature was calculated assuming the diffusivity of the soil varied as a function of the soil thermal conductivity, by depth. For the peak soil temperature conditions used in steady state studies, the dry soil thermal conductivity by depth for each region was used. In the case of transient building load studies in Section 1.18 and Section 6, the soil temperature was calculated in every time step of the simulation using the soil thermal conductivity reflected in the model (for either dry, saturated or iced soil).

To appropriately measure the connection between seasonal ambient air temperature, and soil temperature (T_{soil}), a common soil temperature model was used as shown in Equation 4 [65]:

$$T_{soil}(z,t) = T_M + A_s \bullet \exp\left[(-z)\left(\frac{\pi}{365\alpha}\right)^{\frac{1}{2}}\right] \times \cos\left\{\frac{2\pi}{365}\left[t - t_o - \frac{z}{2}\left(\frac{365}{\pi\alpha}\right)^{\frac{1}{2}}\right]\right\} \qquad (4)$$

This equation utilizes the annual mean air temperature (T_M) , air temperature amplitude (A_s), day of maximum annual temperature (t_0), and ground thermal diffusivity (α) to calculate ground temperature by time (t) and depth below surface (z).

Figure 3.3 shows the temperature distribution for the warmest and coldest days of the year based on historical climate data for five regions (reflecting the zones with permafrost potential).

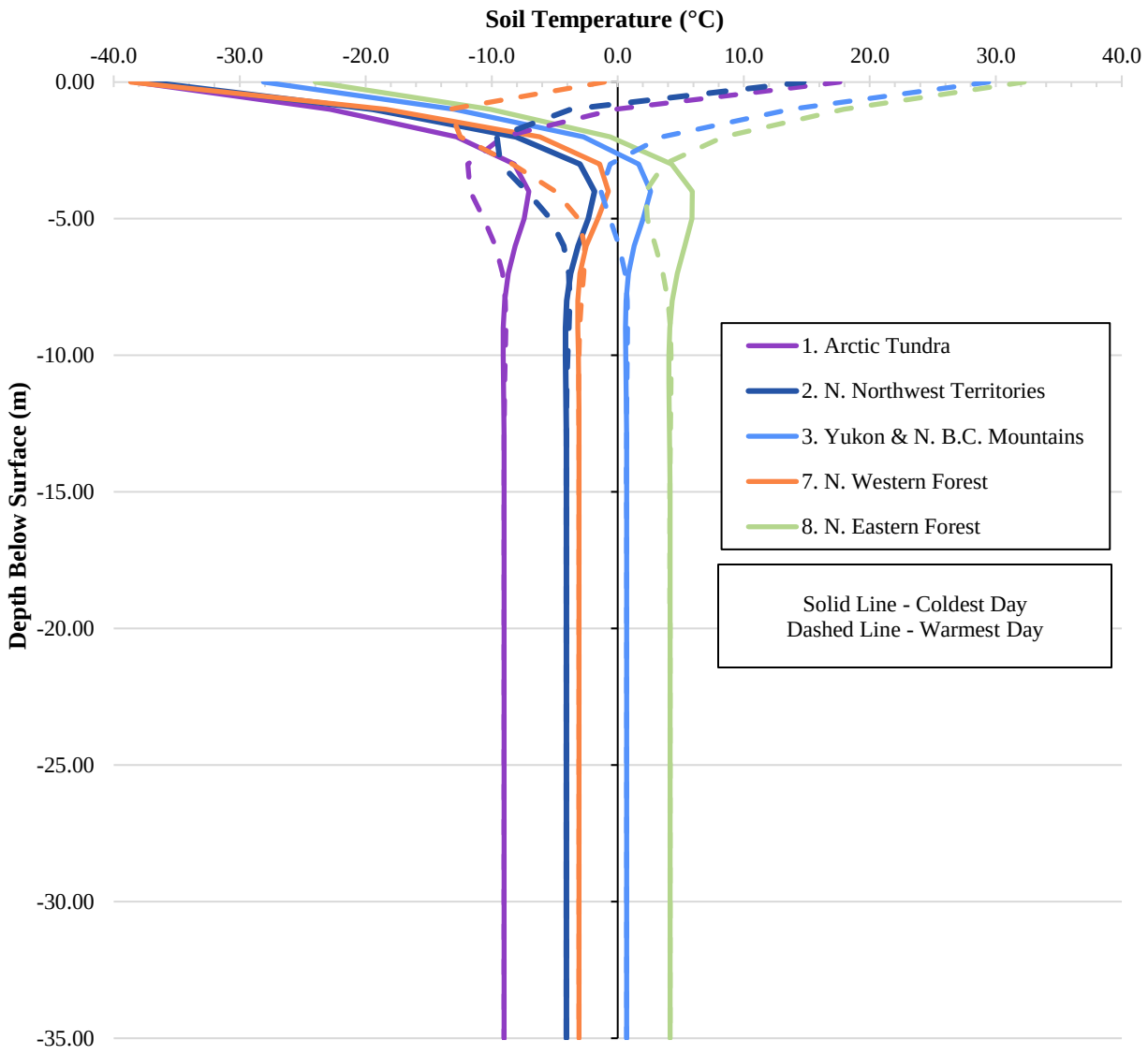

Figure 3.3. Maximum and minimum soil temperature by depth for five zones based on current climate.

This trend of soil temperature by depth follows a typical pattern with both the warmest and coldest temperatures coalescing on an annual mean ground temperature which begins at around 10 m depth. Below this point, the ambient air temperature changes associated with normal seasonal variations do not affect the soil temperature. However, in the case of climate change, even this mean ground temperature is expected to be affected.

To simulate climate change effects, the mean ambient air temperature was increased over 40 years (from 2020-2040) by 2°C as is measured to have already occurred from warming in Canada's polar

deserts [11], and is predicted by climate change models [18]. A recalculation of the soil temperature with this increase led to a shifting of the mean temperature lines for all regions. Figure 3.4 shows the effects on Zones 3 and 7, which have mean ground temperatures closest to 0°C and are therefore the most at risk of permafrost thawing.

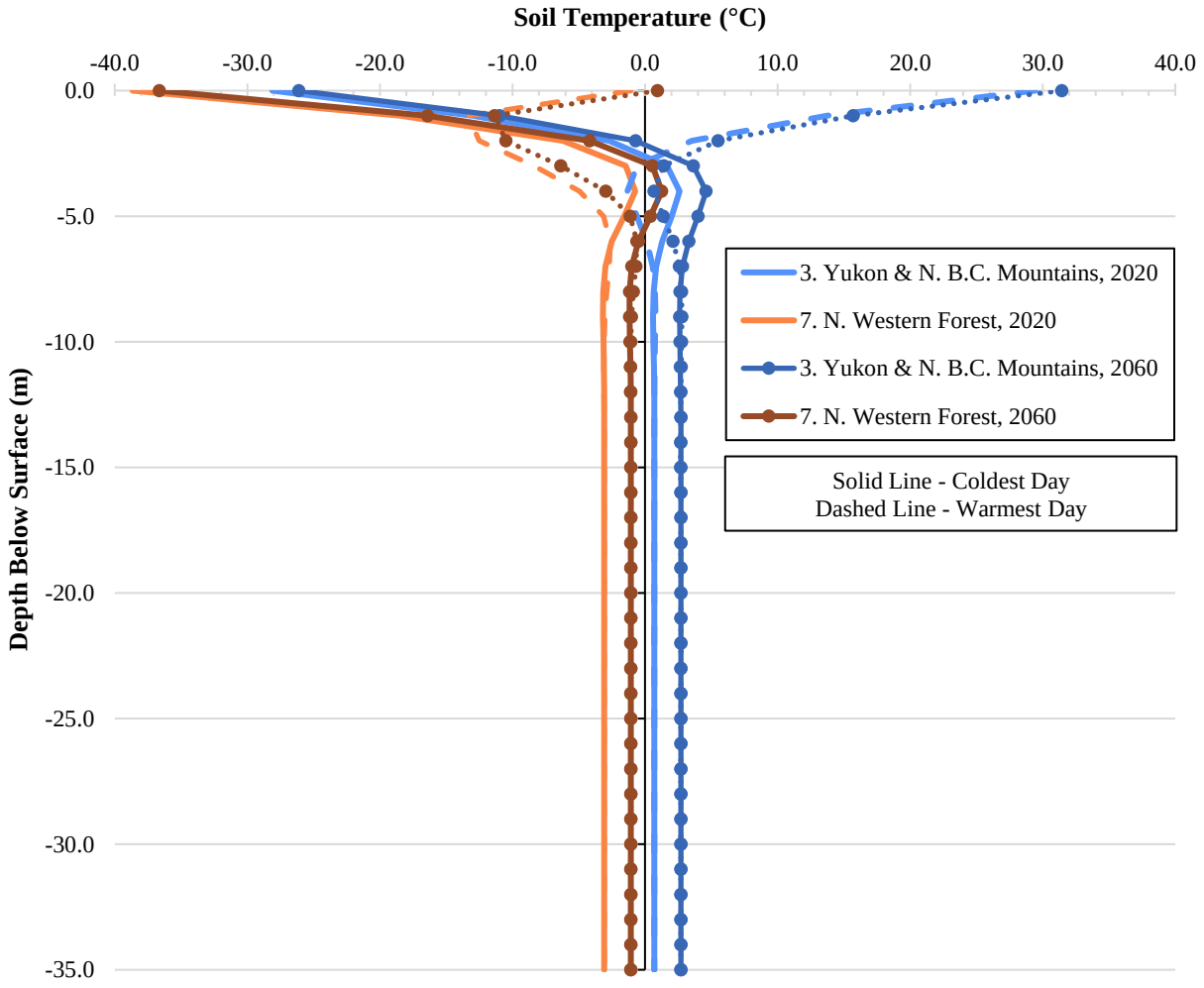

Figure 3.4. Comparison of ground temperatures in 2020 and 2060 in permafrost regions at risk of thawing with a projected 2°C mean ambient temperature rise across 40 years.

The comparison between present day ground temperature and future ground temperatures with climate change increases shows that these zones are clearly at risk for permafrost melting. As well, the analytical method used here for the purpose of GHE simulation has confirmed the predicted ground temperature response by researchers in the field of climate change modelling. The trend shown in Figure 3.4, is comparable to Figure 1.6(a) which shows the shifting of the mean ground temperature to warmer values over time [18]. Overall, it can be seen that the increase in ambient

air temperature will affect the mean ground temperature over time, and that this effect may lead to melting of large areas of permafrost soil.

This soil temperature model is a simplified version of the actual feedback loops which relate ambient air temperature to ground temperature, and many models have shown that there are tipping points of climate change, which will have such significant impacts on environmental factors that the temperature changes could be exponentially increased. This model assumes a constant, and gradual increase of 0.05°C per year for 40 years, but future work should consider that as large areas of permafrost regions begin to melt, the ground temperature effects will not necessarily be linear: there will be latent heat transfer from the conversion of ice into liquid, and there will be a combination of conductive and convective heat transfer between areas of melted and frozen permafrost zones which may play an even greater role in their thawing than the ambient air temperature increases. Research by Subin and colleagues on the impact of increased ground moisture on mean ground temperature in permafrost regions found that as the void volumes in soil were filled by an increasing amount of water, the permafrost warmed by up to 3°C [102]. As solid ice changes phase to liquid this latent heat of fusion was experimentally found to increase the warming of permafrost soils [102]. Furthermore, the flow of this melted water through solid ice (from the upper surfaces most impacted by air temperatures down to the lower soil layers) can dissipate convective heat transfer throughout permafrost regions which would otherwise rely on conductive heat transfer – increasing the speed at which melting occurs. Furthermore, future work should also consider the potential heat flux from a building to the surface – which may increase or insulate the soil from the conventional seasonal temperature formulations.

Nevertheless, the temperature distribution model in this section is useful in simulations of GHEs – as even at the shallow depth of 20 m, the mean ground temperature and seasonal changes will affect temperature conditions around the pile. Finally, it highlights that even with the simplified soil models commonly used in this field – the predicted melting of permafrost studied by experts on climate change can also be roughly calculated by observing the mean ground temperature changes using Equation 4. The shifting of soil temperatures by depth found in this research further validates climate change predictions in the literature and necessitates some intervention to maintain the stability of permafrost soils across time.

4. Geometric Optimization of a Single Helical Steel Pile

After the accuracy of the model's input conditions were checked, the geometry was optimized to increase the thermal performance of these piles as in-ground heat exchangers. The heat exchange rate by depth $\overline{Q}$ in W/m was the key variable by which the optimization was measured:

$$\overline{Q} = [\dot{m}\, c_{p,f}(T_{in} - T_{out})]/L_{st} \tag{3}$$

The mass flow rate of water, $\dot{m}$, in kg/s reflected flow rates of 2 L/min and 1 L/min, the specific heat capacity of the water, $c_{p,f}$, in J/(kg K) was constant at 4187.7, and the length of the borehole, L_{st}, was 20 m. The inlet water temperature (T_{in}) was kept constant at 27°C, and the outlet water temperature (T_{out}) reflects the surface average of the steady state outflow temperature at the cross-sectional exit surface of the outlet pipe. In this case, the parametric sweeps are performed using a summer operation – when the cooling of the water across the pile will inform the heat exchange capability of this in-ground heat exchanger.

1.13 Temperature Distribution

For the cooling operation simulated in this study, the entering hot water fluid, at 27°C, is cooled by the colder soil domain to exit at a reduced temperature. This change in temperature is the heat exchange with the ground by which the GSHP provides space conditioning. Figure 4.1 shows the computed isotherms of the base pile (Pile 2), from (a) a side view, (b) a top view, and (c) a close-up top view with contour lines of constant temperature.

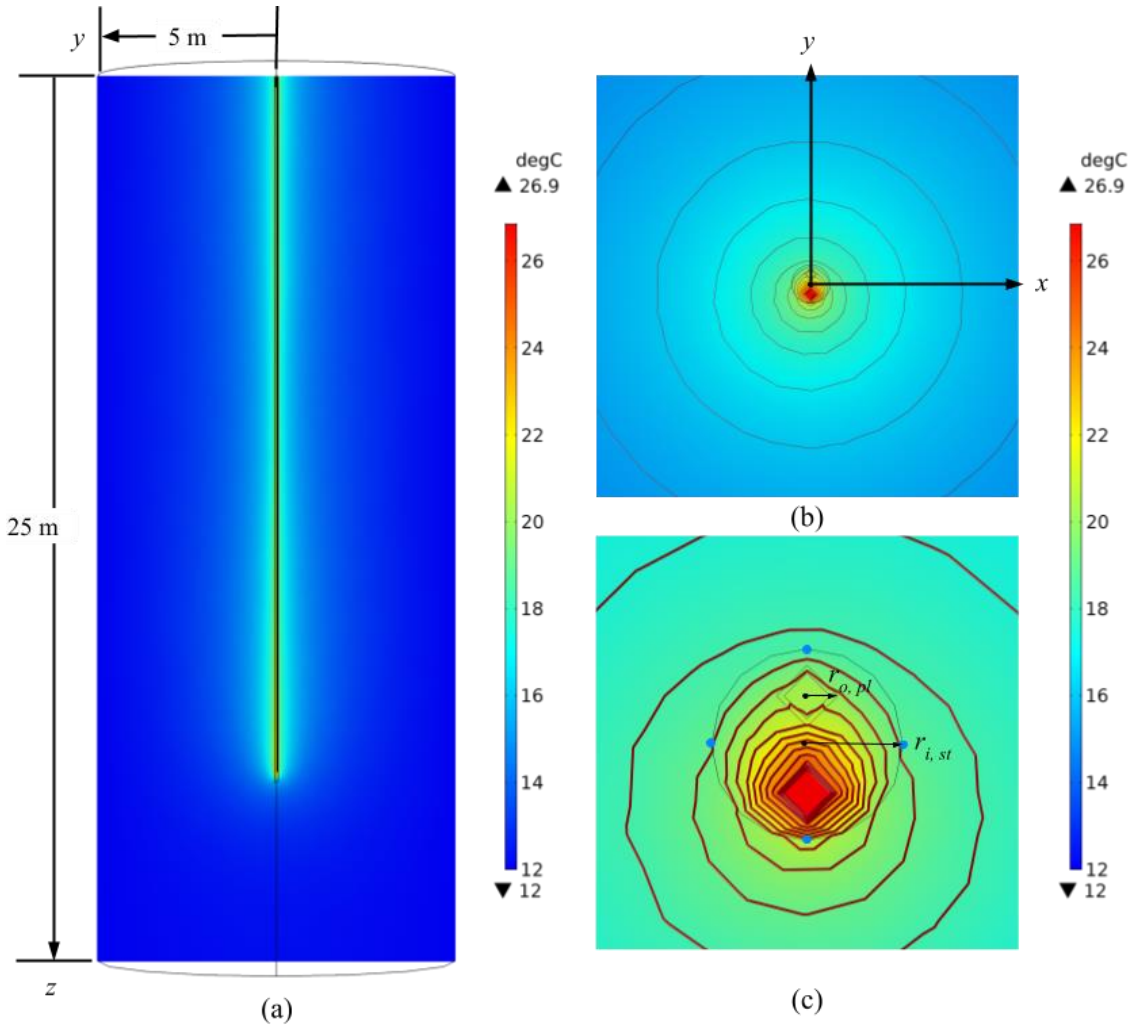

Figure 4.1. Temperature distributions within the pile and soil domains of (a) a side view, (b) top view, and (c) closer top view with contour lines of constant temperature

In Figure 4.1a, it can be seen that the temperature varies from 12°C up to about 27°C, with steep gradients in the radial direction, away from the pile, and minimal gradients in the axial direction, except for in the area immediately below the pile tip. The resulting radial gradient is typical for in-ground heat exchangers, where the temperature radially decreases from the high temperature inlet fluid point. Viewing this temperature distribution from the top (as in Figure 4.1b and c), the radial gradient is highest in value at the inlet pipe wherein the cooling load water temperature is first entering the GHE. The reduction in temperature at the outlet pipe surface reflects the heat exchange across the pile after the fluid has travelled through it. For this novel design, there is an offsetting of the peak temperature (as can be seen in Figure 4.1c) which corresponds to the offset inlet plastic pipe. Compared to a conventional coaxial GHE, with symmetric temperature distributions, this

pile has one edge with a higher heat flux magnitude by depth with an average of 9 W/m^2 greater than that of the other three intersecting axis points of the circle corresponding to the edge closest to the inlet pipe.

1.14 Flow Field

The flow field for the base pile at 2 L/min is shown in Figure 4.2, where the velocity magnitude is shown as a colour gradient with a red streamline indicating flow direction at the (a) bottom section of the pile and (b) top section.

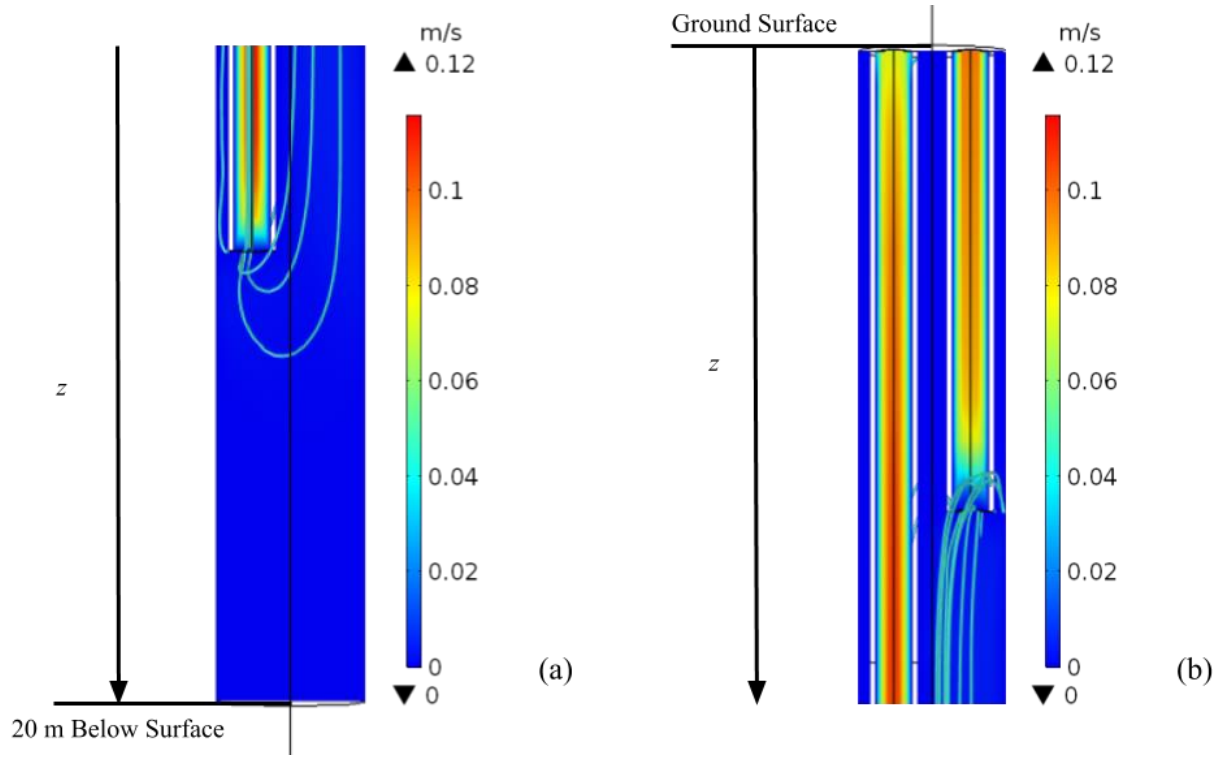

Figure 4.2. Streamlines and velocity magnitudes of flow in (a) bottom section of the pile and (b) top section of the pile.

The streamlines in Figure 4.2 indicate the direction of flow which either curves out of the inlet pipe and back up the pile (in Figure 4.2a) or funnels out of the outlet plastic pipe in Figure 4.2b. The gradient of fluid speed show that the velocity achieves a peak within the centre of the inlet pipe (due to the no-slip wall conditions with the normal inlet flow velocity). This condition represents forced fluid flow within a pipe with friction along the wall. The flow of the larger volume of water within the steel casing void is low, allowing for conductive heat transfer and near equilibrating of temperature with the surrounding domains.

1.15 Influence of Pipe Diameter on Performance

The first parameters that were investigated were the pipe diameters of the interior plastic and exterior steel pipes in the pile. The range of these sizes were chosen from nominal pipe sizing available from manufacturers for these components [89][90]. Table 4.1 shows the range of diameters for which were simulated.

Table 4.1. Diameter sizes used in first parametric sweep

Steel Casing			**Plastic Pipe**			
Nominal Size	*Inner Diameter (m)*	*Outer Diameter (m)*	*Nominal Size*	*Inner Diameter (m)*	*Outer Diameter (m)*	*Pipe Offset (mm)*
API 13.5	.09957	.1069	⅜”	0.00914	0.01270	25.4
API 23	.1186	.1292	½”	0.01232	0.01588	25.4
API 29	.1571	.1673	⅝”	0.01483	0.01905	25.4
API 53	.2205	.2325	¾”	0.01730	0.02223	25.4
API 60	.2736	.2860	1”	0.02223	0.02858	45.7
API 68	.3136	.3267	2”	0.04750	0.05080	63.5

There was some variation in pipe offset from the center due to the increase in pipe size. Furthermore, the API 13.5 casing was not simulated with 2” plastic pipes due to the limitation of size within the casing. Likewise, the 3/8” plastic pipe size was not simulated for the normal sized API 68, and API 23 for some cases due to computational limitations. To gather multiple sets of data within the laminar flow range, four situations were simulated: the range of sizes presented in Table 4.1, and a doubled version of these sizes, both at 1 L/min and 2 L/min flowrates. With these studies the variations of thermal performance by size and flow rate can be evaluated.

Figure 4.3 presents the results from these parametric sweeps for each of the four cases of study. This figure shows the steady state heat exchange rate per unit of depth achieved for each combination of plastic and steel pipe sizes at the two chosen flow rates. The data is represented as a series corresponding to nominal steel sizes (which are doubled in the corresponding simulations), with the independent variable being the nominal plastic pipe size. In this way, the performance changes of each steel casing size can be tracked as inner piping diameters are changed.

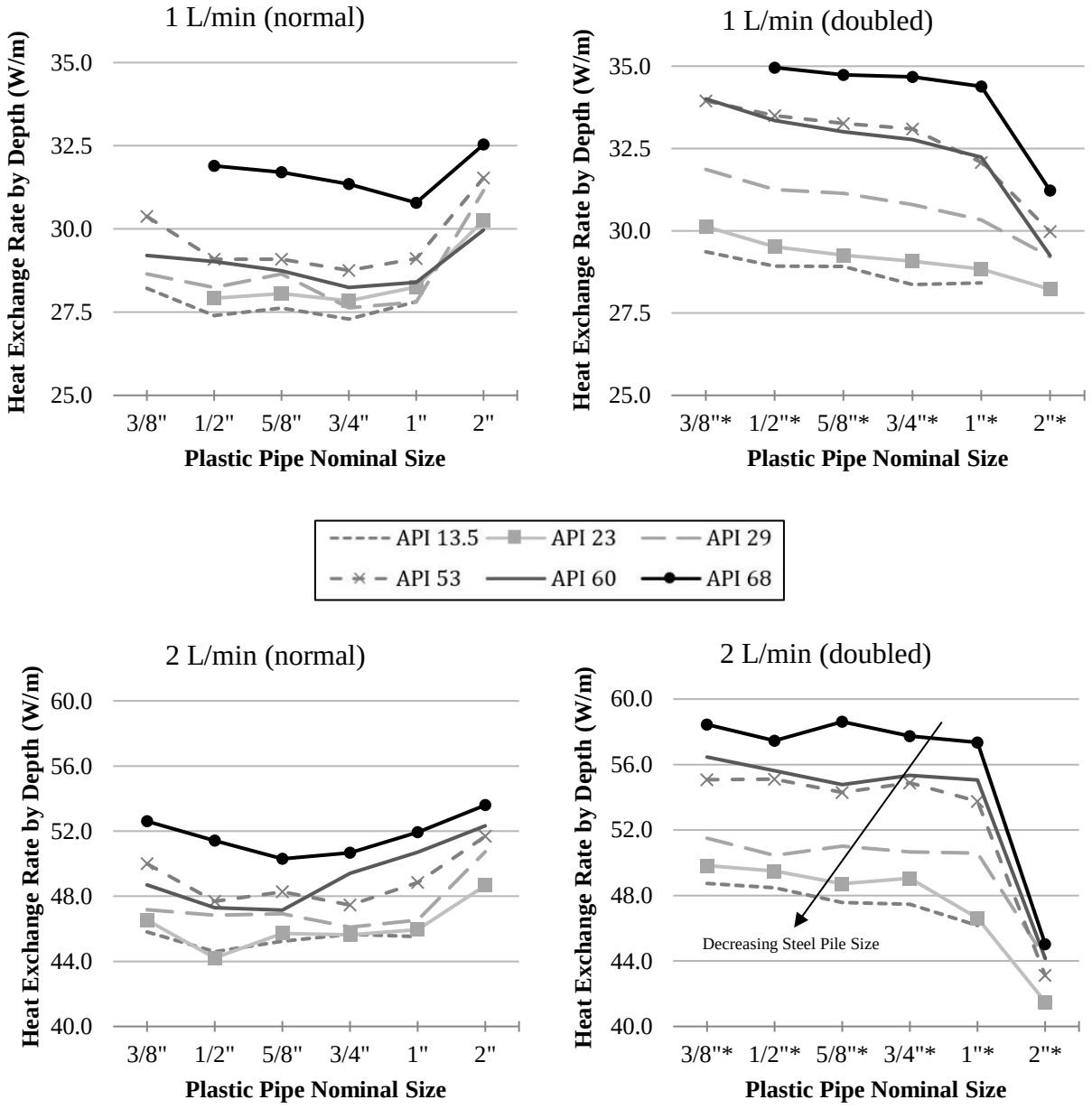

Figure 4.3. Heat exchange rate by depth at 1 L/min using nominal sizes (upper left) and a doubled version of the nominal sizes (upper right), then again at 2 L/min with the nominal sizes (lower left), and the doubled 2 L/min case

(lower right). Showing the effect of changing the inner plastic pipe sizes in combination with changing the outer steel casing size.

These results highlight the importance of flow rate in thermal performance. Across all pipe sizes, increasing the flow rate from 1 L/min to 2 L/min increased the heat exchange rate by an average amount of 383.98 W for the normal sized pipes and 398.70 W for the double sized pipes. The upward trend in the left graphs (nominal sized at 1 L/min and 2 L/min) in Figure 4.3, with the downward trend in the right graphs (double sized at 1 L/min and 2 L/min) indicate that the sizing of plastic pipe and steel pipe optimizes at a middle point, where the normal size showed a general trend of highest heat exchange rate with a 2" plastic pipe, but the 2"* pipe (a 4" nominal pipe from the double size tests) was the lowest heat exchange rate in the double size casing. This trend appears at both flow rates and indicates the role of geometric conditions on fluid flow and heat transfer in these exchangers.

Across each combination of inner plastic pipe diameter change, within the steel casing diameter changes – there exists a stepping of geometric features such as water volume. This stepping is represented using a ratio of inner steel pile diameter to inner plastic pipe diameter, as well as total water volume, and resulting heat exchange rate by depth in Figure 4.4 for the doubled 1 L/min case.

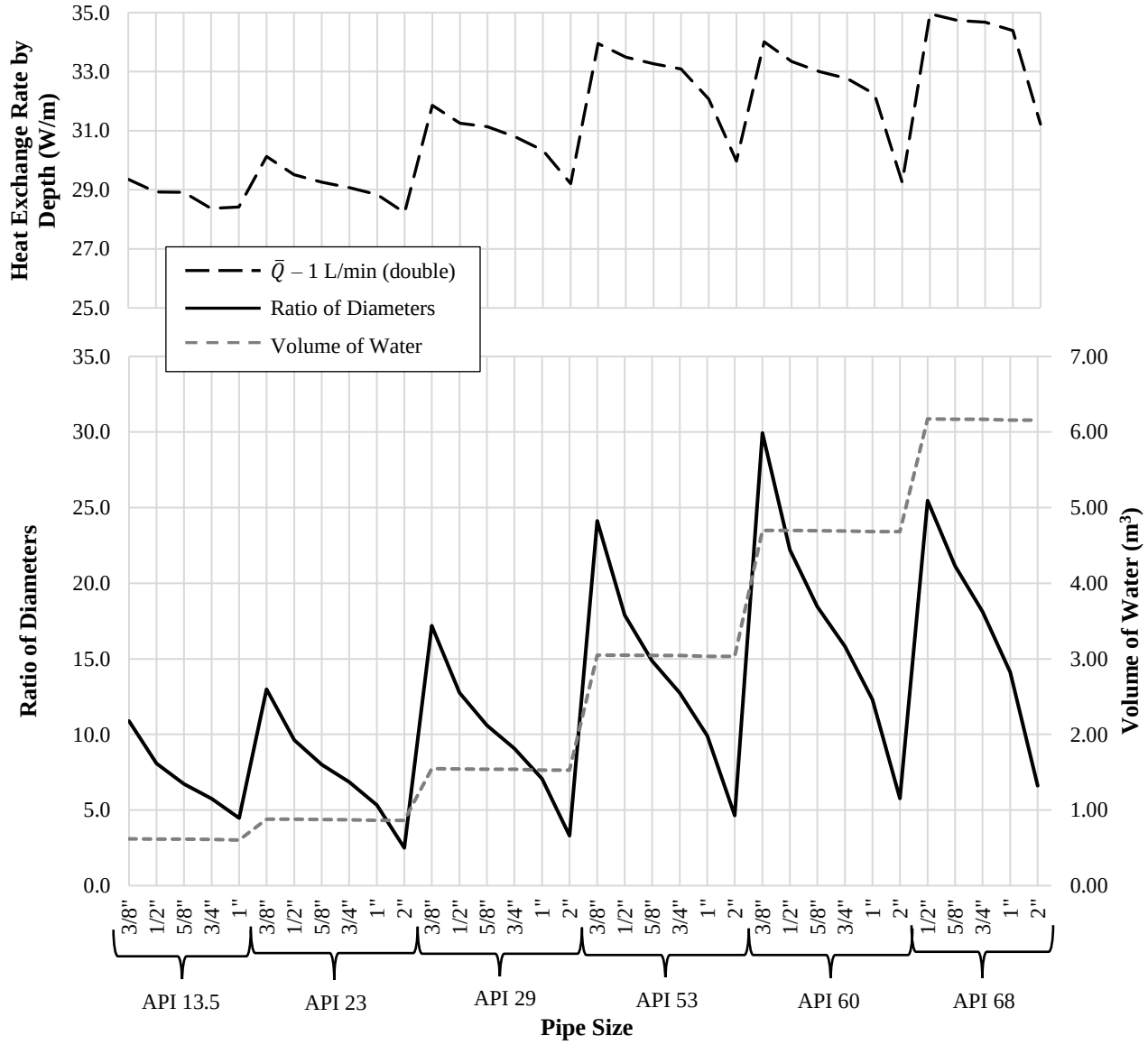

Figure 4.4. Comparison of geometric and thermodynamic parameters across simulation datasets.

The lower graph in Figure 4.4 depicts the full range of steel and plastic pipe diameter changes within the doubled 1 L/min case. The total volume of water within the pile increases significantly as the outer steel casing size is changed. In comparison, the ratio of the diameters jumps with each steel casing size increase, but decays as the inner plastic pipe diameter is increased. The heat exchange rate by depth in the upper portion of Figure 4.4 reflects a combination of the lower two trends across the dataset – wherein there is a general increase in thermal performance as the steel casing size is increased, but this decays as the inner plastic pipe size becomes larger.

The conditions represented by Figure 4.4 give an initial understanding of the relationship between flow conditions, pile size and heat exchange within these GHEs. Fundamentally, these graphs are a representation of the simultaneous effects of conduction and convection in this heat exchanger. The increase in water volume increases the mass of heat transfer fluid acting in both conductive and convective heat exchange with the surrounding domains, and the increasing ratio of diameters results in an increasing Reynold's number - with a higher convective potential.

To further understand this relationship, a geometric factor (GF) in m^3 is defined which multiplies the ratio of diameters by the total volume of water (V_w) within the pile, as seen in Equation 3:

$$\frac{d_{i,st}}{d_{i,pl}} * V_w = GF \tag{3}$$

This geometric factor was applied across the entire dataset in order to transform the stepping behavior seen in Figure 4.4 to a more generalized trend across the entire parametric sweep set. By linking the ratio of diameters to the volume of water within the pile, the competing effects of higher heat transfer by greater Reynold's number, and higher heat transfer by greater water volume (and residence time) are combined into one term (GF).

Figure 4.5 shows the effect of this geometric parameter on heat exchange rate by depth across the entire dataset. Trendlines are drawn for datapoints of the two different flow rate conditions to show a rough pattern between these variables.

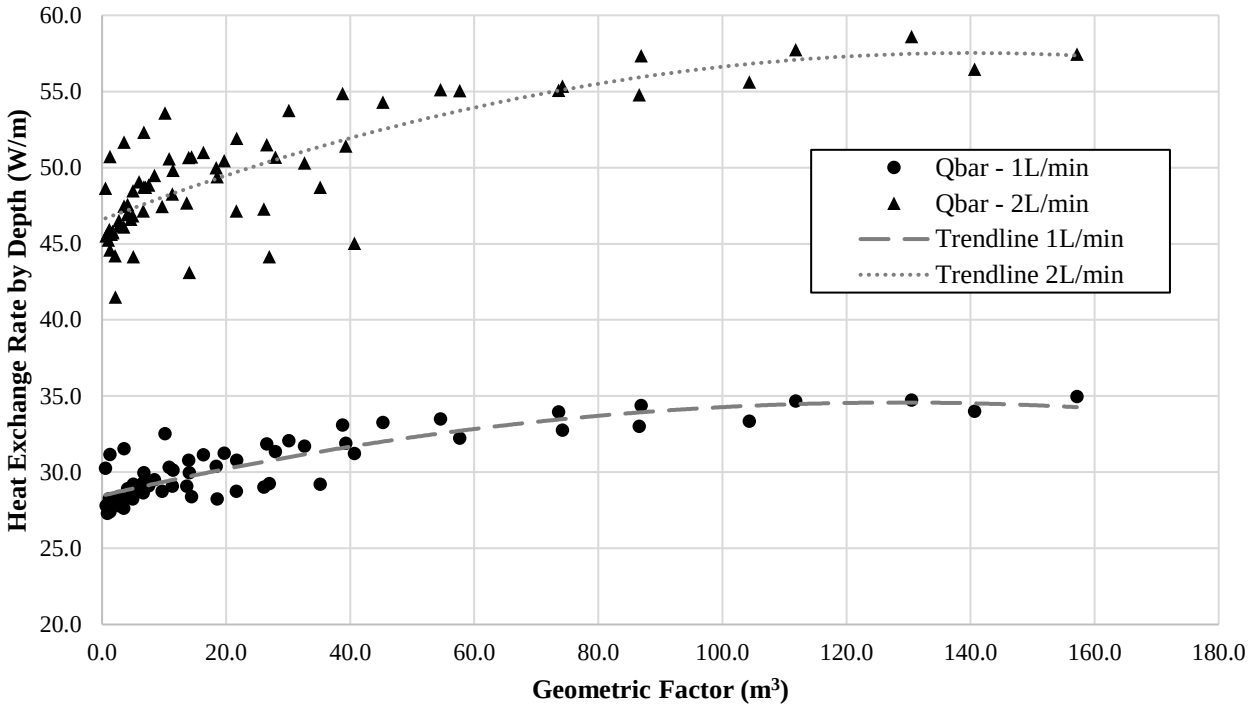

Figure 4.5. Heat exchange rate by depth versus geometric term for all data

Generally, increasing the GF increases the heat exchange rate by depth to a maximum, seen here at approximately 130 m^3, after which the performance improvement begins to reduce. This result supports the trends observed in Figure 4.3 where the thermal performance of the piles improved across increasing steel pile size to a peak, and then decayed after a maximum across both flow rates. The balance of convective and conductive heat transfer ability within GHEs is an important feature in the optimization of their design, and the competing effects of increasing or decreasing size results in this parabolic trend.

The ground temperature distribution changes from these parametric studies are shown in Figure 4.6 for the normal and double sized API 13.5 steel pipe, at the minimum and maximum heat exchange rate (plastic pipe sizes of 1" and ⅜" respectively). This temperature is collected from the y-axis running horizontally through the model at a depth of 15 m.

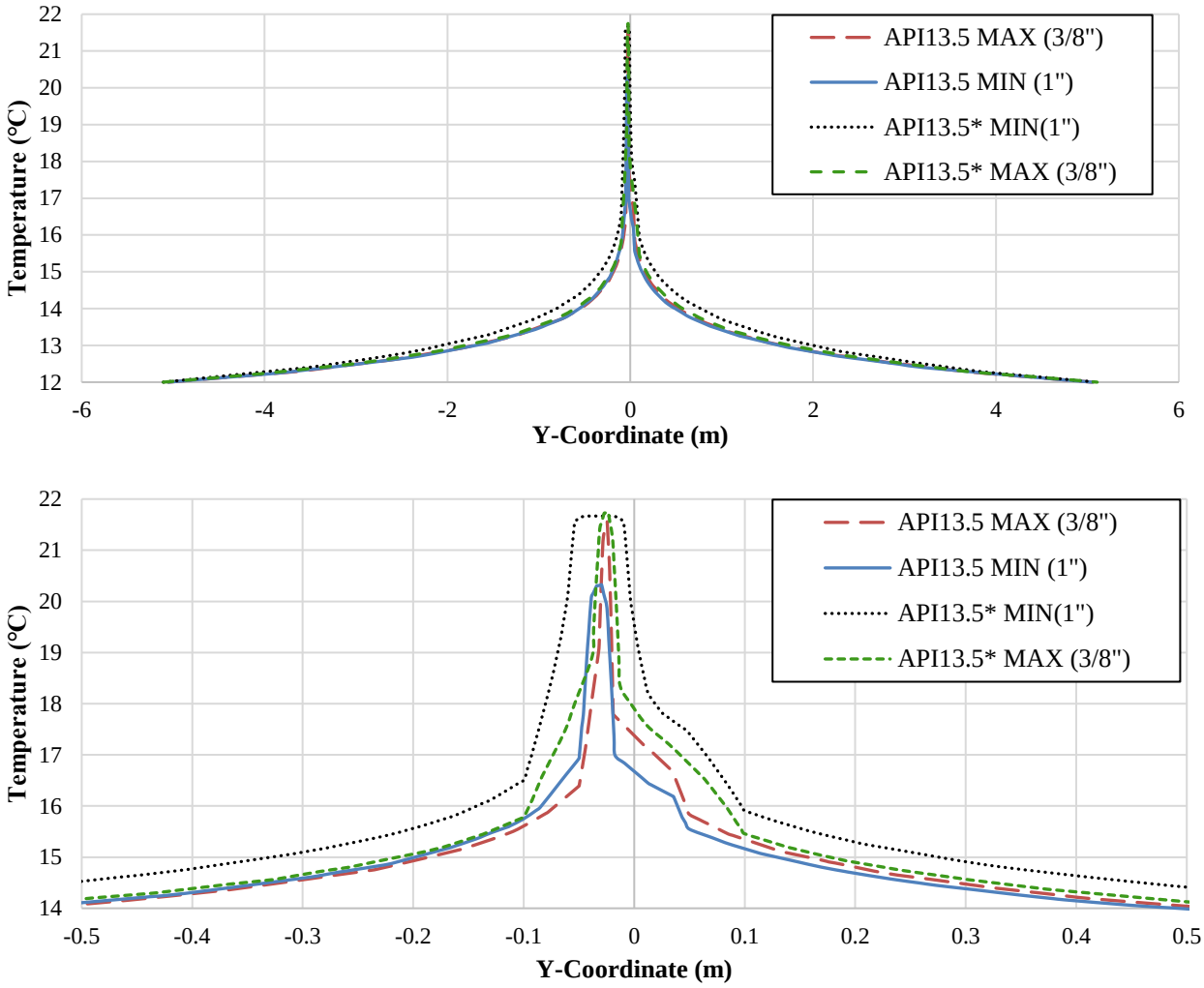

Figure 4.6. Effects on ground temperature distribution by diameter changes 15m down

The center temperature peak represents the fluid temperature, and the offset of this peak is a result of the unique inner geometry (as opposed to conventional coaxial pipe layouts which have a centered and symmetric ground temperature distribution). The double sized piles have a broader temperature distribution due to their larger radius of thermal mass within the soil. However, all sizes reach the same approximate far field temperature, with the same general trend that is consistent with studies of geo-exchange boreholes [77]. This result indicates that the conventional spacing of the piles will be unaffected by optimizing the steel and plastic pipes to improve heat transfer – however, the offset of temperature distribution in the ground close to this novel pile also indicates that novel array orientations may be implemented. At distances less than 2 m from the centre of the GHE, the spacing between piles at their lower heat transfer sides may be reduced – while orienting the higher heat transfer edge strategically away from the surrounding piles. This

result may play a role in thermal foundations which rely on the helical steel piles for the dual function of heat exchange and structural support. If the structural design necessitates a clustered pile array around a central location, the thermal interference between piles may be slightly reduced by careful orientation, as shown in Figure 4.7.

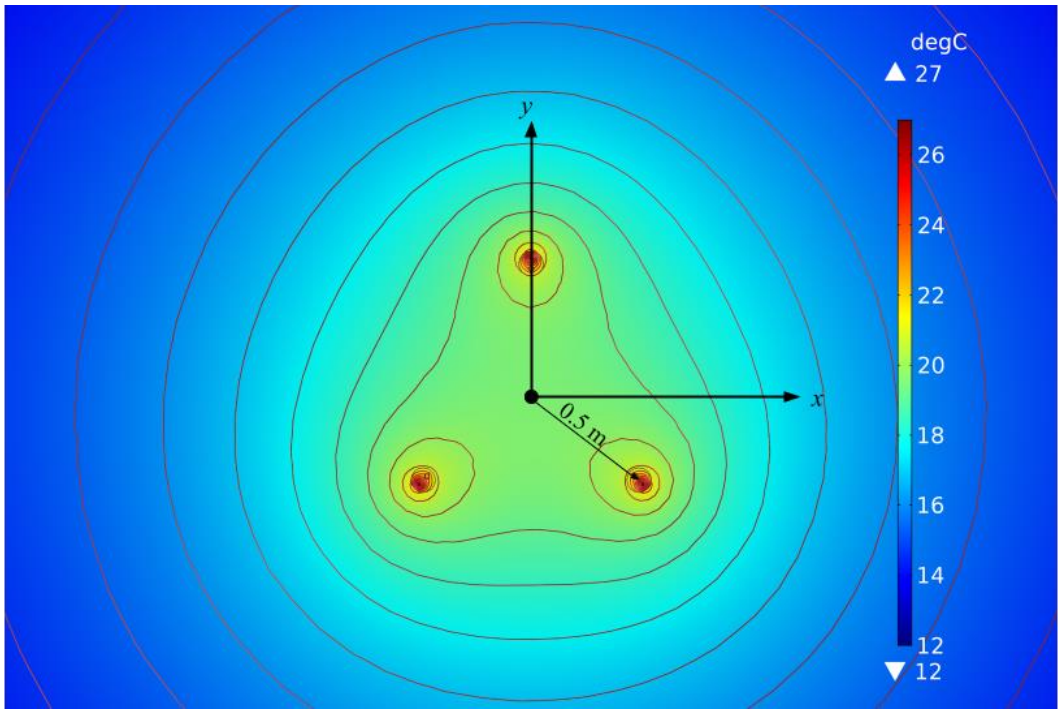

Figure 4.7. Temperature distribution of three piles with radial orientation.

Three piles of the base geometry (Pile 2) were simulated within the soil domain at radial distance of 0.5 m from each other. These piles were orientated such that the inlet pipes (and edges with highest heat flux) were facing directly away from each other. The temperature gradient shows that there is thermal interference between piles, but this clustering may have reduced this effect – as the contour lines of constant temperature are concentrated on the outer edges of this pile array. This proposed layout may increase the number of GHEs within a small footprint and will be a focus for further research and optimization with these piles.

Table 4.2 shows the potential improvements to thermal performance by optimizing for either the steel or plastic pipe from the 1 L/min normal size parametric study results. The maximum difference is calculated as the maximum minus the minimum heat exchange rate for a range of

sizes within the given category (all plastic pipe sizes within the API 13.5 steel casing for example). This table also indicates the combination of plastic and steel pipe sizes which achieved the optimal heat exchange rate for this operating condition.

Table 4.2. Maximum differences in heat exchange rate by depth by plastic or steel pipe changes

Effect of Optimizing Plastic Pipe Diameter			**Effect of Optimizing Steel Casing Diameter**		
Nominal Steel Size	*Max. Difference (W)*	*Optimal Plastic Size*	*Nominal Plastic Size*	*Max. Difference (W)*	*Optimal Steel Size*
API 13.5	18	⅜”	⅜”	43	API 53
API 23	48	2”	½”	**90**	API 68
API 29	**71**	2”	⅝”	82	API 68
API 53	56	2”	¾”	81	API 68
API 60	35	2”	1”	60	API 68
API 68	35	2”	2”	51	API 68

The goal of presenting these results is to guide designers in optimization when one of the diameters is fixed. If, for example, the steel casing size has been determined for structural requirements, the design may still be optimized by choosing an appropriate inner plastic pipe size for that pile. These results indicate that the performance of a 20 m long helical steel pile may be increased by up to 90 W when choosing the appropriate combination of steel and plastic pipe.

When comparing the thermal performance of the optimized API 68, 2” pile to the base pile design (Pile 2) described in Section 4.2.1, using a 2L/min flowrate in cooling operation, the improvements were equivalent to the reduction of 1 pile in the array. With a GSHP cooling coefficient of performance (COP_c) of 5.1 based on the inlet water temperature, 12 optimized geometric piles are required to meet a 3 ton cooling capacity, compared to 13 required for the same load with the base design (wherein each individual pile supplies approximately 0.25 and 0.24 tons of cooling respectively).

These results indicate that there can be a material savings by optimizing the diameters of the pile components - and a potential to reduce the number of piles required to meet a load. As well, these results provide a foundation for the use of laminar flow - a benefit in shallow piles which rely more heavily on thermal equilibration with the soil for their heat exchange than conventional piles - which require turbulent flows to achieve the flow for movement across the deep boreholes.

1.16 Influence of Pipe Lengths on Heat Exchange Rate

Next, the length of the inner plastic pipes was optimized. Figure 4.8 shows the results of the base case (Pile 2) geometry with increasing inner pipe length from 0.5 m to 19.5 m; all other parameters remained constant. This parametric sweep was simulated using a constant soil conductivity model, as well as a variable soil conductivity model which represented the multi-layered soil.

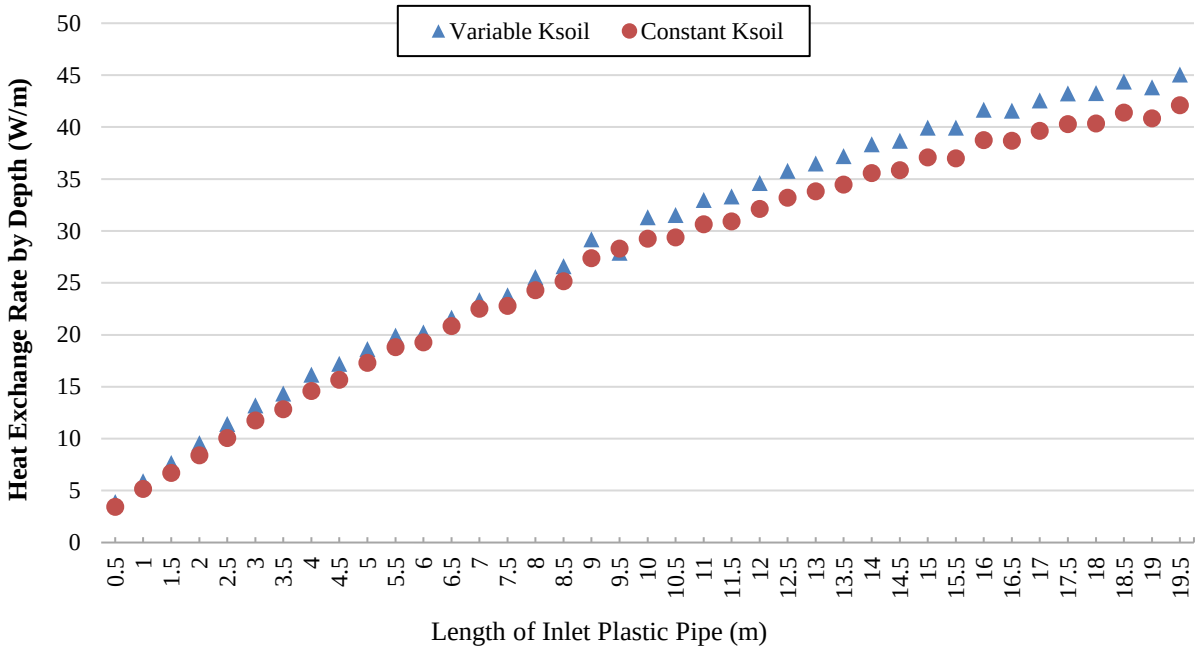

Figure 4.8. Effect of changing inlet pipe length on heat exchange rate by depth.

As reflected in the upward trend of data points in Figure 4.8, the inlet pipe length has a near linear relation with heat exchange rate by depth – where the increase in length leads to a proportional decrease in outlet temperature (and thereby an increase in heat exchange rate by depth for the cooling operation studied in this section) with a slope of approximately -0.4 °C/m for the cooling operation simulated in this study. Therefore, the longer the inlet pipe, the higher the heat exchange rate by depth for the pile. This is an intuitive result, as the inlet pipe dictates how deep into the heat exchanging medium the fluid will travel - increasing the heat exchange capability. The effect of soil thermal conductivity variability by depth was minimal on these results, so too was the effect of considering a variable or constant value for conductivity in the soil.

Similarly, the length of the outlet pipe was simulated for a range of 0.5 m to 19.5 m with a step of 0.5 m. The other geometric features of the pile were consistent with the base case (Pile 2 in Table

2.1). Figure 4.9 shows the resulting overall heat exchange rate by depth of these parametric studies, where the simulations were performed using the variable conductivity of the soil by depth determined from the borehole test, as well as using the average constant ground thermal conductivity (shown as lines with the independent variable depth below the ground surface).

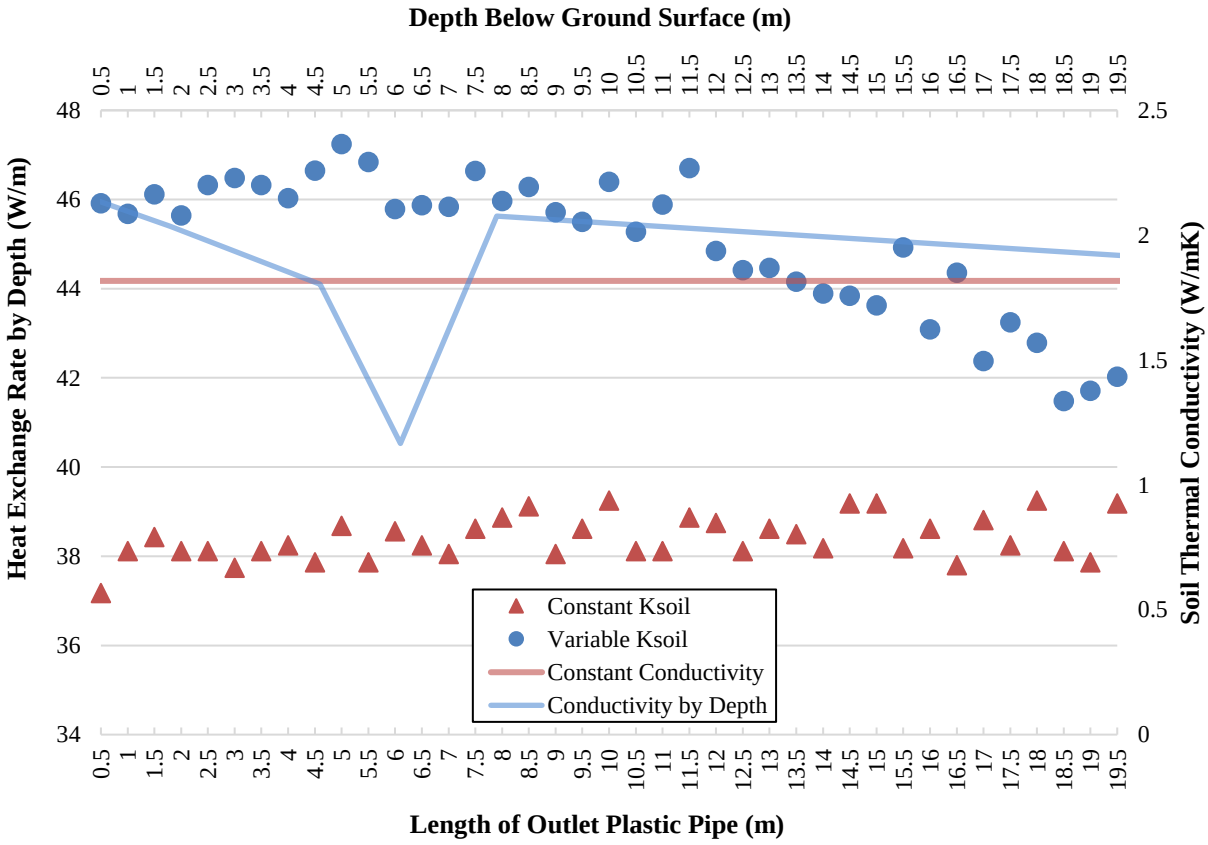

Figure 4.9. Effect of changing outlet plastic pipe length on the heat exchange rate by depth using a constant soil thermal conductivity and one which varies by depth. These thermal conductivity values are shown by line graphs.

While the parametric sweep of the outlet pipe length using a constant soil thermal conductivity (1.817 W/m K) yielded a near constant heat exchange rate by depth of an average 38.4 W/m, the sweep performed with the varying soil thermal conductivity resulted in a range from 47.2 W/m to 42.0 W/m. The thermal performance of the pile within the variable soil conductivity model began to decay after between 8 and 11.5 m below the surface – which correspond to the start of a high conductivity soil layer in the multilayered soil model. These results highlight the significant potential impact that a variable soil conductivity model can have on some thermal performance enhancement conclusions of an in-ground heat exchanger. The constant soil conductivity model

indicates a nearly negligible increase in heat exchange rate potential by increasing the depth of the outlet pipe. However, the results for the variable thermal conductivity show the opposite to be true. In this case, the heat exchange rate by depth was optimized at a pipe depth which corresponded to a soil level of high thermal conductivity (at approximately 8 m depth). This result indicates that there may be an advantage to allowing the fluid to fill the inner steel casing cavity until the optimal soil level is reached before funneling it out of the pile in the outlet pipe. These results were not seen in the inlet pipe length parametric sweep, where a comparison of variable and constant soil thermal conductivity had little effect on the heat exchange trend. Therefore, the soil thermal conductivity has a greater effect on the lower velocity fluid (outlet water), wherein conduction with the soil is a driving feature of heat exchange.

These results imply a potential to save on the material of the outlet plastic pipe - wherein increasing the length of this pipe did not show significant thermal performance improvements and may have a detrimental effect depending on soil layer types and locations. There is also a potential here for site-specific depth optimization using the data collected during the soil testing typically performed by industry before installation. This multi-layered soil approach shows that the conductivity of the soil layers influences the optimization of the outlet plastic pipe length – and this length should be designed to allow for the greatest volume and residence time of the heat transfer fluid to coincide with the soil layers of highest thermal conductivity.

5. Performance of the Helical Steel Pile in a GSHP System

This chapter begins the process of measuring the performance of the piles within a GSHP system. First observing a single pile under peak heating and cooling conditions, a parametric sweep of inlet water temperature in Section 1.17 investigates the potential capacity of a single 20 m pile, along with the predicted coefficient of performance (COP). This capacity is then used in Section 1.18 with normalizing three sets of building loads of varying characteristics to analyze the transient performance of one pile within an array. These results indicate expected operating temperatures of the working fluid, and radial distances of ground temperature impacts in order to inform pile spacing.

1.17 Sizing the Peak Heating and Cooling Capacity

Using the soil conductivity calculated from the borehole log [98] in Section 3.1.1, and the ground temperature distribution from Soil Zone 9 calculated in Section 1.12, two steady state conditions were modelled. The first case investigated a peak summer cooling condition, with a maximum ambient air temperature of 32.8℃, and the second case used a minimum ambient air temperature of -19.4℃ to simulate a peak winter heating condition (the ground temperature distributions reflected the seasonal temperatures on these peak days). A constant flow rate of 2 L/min was conditioned at the fluid inlet surface, within the Base Case (Pile 2 in Table 2.1) geometry, to perform a parametric sweep of inlet water temperature. The winter inlet water temperature was simulated from 0-15℃ in winter, and from 10-30℃ in summer, both with an increment of 1℃.

These inlet (to the pile) water temperatures were used to calculate COPs for each season with Equation 7 from Section 1.10.1. The resulting outlet water temperatures from the parametric sweeps informed the expected thermal energy load ($Q_{building}$) supplied by the pile using Equations 5 and 6. Both of these values are plotted in Figure 5.1 for the entire range of inlet water temperatures.

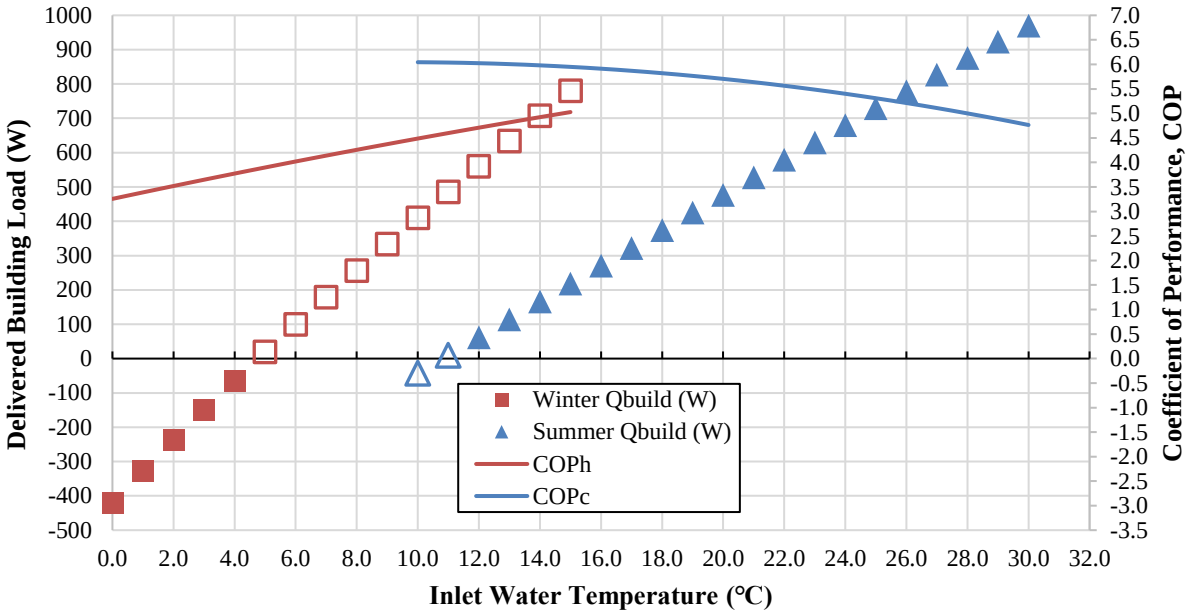

Figure 5.1. Building load ($Q_{building}$) supplied by the pile versus inlet water temperature to the pile for heating (winter) and cooling (summer) modes. This graph includes the variation in COP for heating (COPh) and cooling (COPc).

As the inlet water temperature increases, the heat exchange across the pile and therefore the ability to supply building load also increases with a positive slope in a linear manner. As the incoming working fluid increases in temperature above 11°C in the summer, the pile is able to cool this water at a linearly increasing capacity. Inversely, as the inlet water temperature decreases below 5°C in the winter, the pile is able to heat this water at a linearly increasing capacity (decreasing value of $Q_{building}$, increasing in magnitude). For the summer conditions, this slope is slightly less steep than in the winter conditions but reaches a maximum cooling capacity at the maximum inlet water temperature supplied. The lower inlet water temperatures of 10°C and 11°C were unable to provide useful cooling energy, and so these data points are shown as outlined markers without fill in Figure 5.1 to contrast the other usable inlet water temperatures (markers filled with colour). The heating load capacity in the winter season reaches its peak at the minimum inlet water temperature. The negative refers to the direction of heat exchange, with heat being extracted from the soil into the working fluid (in the opposite direction of the cooling mode which has heat leaving the pile into the soil). Therefore, the lower the inlet temperature, the greater the heating capacity of the pile. However, this inlet temperature is eventually limited by the freezing point of the fluid, and the operating temperatures of the GSHP. The optimal heating capacity must reflect the appropriate operating temperature limits of the working fluid in the GSHP system.

The ability for the pile to deliver space conditioning through heat exchange with the working fluid relies heavily on the temperature of the surrounding soil (the heat exchanging medium). The difference in temperature between the exiting fluid and the incoming fluid to the pile is plotted per inlet water temperature simulated in Figure 6.2. When this difference crosses from a positive to a negative value it indicates that the direction of heat exchange has switched – the pile is moving from a cooling to a heating mode. As the primary heat exchanging medium, the average ground temperature dictates the point of this switch.

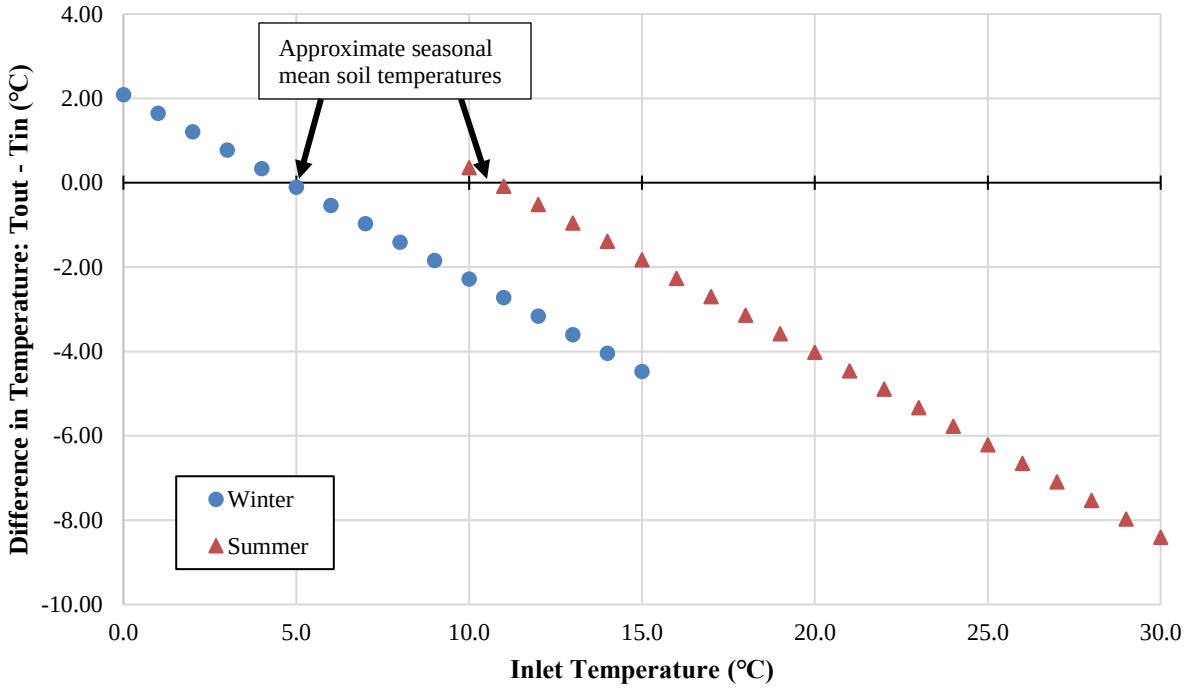

Figure 5.2. Temperature difference versus inlet water temperature for winter and summer peak steady state studies

From Figure 6.2, the winter and summer differences in fluid temperature cross the axis at approximately 5°C and 11°C respectively. These temperatures reflect the average seasonal soil temperatures for the dates of study performed. Through the calculation of ground temperature by depth presented in Section 1.12, the deep ground mean soil temperature (the constant temperature below the depth affected by seasonal variations) was calculated for this region, Zone 9, to be 7.43°C. The average soil temperature to a depth of 30 m for this zone on the peak winter and summer day was calculated to be 6.28°C and 8.81°C respectively. Differences between the calculated average soil temperatures in Section 1.12 and the resulting values shown in Figure 6.2 may be due to the effect of the steel, water, and plastic components within the pile. Since the fluid

is not in direct contact with the surrounding soil but has varying conductivities and thermal mass associated with the necessary pipes for fluid transport, some difference in the numerical simulation temperature with the soil-only analytical model should be expected.

These results confirm that the change in fluid temperature across the pile is closely tied to the local ground temperature. It is also seen that the inlet fluid temperature will dictate the direction of heat exchange to provide heating or cooling at different values in the winter and summer seasons. The inlet water temperature in the summer season should be higher than the average mean ground soil temperature to provide cooling, and the inverse is true for the winter season.

While experimental data for validation of a turbulent numerical model was not available at the time of this research, the difference in heat exchanging performance from the laminar versus turbulent flow was tested for the summer peak conditions at an inlet water temperature of 27°C. A turbulent model was created using a flowrate of 8 L/min, initial values of turbulent kinetic energy of 1.07×10^{-4} m^2/s^2, a turbulent dissipation rate of 6.53×10^{-5} m^2/s^3, an inlet turbulent length scale was 2.80×10^{-3} m, and a turbulence intensity of 0.049. A constant soil temperature by depth of 7.4°C was chosen to reduce computational time, and the steady state cooling capacity of a turbulent flow in this pile was calculated to be 0.07 tons (0.29 kW) per 20 m pile. This is a reduction in capacity by 0.59 kW or 71% when compared to the base pile at 2 L/min. While this result should be further validated with experimental data, the results showed the expected behaviour in temperature distribution and fluid flow – and the model was performed using the same boundary conditions as the laminar comparison model. This finding indicates that thermal performance of shallow GHEs may be significantly improved by using slower, laminar or transitional flows – as the high-speed turbulent flows traditionally used by much deeper GHEs is too fast for the fluid to achieve usable heat exchange within the soil domain. Next steps in research on HSP as GHEs should include a full parametric sweep of various flow rates (laminar to turbulent) in order to optimize the heat and mass transport within a range of pile geometries, and this should be informed by both computational models and experimental data.

To investigate the effect of the geometric optimization of the pile diameters performed in Section 1.15, a steady state summer peak study was performed using the same environmental conditions

above with an inlet water temperature of 27°C. This resulted in an increase in building cooling load by 68.8 W (an 8% increase) and yielded a cooling capacity of 0.25 tons instead of the 0.24 tons resulting from the base pile at this inlet water temperature. This results in a reduction of number of piles in an array needed to meet a 3-ton cooling capacity from 13 piles to 12 piles by optimizing the pile diameter. The reduction in number of piles required for the array from only geometric optimization of the pile features is a significant improvement which may benefit small projects and larger ones wherein hundreds of piles are used. Since many installations will use a range of pile sizes as dictated by installation variables, the cooling capacity of the 20 m pile is said to be approximately ¼ ton (or 1.05 kW). Variations in this capacity can be achieved by changing the pile length and diameters, and this performance is also affected by the soil and climate conditions of each individual installation site. Nevertheless the capacity of ¼ ton is used in the following Section 1.18 to normalize the peak building capacity drawn from one pile in both the heating and cooling seasons.

1.18 Annual Performance with Three Building Load Sets

Next, a full year transient study was performed using the pile in a simulated interaction with a GSHP and building loads. This simulation was performed using time step increments of 10 hours and 1 hour. There were no significant variation in the results for both time step intervals, however the computational cost difference between the two studies was an increase in time of 210 minutes (from 28 minutes computation time to 3 hours and 58 minutes), and a difference in file size from 7.4 GB to 73.5 GB. Therefore, the remaining studies were simulated using a computational 10-hour time interval (the inputs remained hourly).

The performance of the HSP within a GSHP system was tested using three building load sets from [103]. These loads were not preprocessed to remove heating or cooling in off seasons but were left as the variable hourly data from the study in an attempt to maintain variability which might occur. This load was normalized to ¼ ton capacity per pile – such that the peak of either the heating or cooling season (depending on which had the greater magnitude) would be equal to a maximum thermal load of ¼ ton. The peak hourly heating and cooling load across the year is presented in Table 5.1 along with the percentage of the year with hours devoted to the heating mode.

Table 5.1. Building load peak demands and proportion of heating time

Building No.	**Peak Heating Load**		**Peak Cooling Load**		**Annual Portion of Hours in Heating Mode (%)**
	(kW)	*(tons)*	*(kW)*	*(tons)*	
1. Oakville	-283.9	-80.7	817.2	232.4	29
2. Keele	-4945.8	-1406.3	1690	480.5	76
3. Carmen	-521.8	-148.4	497.8	141.6	55

These three building load sets reflect a range of imbalance: the first is cooling dominant (spending only 29% of the annual hours in the heating mode), the second is heating dominant (76% of the annual hours in heating), and the last is nearly evenly distributed (with 55% of the annual hours spent heating).

The range of peak demand across the buildings reflects medium to high thermal energy demands which were normalized to assume that the number of piles required to meet this load were present in the array, and that these piles were spaced far enough from each other to cause no thermal interference. It is also assumed that the flow rate is constant at 2 L/min across all piles. By normalizing the building load for one single pile, the approximate ability for this GHE design to deliver the building loads through a GSHP system (with an array of piles) can be understood, given the assumption that each pile in the array exchanges the same ¼ ton capacity, and the load is divided evenly between them. This performance is modelled through an hourly temperature input to the water inlet surface, which is pre-calculated using the equations presented in Section 1.10.1. The resulting transient outlet water temperature from this simulation reflects the ability of the pile system to deliver the capacity required by the building load dataset. The temperatures of the surrounding soil domain change through this process of extracting or inserting heat through the working fluid in the pile. At the end of the simulation, this ground temperature will give insights into the capacity of the soil to deliver the load profiles tested using these three buildings.

Figure 5.3 to Figure 5.5 plot the transient results for each building. Showing the hourly normalized building load alongside the hourly average temperatures of the soil domain volume, the inlet fluid surface and the outlet fluid surface. For all three graphs, the difference between the inlet and outlet temperatures indicates the type of heat exchange being supplied. With a higher inlet than outlet temperature (a positive heat exchange), cooling is occurring, a lower inlet than outlet temperature

indicates that heating is occurring (a negative heat exchange). The average hourly soil volume temperature is also shown in the figure, as calculated for the soil domain cylinder. The difference in magnitude between the fluid temperatures and the soil temperature roughly indicate the amount of thermal energy being drawn or released into the soil domain to deliver the building load. For a cooling demand, the fluid temperatures will be warmer than the average soil temperature, and this difference will increase to reflect the magnitude of cooling load.

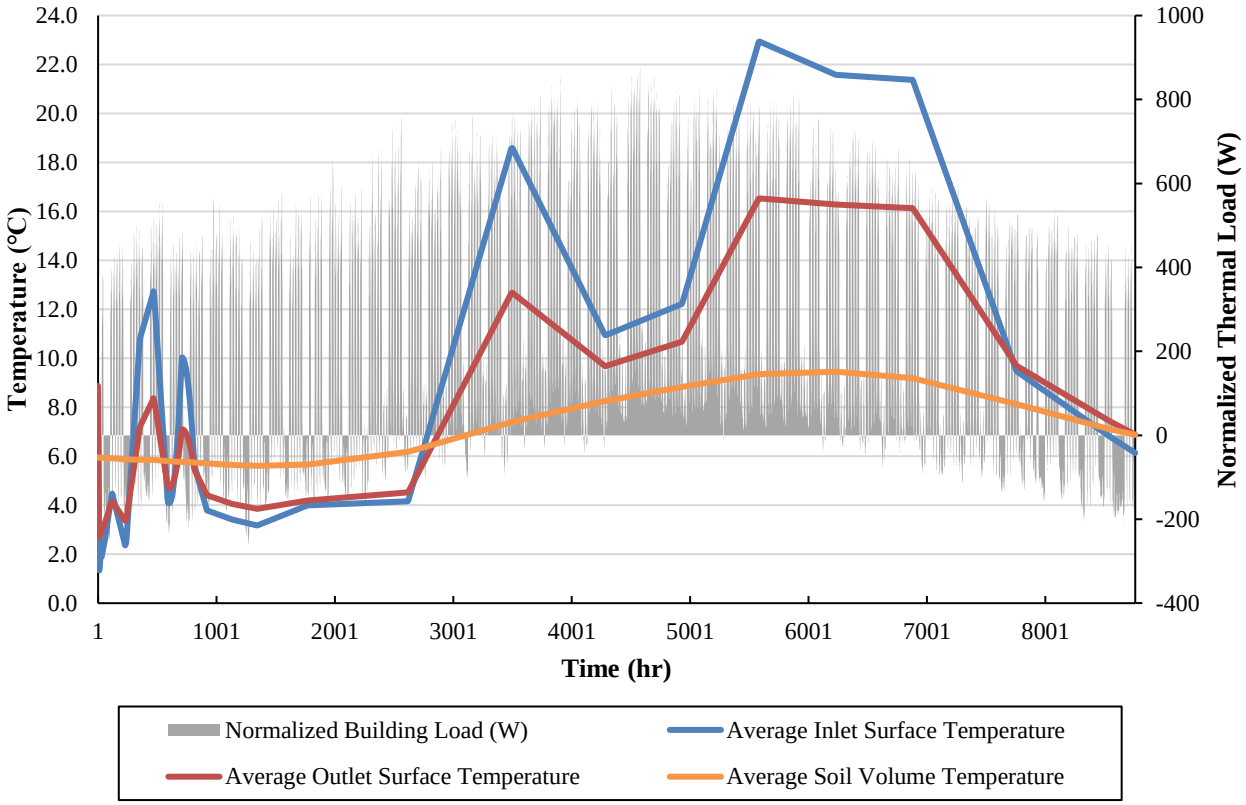

Figure 5.3. Annual hourly building load and key average temperature results for Building 1 – Oakville.

This cooling dominant building has cycles of cooling demand across the entire year – reflecting the unique use of the building. As such, the inlet fluid temperature is greater than the outlet for most of the year, with the notable exception of much of November through March (approximately hour 7700 – 2800). The jagged nature of the first 1000 hours is a result of transient simulation start-up effects with undisturbed ground conditions. The seasonal variation of average soil volume temperature is shown by the curve which peaks at a warmer temperature in the end of the summer season (near hour 6000), and a minimum in the end of the winter season (near hour 1500), with an approximate middle value of 7-8°C as discussed in Section 1.17.

Figure 5.4 shows the transient results for the second building load tested, with a heating dominant characteristic.

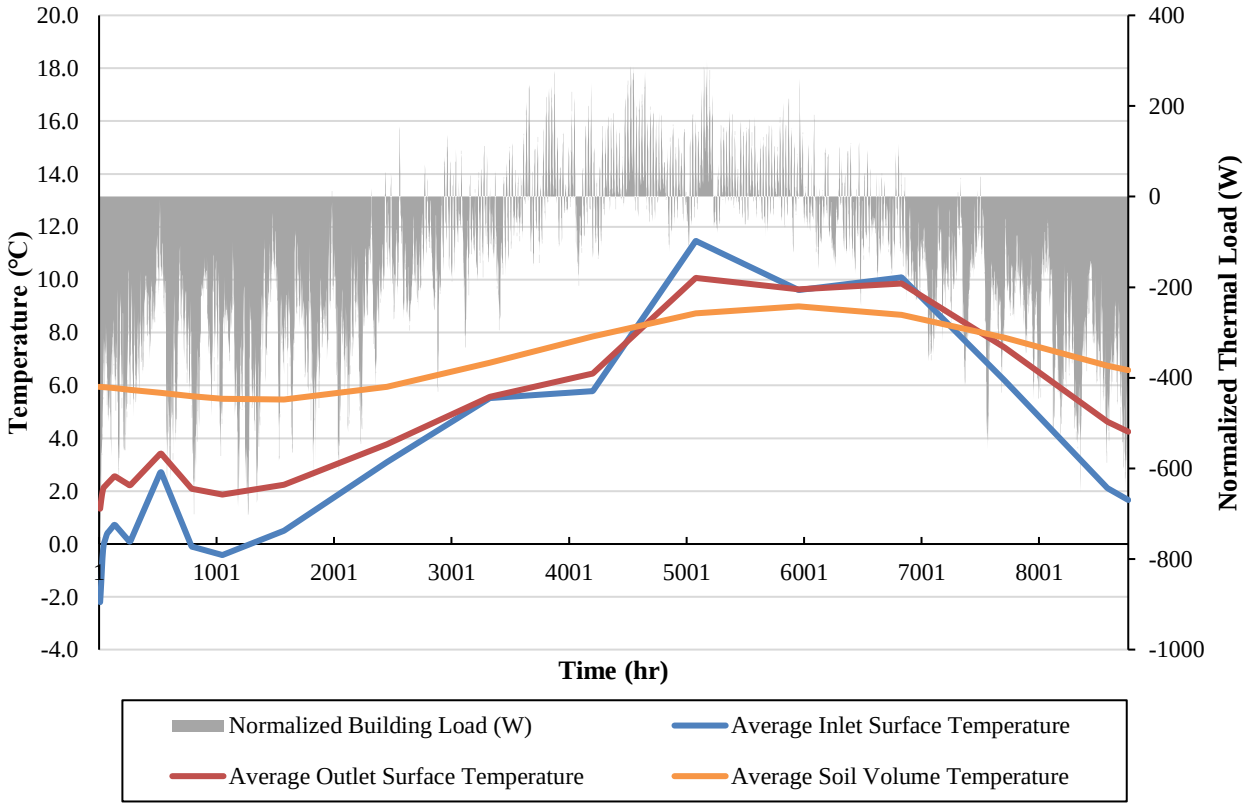

Figure 5.4. Annual hourly building load and key average temperature results for Building 2 - Keele.

Unlike in Figure 5.3, the inlet fluid temperature in Figure 5.4 tends to be lower than the exiting fluid temperature across the year. As well, this building load is divided more clearly into two seasons, and so the curves of fluid temperatures are less varied than for Building 1. The operating range of the inlet water temperature initially goes below 0°C to supply heating on this January 1 operation date. In contrast, the inlet water temperature at the last hour of the year is above 0°C, since there is more heating energy stored in the ground after the year of operation, and the water temperatures are not then needed to be so low to gather the required heat for the building load. This is also a reflection of the assumption in Section 1.17, wherein the thermal capacity of one pile was chosen to be ¼ ton based on the cooling season results, but it is actually slightly less in the heating season – as such buildings which are normalized by a peak heating value to ¼ ton may have initial temperatures below 0°C, to signify the pile and soil domain require a reduction in inlet water temperature to meet the demanded heating load.

Finally, Figure 6.5 shows the transient temperature results for the normalized building load of Building 3.

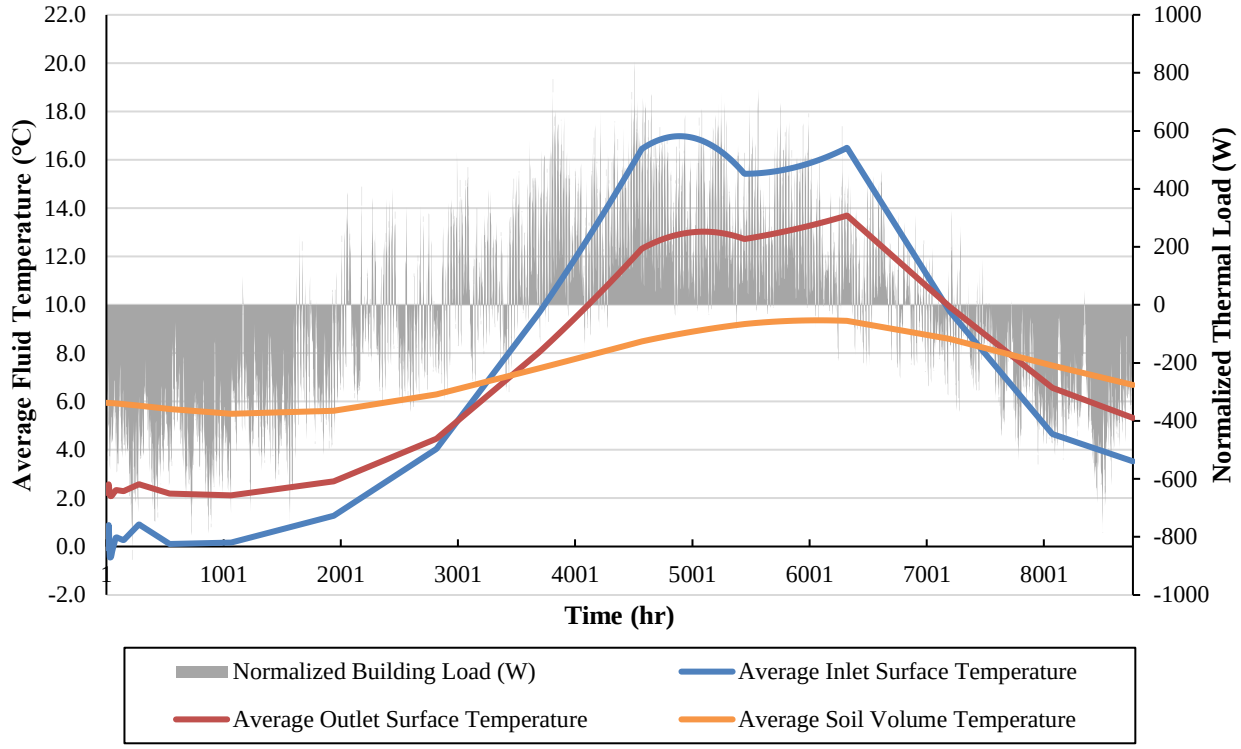

Figure 5.5. Annual hourly building load and key average temperature results for Building 3 – Carmen.

As this building has the most balanced heating and cooling demand of the three, it also shows the most consistent transient curves for inlet and outlet fluid temperature. Starting at a low inlet temperature to deliver the heating demand, the temperatures climb to a peak near the hour 5000, and then reduce for the winter season again at hour 7000 to provide heating for the rest of the year. The gap between the inlet and outlet fluid temperature curves (the area which represents the heat which was exchanged while the fluid travelled through the pile) remains relatively consistent compared to the other two building results – another consequence of the more balanced load in Building 3. The average soil temperature follows a roughly similar path as the other two buildings, showing that the seasonal variations of temperature within the soil volume chosen are similar regardless of the load characteristic. This may signify that the capacity of ¼ ton per pile was an appropriate choice to minimize ground thermal imbalance across the year.

A comparison of the minimum and maximum temperatures across these three building simulations is presented in Table 5.2, for the fluid, soil volume average and average instantaneous difference in fluid temperatures, ΔT (inlet minus outlet).

Table 5.2. Maxima of inlet fluid, change in fluid, and soil volume temperatures.

Building No.	**Inlet Fluid Temperature (°C)**		**Soil Volume Average Temperature (°C)**		**Average Change in Fluid Temperature, ΔT**	
	Minimum	*Maximum*	*Minimum*	*Maximum*	*Heating*	*Cooling*
1. Oakville	1.39	22.9	5.61	9.45	-0.44	3.45
2. Keele	-2.20	11.5	5.47	8.99	-1.14	0.47
3. Carmen	-0.44	17.0	5.49	9.36	-1.44	2.36

These results show that the cooling dominant building (Oakville) had a higher maximum fluid temperature than the other three buildings, it also had the highest soil volume average temperature and change in fluid temperature during the cooling season. In contrast, the heating dominant building (Keele) had the lowest fluid temperature, average soil volume temperatures, and cooling season fluid temperature difference. The relatively balanced load, (Carmen) was in the middle of these two buildings in terms of magnitude of temperatures across all three variables. The balancing of the load resulted in a more moderate operating temperature conditions for the soil and fluid domain. These results are useful for choosing the optimal GSHP mechanical equipment, as the change in fluid temperature, and entering/exiting fluid temperatures to the heat exchanger equipment of the GSHP are key factors in determining its efficiency. Furthermore, when examining the average soil volume temperatures across the studies, the likely long-term effects on ground temperature can be predicted. The cooling dominant building has the highest average soil volume, and would therefore increase the mean soil temperature within that area (eventually leading to a failure to produce cooling unless a balancing intervention is applied). Similarly, the heating dominant building might lead to a reduction of the mean ground temperature within this volume – reducing the ability of that heat exchanging domain to deliver the heating demanded by the building load. In the climate studied here, wherein there is a natural cycling of temperatures across the heating and cooling season, the longevity of the GHE system depends on the ability for the soil to continue to deliver the heat exchange required by the GSHP. In general, creating a balanced thermal load will protect this longevity of performance and allow the GSHP to operate within optimal efficiency.

The effect of these building loads on the mean ground temperature is analyzed at four-time intervals across the year using a horizontal radial temperature distribution taken at 10 m below the top of the pile. This depth will approximately represent the temperature changes that occur at the ground which is unaffected by the seasonal ambient temperature changes. The impact of the thermal load being applied within the pile on this mean ground temperature is shown for all three buildings in Figure 5.6, Figure 5.7, and Figure 5.8. The first and last time steps (hours 300 and 8760) occur within the winter season, and the middle two occur in the summer season (hours 4000 and 6000). The characteristics of the annual loads modify the temperature distributions at these times for the three different buildings studied in this Section. Temperature is plotted as a radial distance from the centre along the horizontal y-axis, with the centre of the pile located at 0 m. Figure 5.6 shows this horizontal temperature distribution for Building 1 – Oakville.

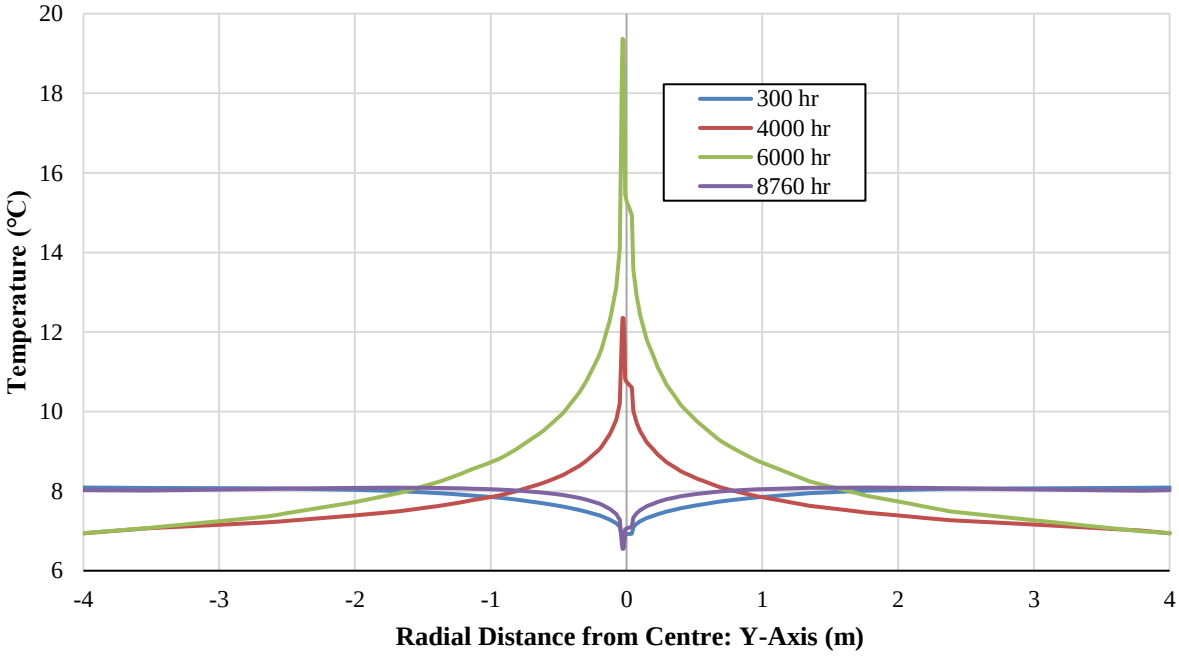

Figure 5.6. Horizontal temperature distribution at a depth of 10 m for Building 1 - Oakville at four time intervals.

The temperature of the winter season time steps is nearly constant at 8°C, with a slight decrease in temperature directly beside the pile up until around 0.5 m radially in each direction. However, the temperature difference at this point is minimal, especially in contrast to the temperature distributions at hours 4000 and 6000. In these summer time intervals, the temperature around the pile reaches a peak near 19°C before gradually decreasing to a mean ground temperature of

approximately 7°C 4 m radially from the centre of the pile. The trends in Figure 5.6 reflect the ground temperature impact a cooling dominant building load can have. Here, heat is being extracted from the working fluid and exchanged into the surrounding soil domain at a high rate across nearly the entire year – as such, the ground temperatures in the summer show a warmed radial distribution up until 2-3 m radially from the centre of the pile. In contrast, the winter season shows negligible cooling of the soil domain surrounding the pile. If applied across many years, this imbalanced thermal load could lead to an overheating of the surrounding soil – the temperature increase seen in the summer season is not balanced by a temperature decrease of similar magnitude in the winter season. If the GHE is used in the manner simulated here, this could eventually lead to GSHP failure, wherein the soil would no longer be able to supply the cooling capacity required by this uneven demand. A hybrid system should be designed for this building load, or an alternative method of thermal energy supply investigated.

Figure 5.7 shows the radial temperature distribution 10 m below the surface, of Building 2 – Keele, across four time intervals in the year.

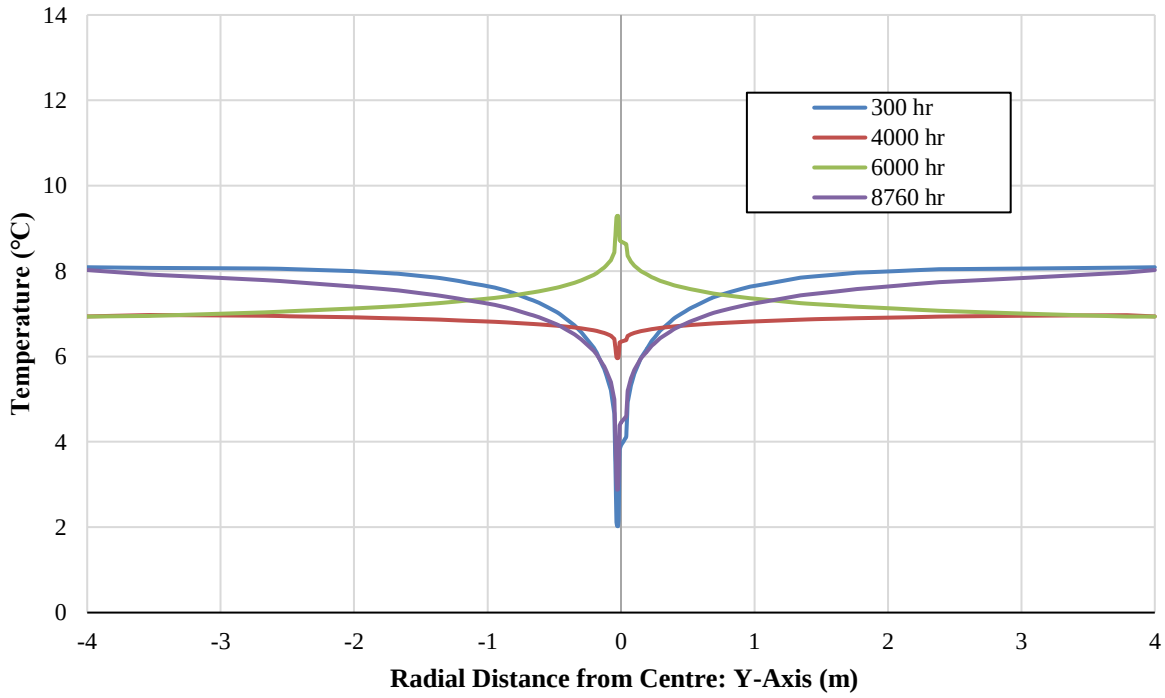

Figure 5.7. Horizontal temperature distribution at a depth of 10 m for Building 2 - Keele at four time intervals.

While Building 1's cooling dominant load resulted in a more significant range of increased temperatures around the pile, Figure 5.7 shows a more significant lowering of temperatures around

the pile. The greatest difference in radial temperatures is seen in the winter season intervals (hours 300 and 8760), which reach minima of 2-3℃ before gradually returning to a temperature of 8℃. In contrast, the summer season time interval of 6000 hours, shows a smaller temperature range of approximately 2℃, increased from around 7-9℃ at its peaks. The hour 4000 is nearly constant in its temperature. These results reflect a heating dominant building load, wherein the soil is reduced in temperature as heat is exchange into the working fluid to increase its temperature. Over years this load is also likely to result in failure due to ground thermal imbalance – wherein the soil would lose too much heat to the heating load, and eventually become too cool to warm the working fluid. Again, a hybrid system or alternative solution is suggested before supplying this load wholly by the GHE simulated in this study.

Finally, Figure 5.8 shows the horizontal temperature distributions 10 m below the surface of the pile supplying Building 3's thermal load.

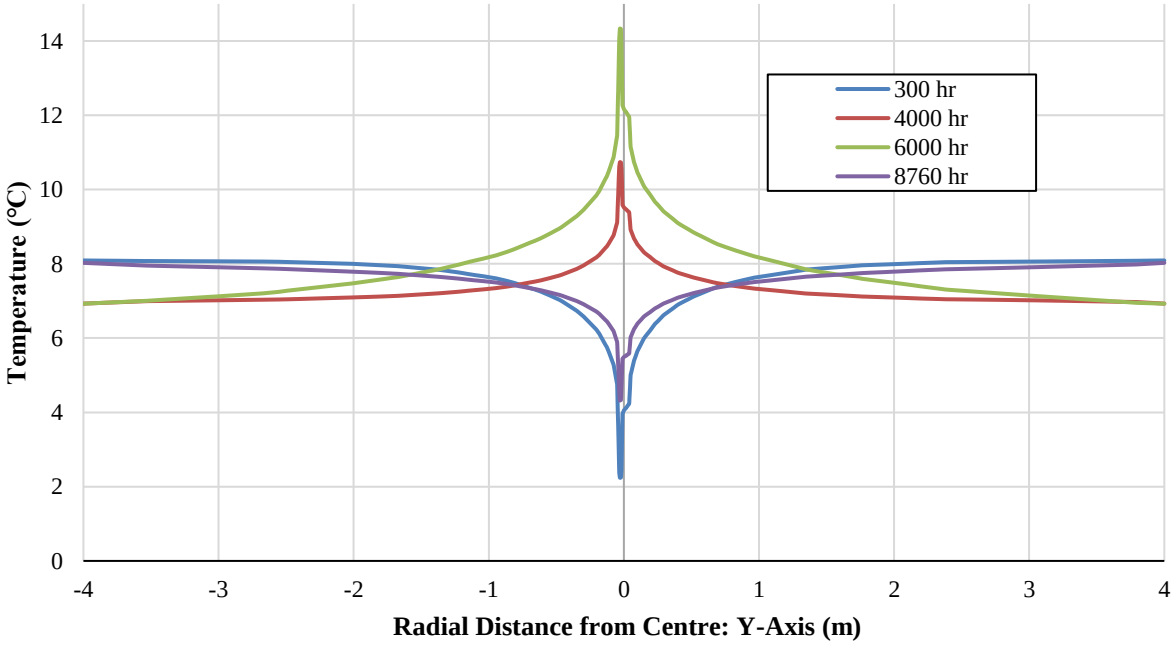

Figure 5.8. Horizontal temperature distribution at a depth of 10 m for Building 3 - Carmen at four time intervals.

The temperature ranges for all time intervals show peaks at the centre within the pile that gradually converge on mean ground temperatures with increasing radial distance. Unlike the previous two building results, here the summer and winter time intervals both show significant changes in temperatures at the origin of the graph (the centre of the HSP). The peak increase in temperature

occurs at hour 6000, with an approximate increase of 7.5°C, and the peak decrease in temperature at hour 300 goes from 8°C to 2°C. This load set shows a greater balance between heating and cooling across the year; it is more likely that this system would perform for many years without experiencing failure due to ground thermal imbalance, and thus this building is a better candidate for the GHE proposed in this research.

All three buildings show that the temperature effects of the pile decay as the radial distance from the centre of the pile increases. The most significant of these effects are found within the 2 m radial distance, with nearly negligible changes in temperature beyond that. Therefore, 2 m may be an appropriate starting point for guiding pile spacing in the design of a system's array. Future work may optimize this distance, and lead to further understanding of the impacts of the system as a whole by applying the loads and flow rates across a model which includes multiple piles. Such a multi-pile model would also have the opportunity to represent the flow rate losses that may occur as the working fluid travels between piles and through a manifold to deliver flow to each pile (in either a series or parallel pipe network). This would result in an improved understanding of the functionality of individual piles within an array.

Nevertheless, this section provided some key initial insights into the annual performance of this GHE in a GSHP system with a variety of operating temperature tested. The approximate capacity of ¼ ton for the 20 m base pile (non-geometrically optimized) was roughly appropriate and can begin to guide future installations in similar climate and soil conditions to those studied here.

6. Performance of a Helical Steel Pile in Remote Canadian Communities and in Permafrost

1.19 Steady State Heat Exchange Maxima Across 11 Canadian Zones

The capacity of the piles is highly dependent on soil and climate conditions. Therefore, this section investigates the steady state capacity of the piles across 11 zones. For the purpose of comparison, these capacities were measured on the same day and time for all cases (12:00 AM January 1 for the winter peak, and 12:00 PM August 1 for the summer peak).

Figure 6.1. Winter heat exchange rate by depth per zone compared to the inlet water temperature to the pile and mean soil temperature per zone. plots the heat exchange rate by depth in the winter conditions for each zone for three soil cases: dry soil, soil fully saturate by water, and soil with ice. The thermal conductivities for each simulation were changed to reflect these conditions using the values from Figure 3.1 and Figure 3.2 in Section 3.1.1. The inlet water temperature and mean soil temperature for each zone are included in the figure's right-side axis for comparison.

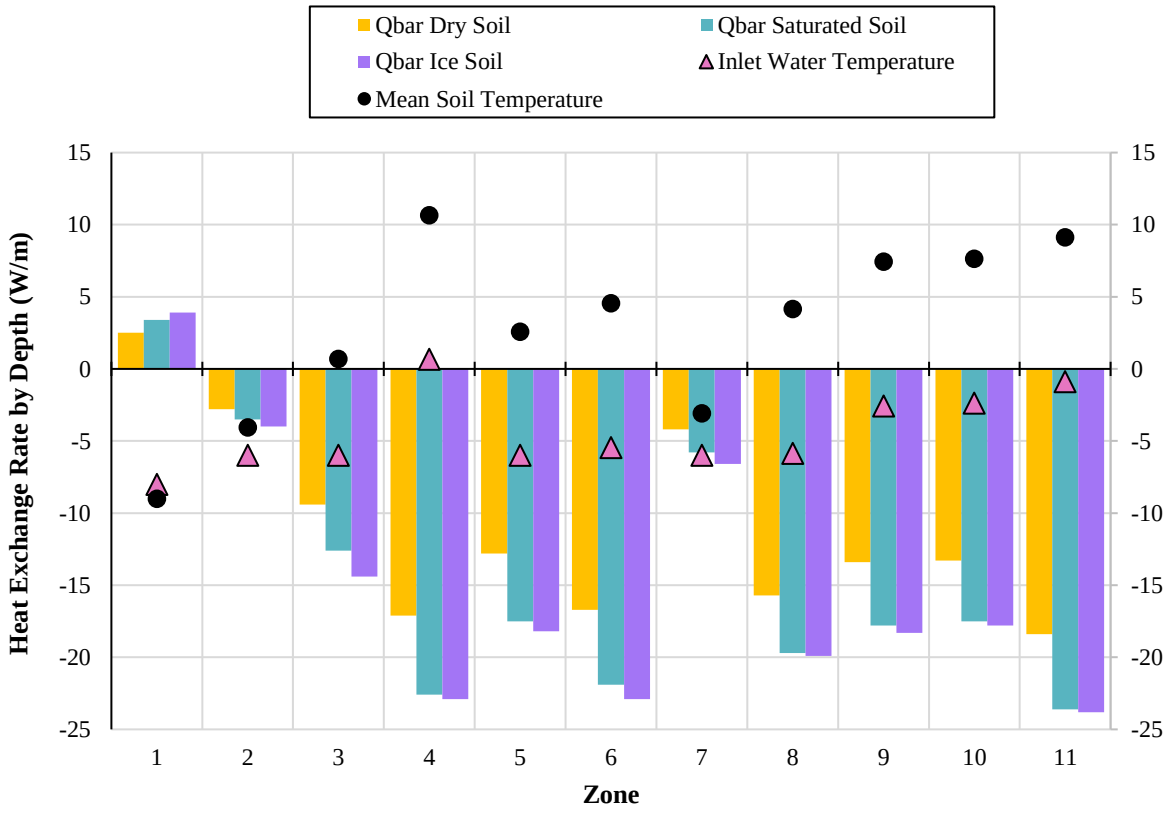

Figure 6.1. Winter heat exchange rate by depth per zone compared to the inlet water temperature to the pile and mean soil temperature per zone.

To deliver heating, the GHE must exhibit a negative heat exchange value (signifying the fluid exits the pile at a higher temperature than it enters – the fluid is heated in the pile). Therefore, Zone 1 can immediately be disregarded for its heating ability. The zone does not have the conditions to yield a heating load through the proposed GHE design. This is a result of the low mean ground temperature of the soil in this region – which is lower than the limit of inlet water temperature, meaning the fluid will be cooled rather than heated by this soil. Zones 2 and 7 also have lower mean ground temperatures, and their resulting heat energy capacity is lowered because of this condition – however, they are simulated to provide around 5 W/m of heating heat exchange rate by depth. If the working fluid were changed to an antifreeze (that meets the appropriate environmental restrictions) these low winter heat exchanging zones may be feasible for the GHE. Further improvements and research can focus on operating these piles in cold regions with a range of fluid solutions and at lower inlet fluid temperatures to the pile.

Zones 4, 6, and 11 have the maximum heating heat exchange rate by depth values for this case. This corresponds to the high mean ground temperatures in these zones – the fluid is heated more effectively due to the higher temperatures of the soil domain with which it is exchanging heat. Across most zones, the ice and saturated soil conditions yielded higher heat exchange rates. This difference in performance is due to the increased thermal conductivity of the soil when water and ice are present. The effects of these conditions are more noticeable with higher mean ground temperature – indicating that the temperature of the ground has a greater influence on heat exchange rate by depth in the winter conditions. The differences between the ice and saturated water soil conditions are negligible for most cases, as the ice was only assumed to exist at soil layers which were calculated to have ground temperatures below the freezing point of water (a mean ground temperature above zero would therefore not have ice in the deep ground temperature regions). However, for Zone 3, which has a near zero mean ground temperature, the effect of the ice soil condition on heat exchange rate by depth was most noticeable – as there was a larger region of soil whose thermal conductivity was increased by the presence of ice.

Figure 6.2. Summer heat exchange rate by depth per zone compared to the pile inlet water temperature and mean soil temperature in each zone. presents a similar plot for the summer cooling conditions. Again, the inlet water temperature and mean soil temperature are presented for comparison with thermal performance – which is measured as the heat exchange rate by depth. Two soil conditions were modelled in these results: dry soil and soil saturated with water. Though there may still exist ice soil conditions in zones where in the mean ground temperature is below zero, those were not included in this analysis and the focus was on saturated and dry soils in the summer period.

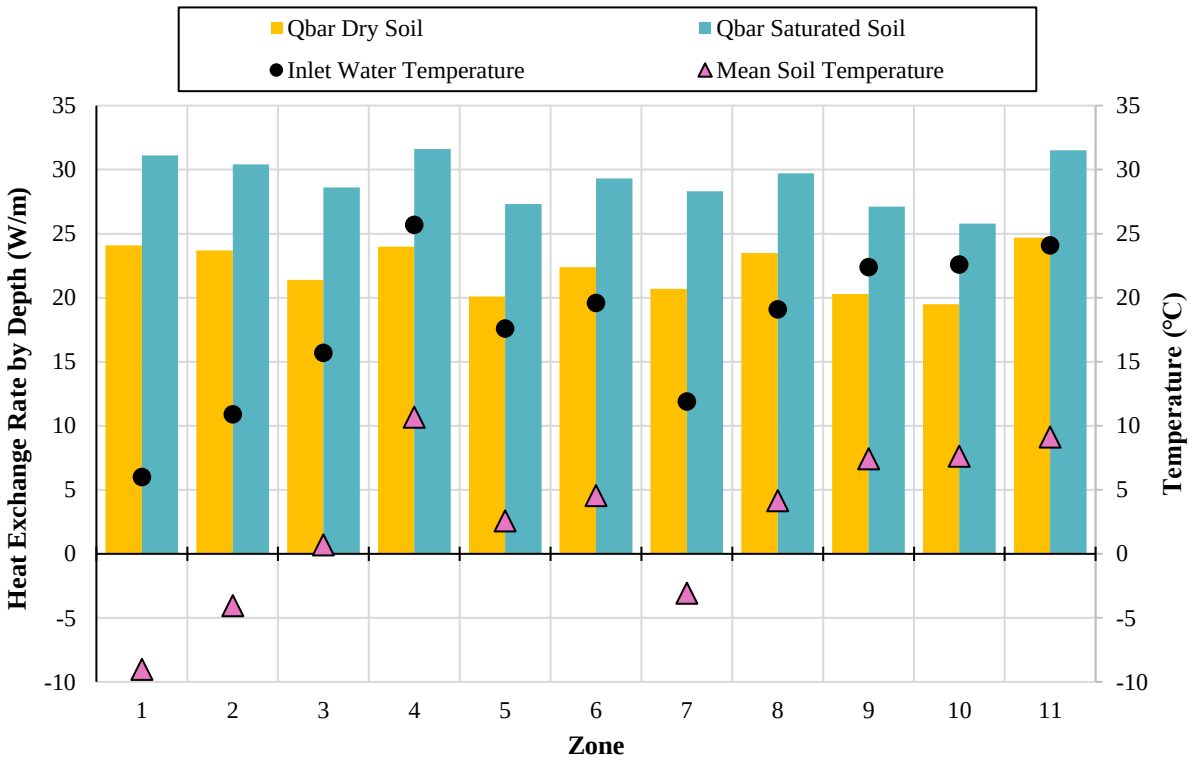

Figure 6.2. Summer heat exchange rate by depth per zone compared to the pile inlet water temperature and mean soil temperature in each zone.

The variation in heat exchange rate by depth for each zone was less for the summer cooling results than the winter heating results. This difference indicates that the cooling capacity may be less affected by soil and climate conditions than the heating capacity is for the range of soils and climate studied here. Since the inlet water temperature was governed by a maximum temperature difference with the soil, the plots of these two temperatures follow the same path across the zones, with an equal difference between them. This as not the case for the heating capacity plot in Figure 6.1, as the minimum inlet water temperature was limited by the freezing temperature of the fluid, and operating ranges of a GSHP.

The highest heat exchange rate by depths for the summer case were in Zones 1, 4, and 11. Zones 4 and 11 were in the regions with higher thermal conductivities and it is likely that this is the reason for the larger heat exchange potential in these zones. Zone 1 has a moderately high thermal conductivity, but also has the advantage of a very low mean ground temperature, and so the entering fluid may be cooled at a higher heat exchange rate for this reason. Across all cases, the differences between the dry and saturated soil conductivities show the impact soil thermal

conductivity values have on heat exchange rate in a GHE. Regardless of region, the saturated soil conditions yielded higher heat exchange rates by depth by an average increase of 6.9 W/m. In combination with the insights from the winter results, this shows that the effect of water saturation in the soil yields increases the total heat exchange rate for the 20 m base pile by 26-37% in the summer, and 25-38% in the winter. This increase yields the highest impact in soil regions with high mean ground temperatures, or across all soil types in the cooling season.

These results are limited by the averaging of conductivities across a large region, which could have a wide variation of soil types and conditions locally. However, the aim is to begin to develop a guide for installation of this technology across large regions of climate and soil conditions. In the context of the northern and remote communities which might benefit from this technology, this general capacity by large zone can be used to mobilize towards installation of these systems in certain regions where their impact may be greatest felt.

Figure 6.3 plots the saturated heating and cooling capacity results on a map for each zone (whose boundaries are drawn with a grey line). These results are also presented with an averaged overall saturated conductivity per zone – one which is averaged across depth and does not account for variations by depth but provides a general trend of the variation of conductivities by zone. This figure also presents the locations of off grid communities as recreated from Figure 1.1 (shown as dots), in contrast to the locations of permafrost with high, moderate, and low responses to warming recreated from Figure 1.8 (shown as colour regions).

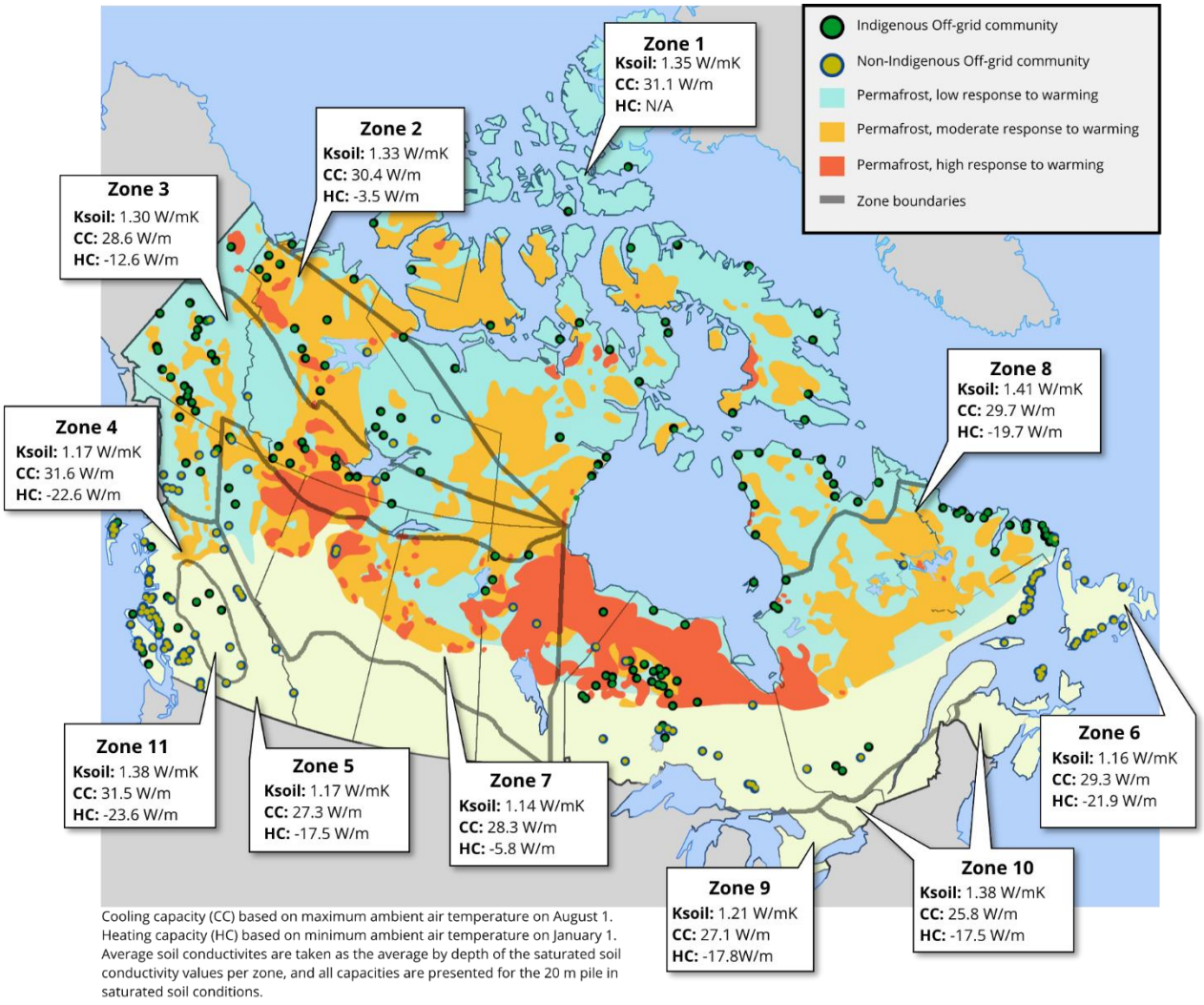

Figure 6.3. Map generalizing the average soil conductivity and saturated heating and cooling capacities per zone in comparison to the location of off grid communities and areas of permafrost at varying risk of thawing. The capacities are not modified by a COP but reflect the direct heat exchange rate by depth of the pile.

The combination of permafrost melting potential, location of remote communities, average thermal conductivity, and capacities brings together the insights of energy use and demand, geological and climate change models with GSHP design and use. Figure 6.3 shows that certain zones may be of highest priority for the proposed application of this GHE. Zone 8 has a high density of off grid communities located within areas of permafrost at highest risk of thawing due to climate change. This zone also has the highest average saturated soil conductivity – which further validates that the permafrost soil in this region is likely to have the highest response to ambient air temperature changes. The heating and cooling capacities in this region are also relatively high (due to the high soil conductivity and warm mean ground temperature), meaning this zone could be a good first candidate for implementation of this HSP system. Zone 7 is also a region with large area of

permafrost soil at risk of thawing due to climate change, however the average soil conductivity for this zone was low – therefore the risk of thawing might be more of a factor of the climate conditions, or geographical features such as the presence of many lakes as is characteristic for this region. Zones 10 and 11 have high thermal conductivities and capacities, but are not located within permafrost regions, and have few or no off-grid communities recorded there. Nevertheless, these regions have great potential for a HSP installation, and may benefit from the sustainability of GSHP systems to supply their thermal energy.

Overall, this initial generalizing of the capacity of HSPs as GHEs across 11 zones of varying soil and climate conditions has given insights into the key role that mean ground temperature, saturation, and soil type play on the thermal performance of a GSHP system. It also indicates that many of the northern and remote communities are in locations with a high potential capacity for cooling and/or heating – which improves the feasibility of this system in these regions.

1.20 Effect of a Constant Heating Load on Ground Temperatures with Climate Change Induced Thawing of Permafrost Over 40 Years

This section characterizes ground temperature changes across five 40-year long transient studies, with the effects of climate change applied as a constant ambient air temperature increase of 2°C across this time frame. For the purpose of consistent comparison, all cases were studied within the Northwestern Forest Zone (Zone 7) – a region previously flagged for being at risk of permafrost thawing due to the present near-zero mean soil temperature found in Section 1.12. A constant heating load was applied to cases with the GHE pile, and this load was selected at a temperature of -5°C, the lowest temperature at which a GSHP would be able to provide space heating given the present mean ground temperature in Zone 7 of -3.07°C. A description of these five studies is presented in Table 6.1.

Table 6.1. Model input parameters for five cases in permafrost mitigation study

Study	Model Input Parameters	
All	Ambient Air Temperature (T_{air})	Hourly input, $T_{air,CC}$ (t)
	Ground Temperature (T_{soil})	Equation 4, T_{soil} (z,t)
No Pile – Dry Soil	Pile Geometry	No Pile
	Soil Conductivity	Dry conductivity by depth for Zone 7, $k_{dry}(z)$
	Inlet Flow Conditions	No flow
	Inlet Water Temperature (T_{in})	None
Base Pile – Dry Soil	Pile Geometry	Pile 2, Table 2.1
	Soil Conductivity	Dry conductivity by depth for Zone 7, $k_{dry}(z)$
	Inlet Flow Conditions	2 L/min, water
	Inlet Water Temperature (T_{in})	Constant -5°C
Optimized Pile – Dry Soil	Pile Geometry	API 68 Steel casing with 2" nominal pipes
	Soil Conductivity	Dry conductivity by depth for Zone 7, $k_{dry}(z)$
	Inlet Flow Conditions	2 L/min, water with 20% glycol
	Inlet Water Temperature (T_{in})	Constant -5°C
No Pile – Ice Soil	Pile Geometry	No Pile
	Soil Conductivity	Ice conductivity by depth for Zone 7, $k_{dry}(z)$
	Inlet Flow Conditions	No flow
	Inlet Water Temperature (T_{in})	None
Optimized Pile – Ice Soil	Pile Geometry	API 68 Steel casing with 2" nominal pipes
	Soil Conductivity	Ice conductivity by depth for Zone 7, $k_{dry}(z)$
	Inlet Flow Conditions	2 L/min, water with 20% glycol
	Inlet Water Temperature (T_{in})	Constant -5°C

An initial validation of the time stepping was performed using the Optimized Pile – Dry Soil case. Due to the large time scale of 40 years of simulation, the time stepping intervals must be optimized for a reasonable computational time. A simulation with 1-hour timesteps for one year of the Optimized Pile – Dry Soil case took approximately 1 hour of wall-clock time to compute. It is likely that a 40-year simulation would then require around 40 hours, across five cases. In comparison, a time step of 876 hours/year (one tenth of a year) for 40 years of the same case (Optimized Pile – Dry Soil) took approximately 1 hour of wall-clock time to compute.

Therefore, this larger time step was utilized for the five cases in order to perform their simulations within a reasonable amount of time, and computational memory requirements. The accuracy of the larger time step model was investigated by measuring the outlet water temperature of the hourly simulation with the 876 hours/year time step simulation for the first year. These results are

presented in Figure 6.4, with the larger time step shown as square markers, and the hourly time stepping shown as a line.

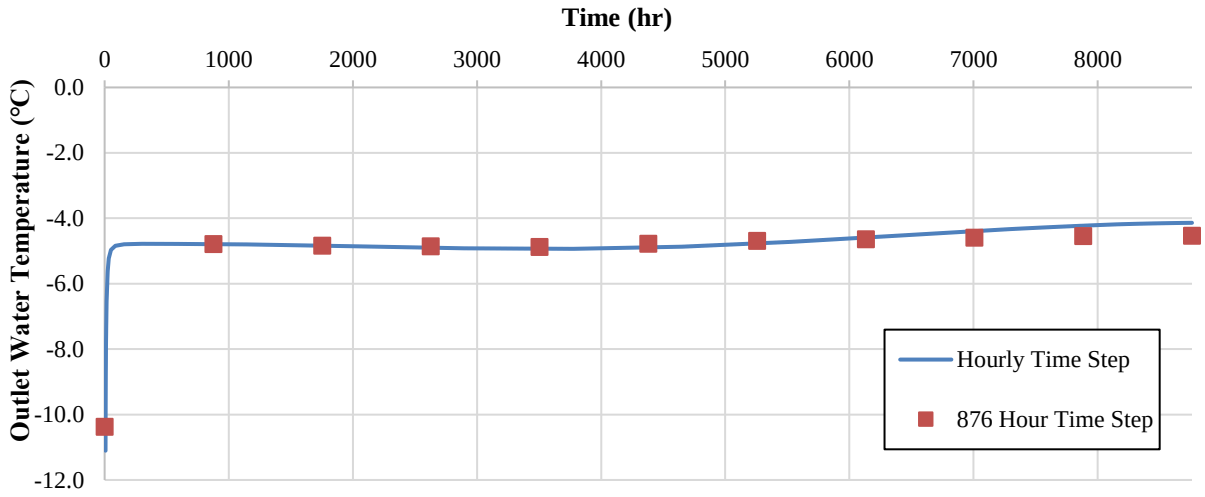

Figure 6.4. Validation of time stepping using the Optimized Pile – Dry Soil case across the first year.

This check shows the expected initial temperature increase of transient start up matched by both time steps, and the subsequent temperatures are simulated with good agreement between both results, and an average outlet water percentage difference of 2% across the year. Future studies may improve upon the time stepping dedicated to the research presented here.

Investigating the ability of the HSP to mitigate climate-change induced permafrost thawing is shown via ground temperature changes across the five cases. First, the results for the 40 year-long transient study (Base Pile – Dry Soil) in the Northwestern Forest zone are shown below in Figure 6.5. This figure compares the average ground temperature across time with no load applied, and one wherein the pile is operating with a constant load, with linear dashed curves to highlight the trend. The temperature is measured as an average of the entire soil domain (5 m radius, and 23 m depth).

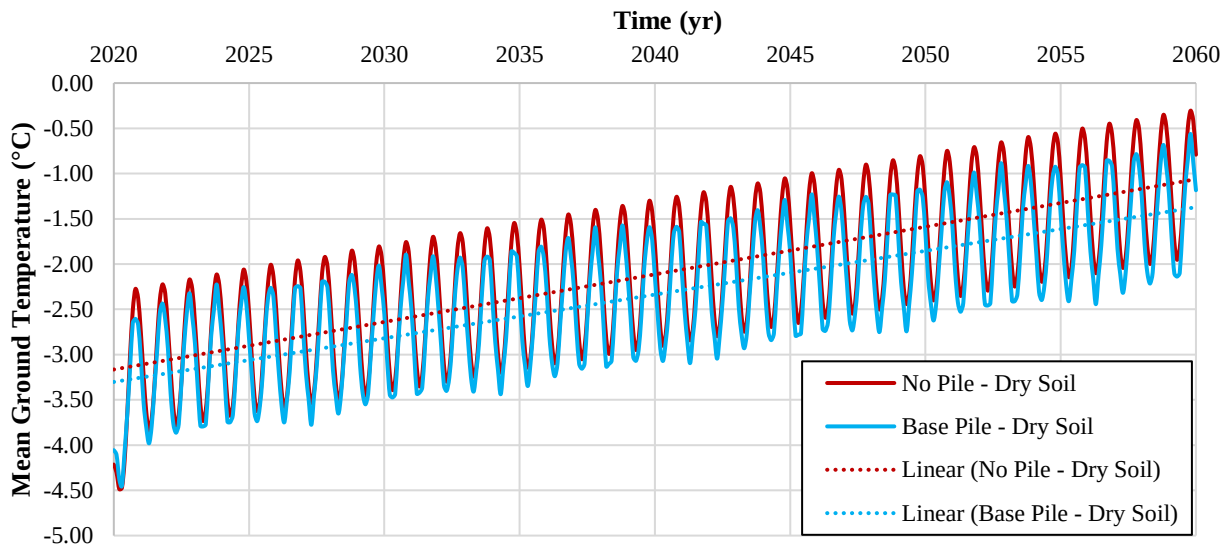

Figure 6.5. Average soil temperature in Northwestern Forest zone with and without a load applied.

These results show the expected rise in ground temperature over time, starting with undisturbed ground, wherein the average ground temperature in 40 years increased slightly more than 3.25°C. When the load is applied, this increase is minimally reduced, with an increase in ground warming of approximately 3.00°C. Interestingly, the constant annual load had a more significant impact on the maximum (summer) average ground temperature than it did on the minimum (winter) ground temperature. This might indicate that seasonal-based operation could be optimized to schedule for greatest overall temperature reduction in mean ground temperature (rather than using a constant annual load). As well, areas of naturally thawing summer permafrost may be artificially frozen utilizing a heating load during the summer (for domestic hot water production for example).

At this point, it might seem that the pile has not been able to deliver a significant effect to mitigate climate effects. However, the approximate percentage of the soil domain affected by the pile's heat transfer is only 14% (assuming the radius and depth of impact are 2 m and 20 m respectively). Therefore, 86% of the volume of soil in the average with the load applied is the same as the soil temperatures with no load applied - hence the similarity in the results presented in Figure 6.5.

The effectiveness of the pile can be better understood by looking at individual ground points across time. As such, four locations were chosen at a depth of 15 m below the surface of the ground: Point 1 is located at the interface between the steel casing and the soil, Point 2 is 0.5 m from the centre

of the pile, Point 3 is 2 m from the centre of the pile, and Point 4 at the edge of the soil domain. The locations of these points are indicated in Figure 6.6 which is a schematic of the top and side view of the computational domain with the points denoted as Pt. 1, Pt. 2, Pt. 3, and Pt. 4.

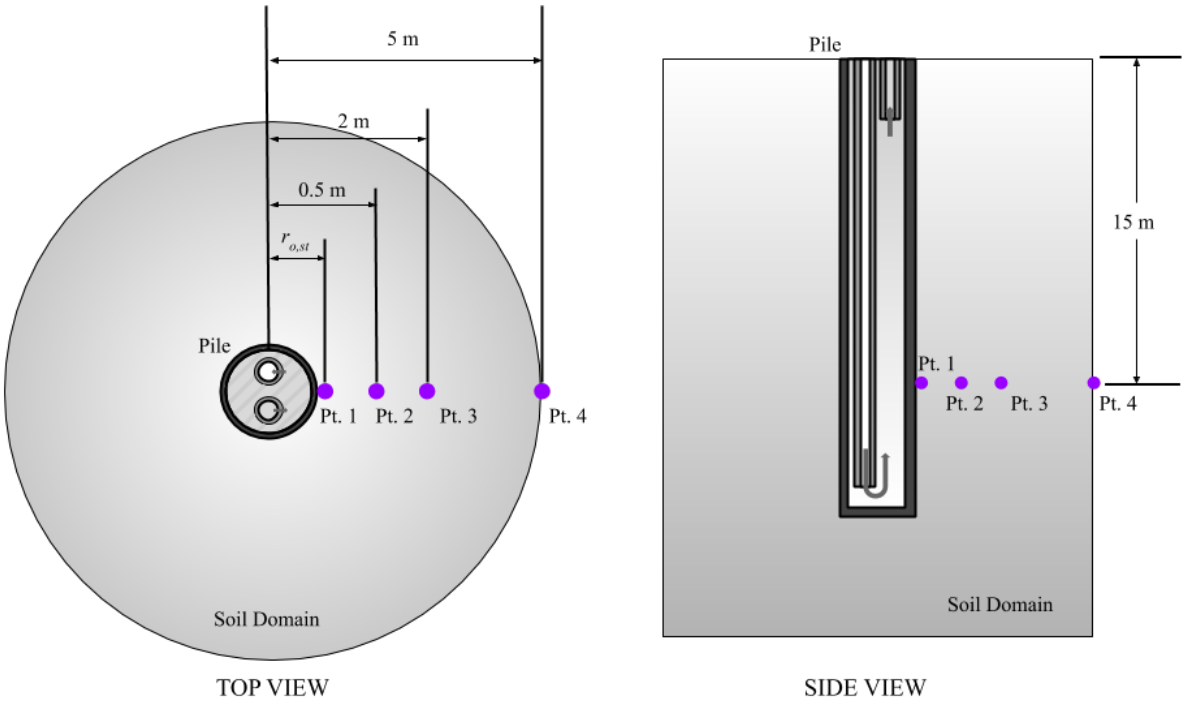

Figure 6.6. Schematic of the location of four soil points for analysis.

The depth of 15 m was chosen for this analysis because it is well below the active layer in this region and so represents the layer of soil within the permafrost which is less affected by seasonal temperature changes. This depth also allows for the measurement of ground temperature effects by the 20 m long pile. In the No Pile – Dry Soil, and No Pile – Ice Soil case, these points are located in the same positions even though there is no pile present in the model and it is solely made up of a cylindrical soil domain.

Figure 6.7 compares the No Pile – Dry Soil with the Base Pile – Dry Soil simulation results at Point 1 and Point 3. This graph shows the trend of soil temperature which is affected by either the ambient air temperature increases (due to climate change) alone, or the air temperature increases and the pile temperature effects (due to the constant heating load applied). The initial variations of slope for all curves reflect the transient effects of startup in undisturbed ground temperatures.

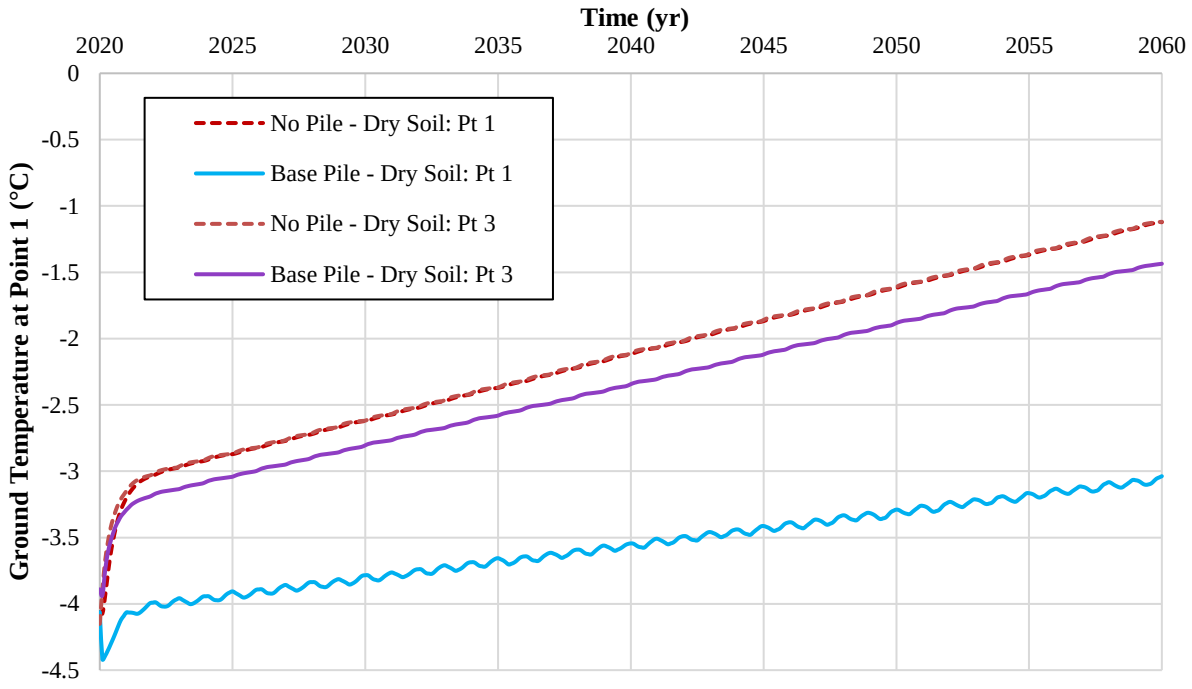

Figure 6.7. Northwestern Forest ground temperature at Point 1 and Point 3 with and without a load applied.

The temperature of the No Pile – Dry Soil case at both points shows very minimal seasonal variation, with a long-term temperature increase – reflecting the climate change warming. This data indicates that the temperature at these points is indeed in the permafrost region, as the active layer would otherwise show greater seasonal variations. It also revalidates climate change predictions of soil temperature increases, by utilizing the heat transfer conditions of the numerical model to show that the ground temperature at this point is increased due to the increasing temperature at the ground surface. The Base Pile – Dry Soil case shows the variation in temperature that may be achieved in the same soil and climate conditions if a constant heating load is inserted into the soil domain. Now the potential of the pile is more noticeable; the ground temperature at these two points indicates the close-range soil temperature effects possible by the pile. The ground temperature at Point 1 when a load is applied is nearly constant across the 40 years, with an increase of around 1°C, whereas the no-load case shows the soil temperature rise almost 3°C at this point in the ground. The Point 3 comparisons show that the ground temperature effects of the pile have reduced at 2 m radial distance, as the difference between the load and no load cases are around 0.5°C (though the pile case still has the lower ground temperature after 40 years at this point).

These results indicate that there is a potential for these piles to dampen the ground warming effects of ambient temperature rise across the next 40 years, but that these results are localized to a distance within around 2 m radius of the piles. To investigate a potential increase of this effect to a wider radius, the geometry of the pile was changed to reflect the optimized pile from Section 3.3 – with an exterior steel casing size of API 68, and interior plastic pipes with nominal diameters of 2”. This pile was simulated within the dry conditions as well as soil with ice conductivity. The No Pile – Ice Soil utilized the conductivity of soil with ice across the entire time step. This method treats the ice as a solid, without the effects of phase change or water transport. In order to maintain the permafrost, the temperature of the ground must remain below 0°C, thereby justifying modelling the ice as a solid – without melting. The effect that the higher conductivity of ice might have on the distribution of temperature throughout time is investigated through the Ice Soil cases.

Performing a similar comparison as seen in Figure 6.5, with the optimized pile geometry in the ice soil, Figure 6.8 presents the average soil domain temperature across time with linear trendlines, both with and without the pile.

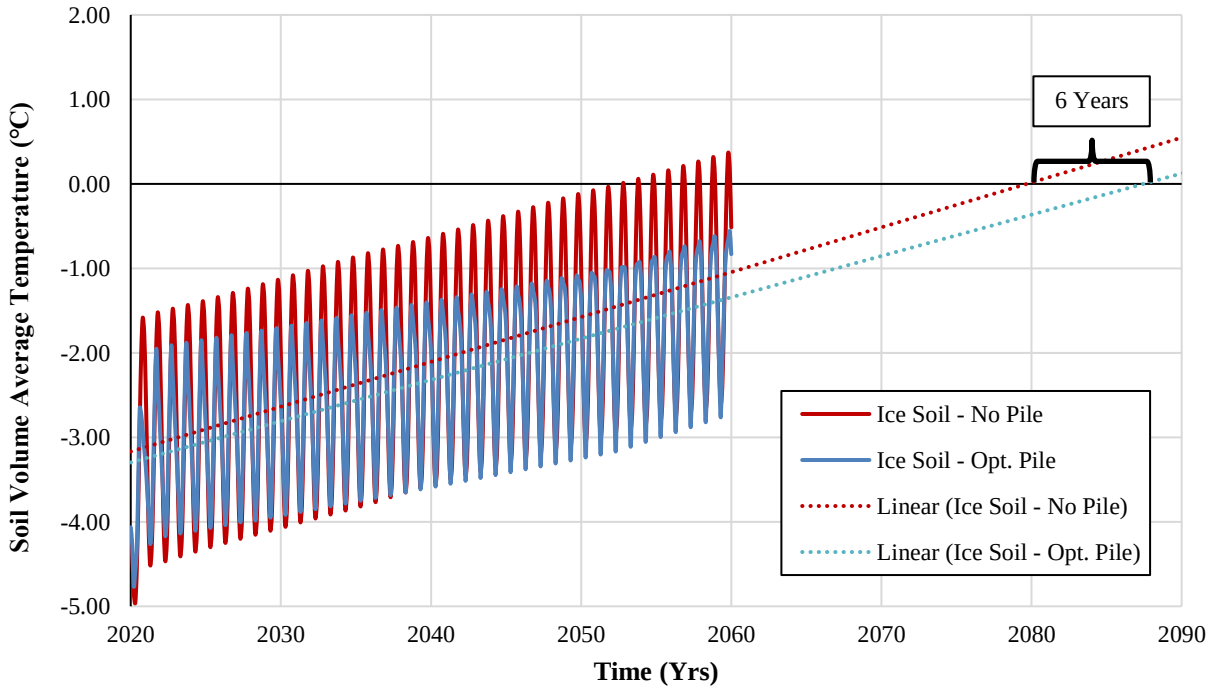

Figure 6.8. Average soil domain temperature in iced soil conditions across time, with linear projections till the mean temperature is above 0°C.

Seasonal variations in these results again highlight that applying a heating load all year has a more significant effect on mean soil temperature in the summer than in the winter. However, the decrease in soil temperature in the summer by the pile is more extreme in the soil with ice conductivities than the soil with dry conductivities and the base pile (from Figure 6.5). Also, the temperature variations even without a pile are more extreme for the soil with ice – due to the higher thermal conductivity of the soil.

The trendlines predict the moment at which this average soil domain temperature will reach above the freezing point of water. Without the pile it is predicted to occur around 2080, and with the intervention of the GHE, this soil volume's average temperature is predicted to reach 0℃ during the year of 2086, a six-year delay of these effects. The Optimized Pile – Dry Soil case reaches this mean temperature of zero during the year of 2089. Again, these results reflect a thermal interference within the size of approximately 14% of the total volume of the soil domain – yet the pile was still able to delay the projected thawing by 6 to 9 years.

Characterizing these effects at each of the four points described in Figure 6.6, Figure 6.9 shows the temperature change across time for the optimized piles in dry (solid lines) and ice (dashed lines) soil conditions.

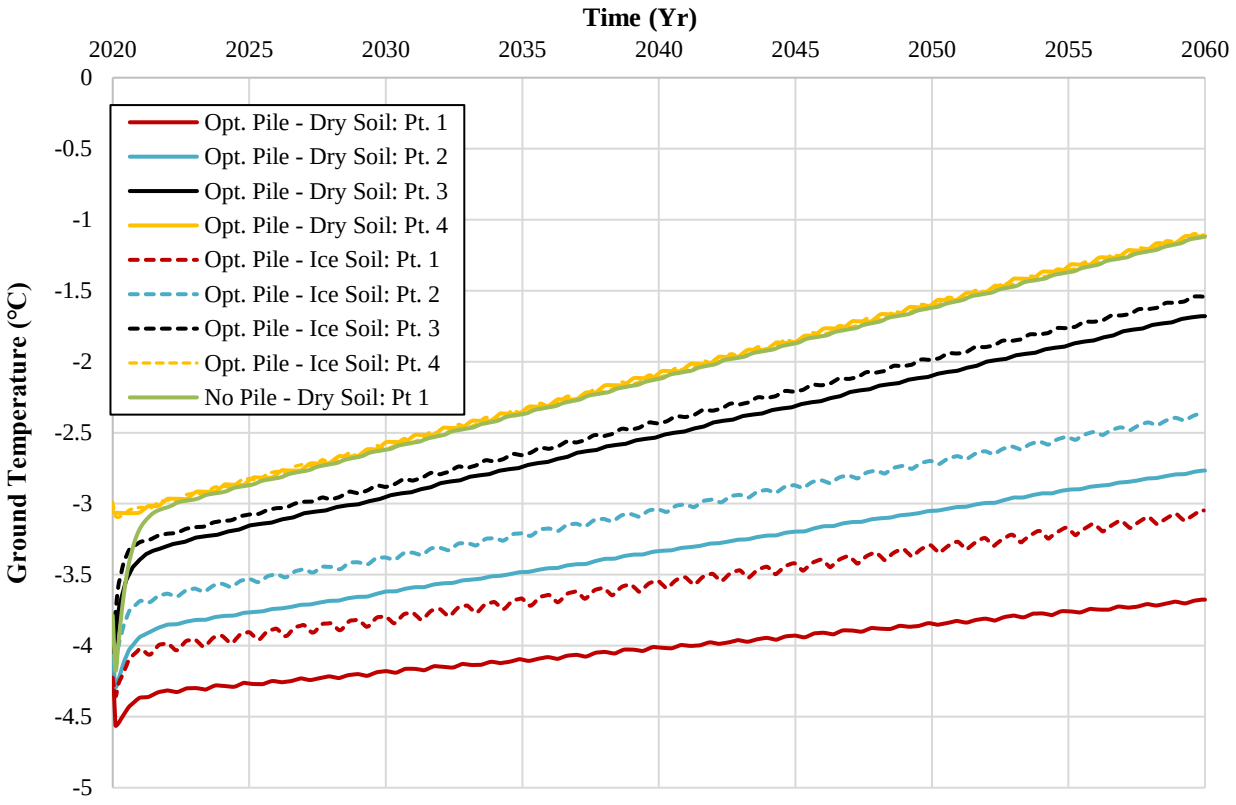

Figure 6.9. Temperature at Points 1, 2, 3, and 4 for the optimized pile cases within dry and ice soil conditions across forty years of time.

The temperature at Point 4 (for both dry soil and ice) tend towards the same climate change thawing output and is not affected by the piles. This is shown by the No Pile – Dry Soil temperature across time at Point 1, which follows nearly the same distribution as the temperatures at Point 4 with the piles that are in ice and dry soil. Moving closer to the edge of the GHE, Point 3 at 2 m radially from the pile exhibits a slight climate change mitigation effect: the increase in temperature due to climate change is reduced. Points 2 (0.5 m radially from the centre of the pile) and Point 1 (on the outer edge of the pile) show significantly mitigated temperature increase due to climate change over the period of study, with Point 1 having the most impacted temperature distribution with respect to time from the pile. The differences between the ice conductivity case and the dry conductivity at these closer locations show that the higher conductivity of the soil (when solid ice fills its void volume) may reduce the pile's ability to mitigate climate change effects. The heat transmission of the increasing temperature ambient air has a higher impact on the soil than the cooling effect of the thermal load applied to the GHE – though there is still a reduction of this thawing.

Projecting the predicted time at which the ground temperature surpasses 0°C at Point 2 shows the potential local thawing mitigation ability of the pile (as opposed to the generalized average soil domain temperature prediction in Figure 6.8). Figure 6.10 plots the ground temperature of Point 2 with the pile for dry and frozen wet soil and Point 1 without a pile in the dry soil across time. Linear trendlines are used to predict the expected time at which this temperature will surpass 0°C - at which point it will no longer be permafrost.

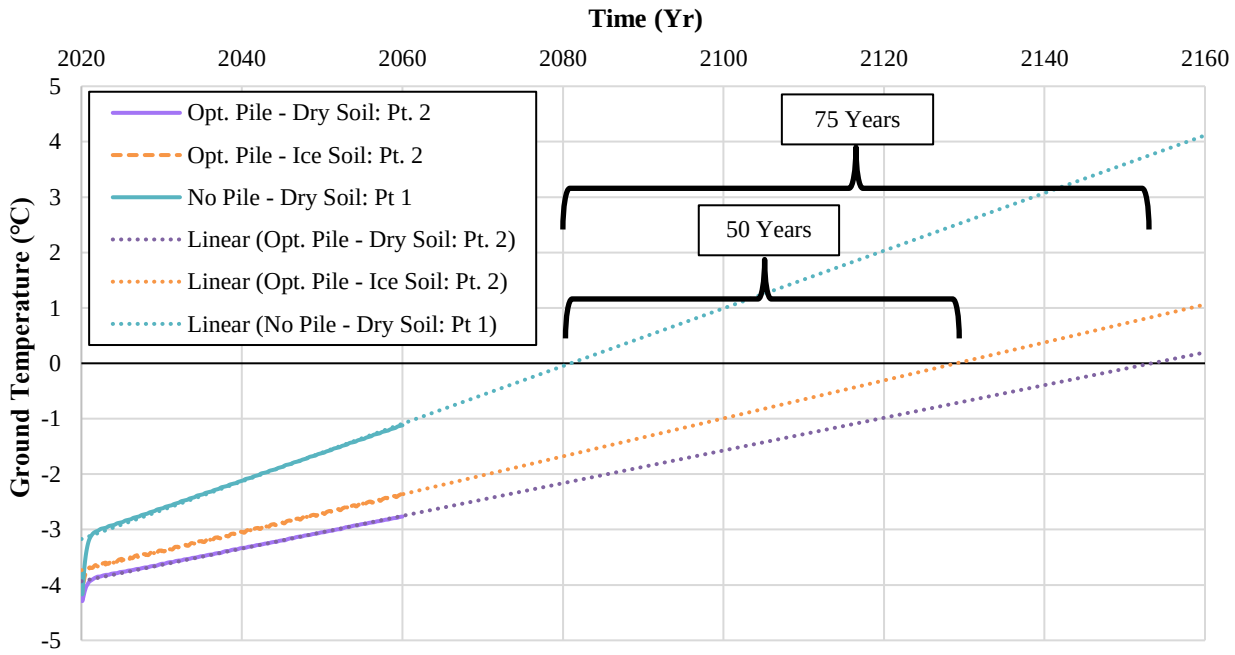

Figure 6.10. Prediction of time until soil temperature surpasses 0°C

The results in Figure 6.10 show the utility of this pile system in maintaining permafrost within a local radial volume surrounding the pile. At Point 2, the application of a thermal load in the dry and iced soil have extended the predicted trendline to follow a less steep slope of thawing due to climate change. Without the pile, this ground is simulated to thaw to 0°C at around 2080, but with the pile in the iced and dry soil it will occur at approximately 2130 and 2155 respectively. This is a delay of 50 and 75 years for the thawing of permafrost within a 1 m diameter radius around the pile.

This prediction assumes that the increase of temperature due to climate change is linear with a constant slope. In reality, the thawing of permafrost due to climate change may happen non-linearly, with a levelling off of temperature due to latent heat as ice changes phase from solid to

liquid. Nevertheless, these results are showing possibilities for the long-term reduction of thawing in permafrost soils – and should inspire more research into the optimization of the positioning of these piles, and their design to delay permafrost thawing in strategic ways.

Visualizing this local temperature effects around the pile, Figure 6.11 plots the distribution of ground temperature across the horizontal radial distance from the centre of the pile (point 0 on the x-axis) at a depth of 10 m below the ground surface. These results are presented for all 5 cases at the first time interval (2020.1 years), and the last (2060 years).

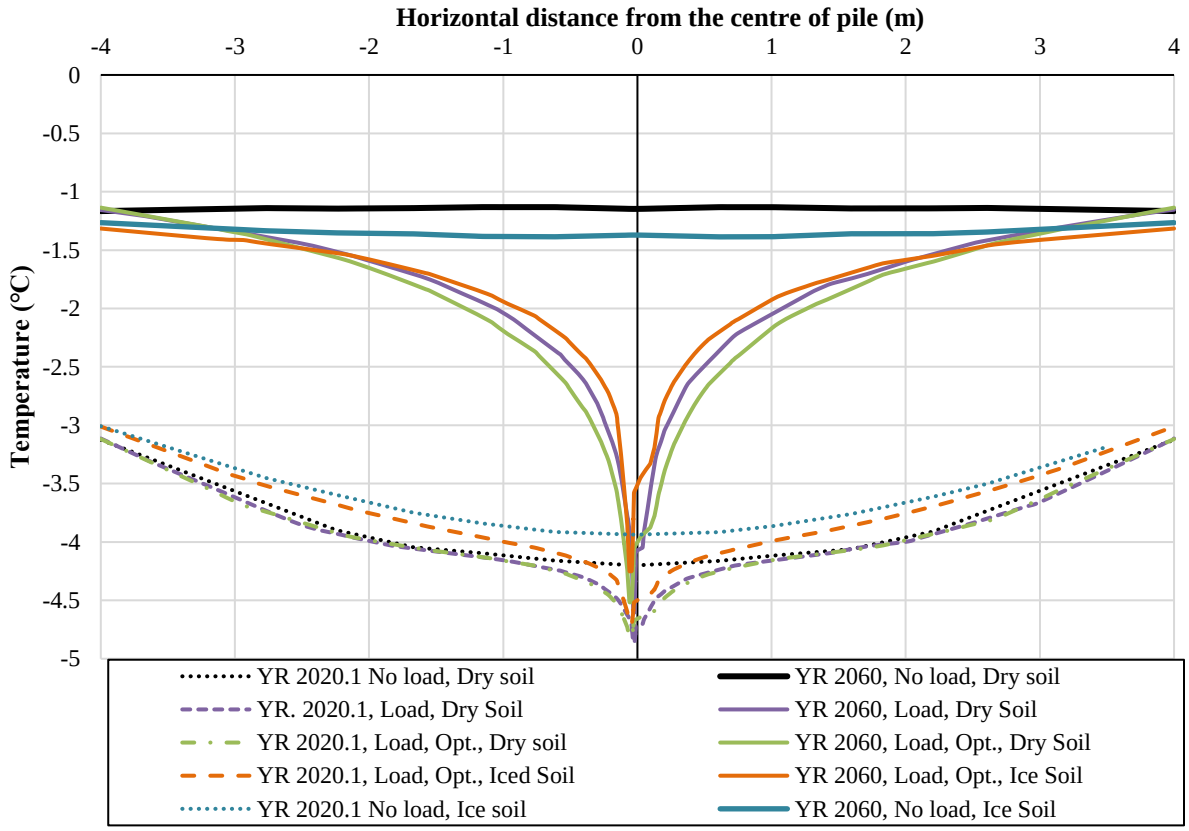

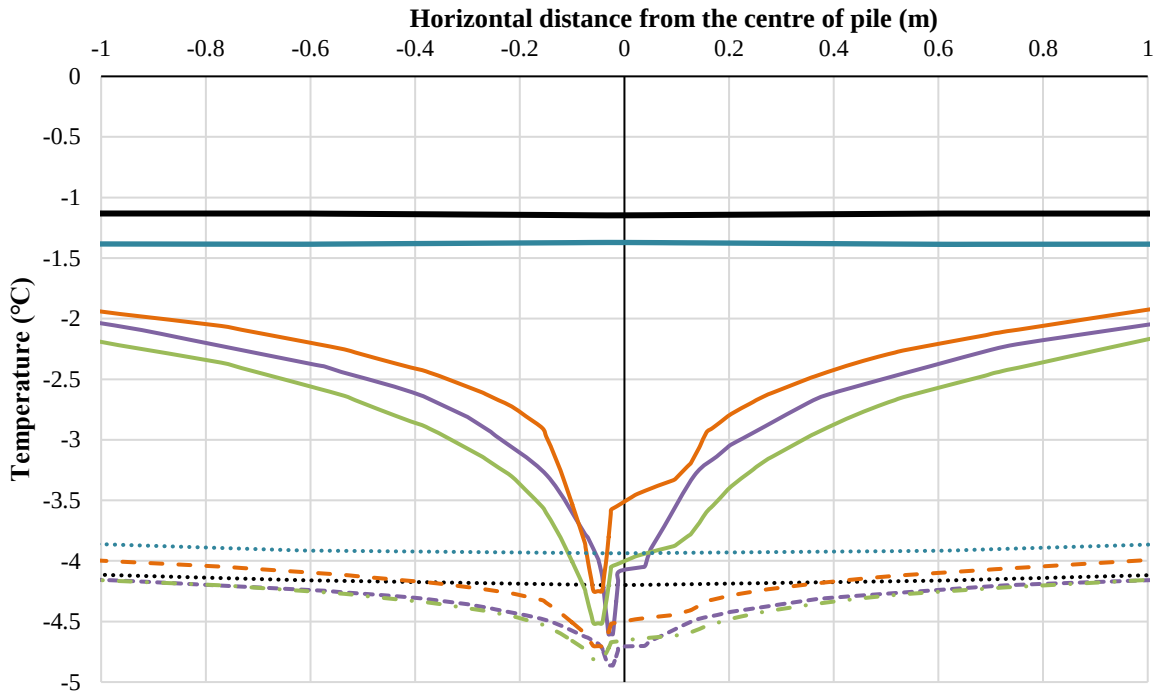

Figure 6.11. Horizontal temperature distributions along the y-axis at 10 m below the soil surface for 3 cases at the first time interval and the last (above), and a close-up view of the same results (below).

The starting temperatures across all cases shown in Figure 6.11 (the non-solid lines) show near constants at this depth, which reflects the mean deep ground temperature. As the climate change heat gain is applied via the ambient air, and the cases with the piles then also receive heat loss via the heating load, the temperature at the last time step reflects the change in ground temperature at this depth. Without the pile, the dry and frozen wet soils have temperatures which increase by approximately 2.5-3°C. However, when the pile is added, the ground temperature immediately surrounding the pile remains close to the starting ground temperature, with a gradual increase as the radial distance from the centre of the pile also increases. In the lower graph (with a closer view of these temperatures immediately surrounding the pile), the temperature is offset slightly to the side of the pile with the inlet fluid pipe (on the left). This offset is also shown in Figure 4.6, and is a result of the unique inner pipe design chosen for this work, which yields greater heat flux at the edge closest to the incoming fluid than the opposite edge wherein a larger volume of fluid is flowing towards the outlet of the pile. with The case which experienced the least amount of ground temperature increase was the Opt. Pile – Dry Soil case, which had lower final ground temperatures up until a radius of nearly 3 m for the No Pile – Ice Soil case, and 4 m for the No Pile – Dry Soil case.

The vertical temperature distributions across time are shown in Figure 6.12 for the first time step, labelled 2020.1 (one timestep, or 876 hours, into the year 2020) and the last (2060). This temperature is extracted from a line 0.5 m radially from the centre of the soil domain starting at the surface of the ground, straight down until the end of the pile at 20 m depth for all 5 cases.

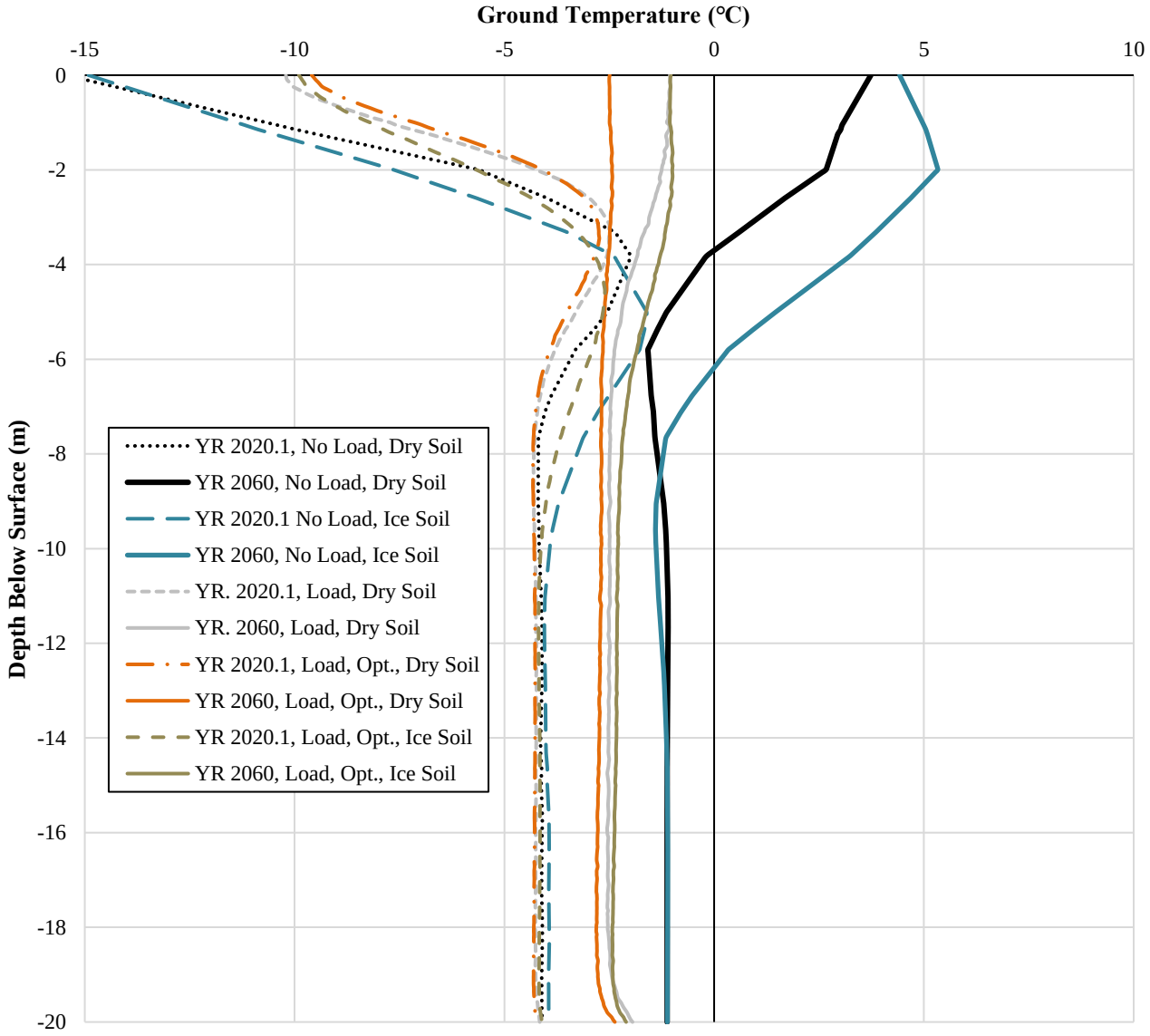

Figure 6.12. Vertical temperature distributions at first time interval and last.

In Figure 6.12, the cases without a pile show a similar starting temperature at the surface of the ground for the first time interval, following a typical soil temperature distribution down until reaching the mean soil temperature at around 10 m depth. The cases with a pile have a slightly warmer starting temperature at the surface of the ground (-10°C versus the -15°C without a pile)

because the temperature effects of the pile are already influencing the distribution at this point. The surface ground temperature is slightly warmer because it is not only affected by the ambient air temperature (as the no pile cases are), but it is modified somewhat by the volume of water, plastic and steel of the pile.

At the year 2060 in the simulation, the No-Pile cases show significant warming. Above 8 m depth, the active layer has a nearly seasonal alteration with the highest ground temperature occurring at the surface (versus this point having the minimum ground temperature in 2020.1). This shows the effect that the warmer ambient air temperatures have on the ground temperature distribution – raising the mean deep soil temperature (an increase in 3°C) as the air increases in temperature due to climate change effects. When the piles are added and their heating load applied, the ground temperature distribution at this point is nearly a straight line; the Opt. Pile – Dry Soil case was again the most effective at keeping the ground temperature near its starting point.

Representing these temperature gradients within a section view, cutting through the centre of the pile, Figure 6.13 shows temperature contours of the five cases at the starting interval and the final one.

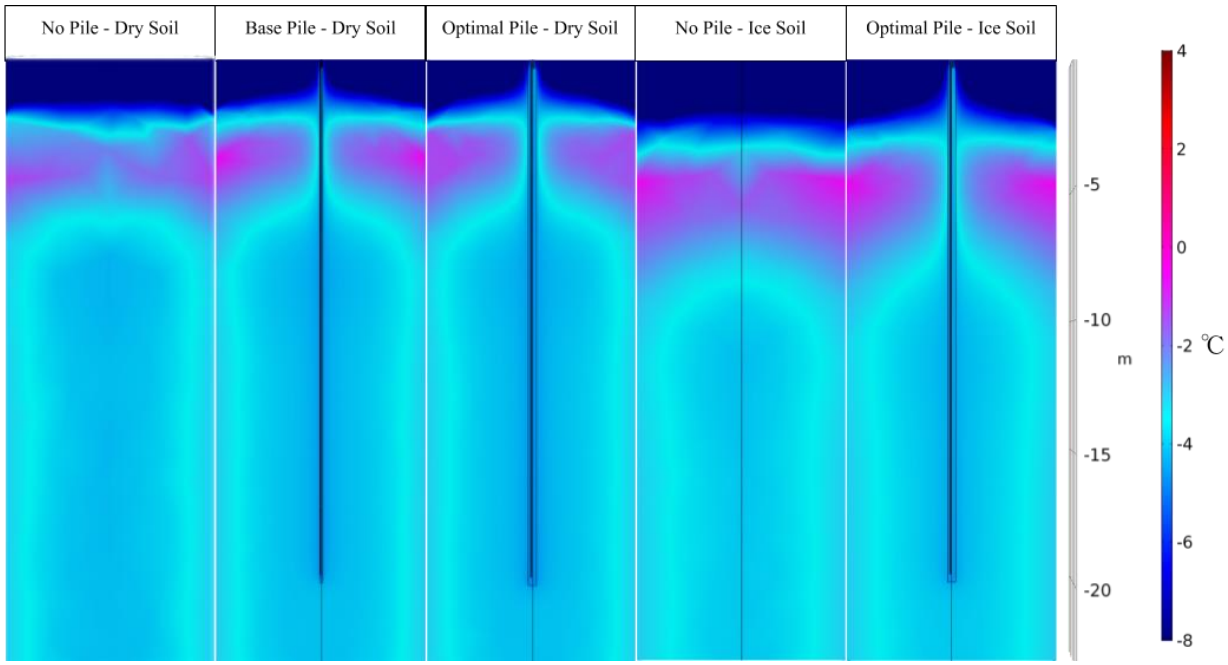

(a)

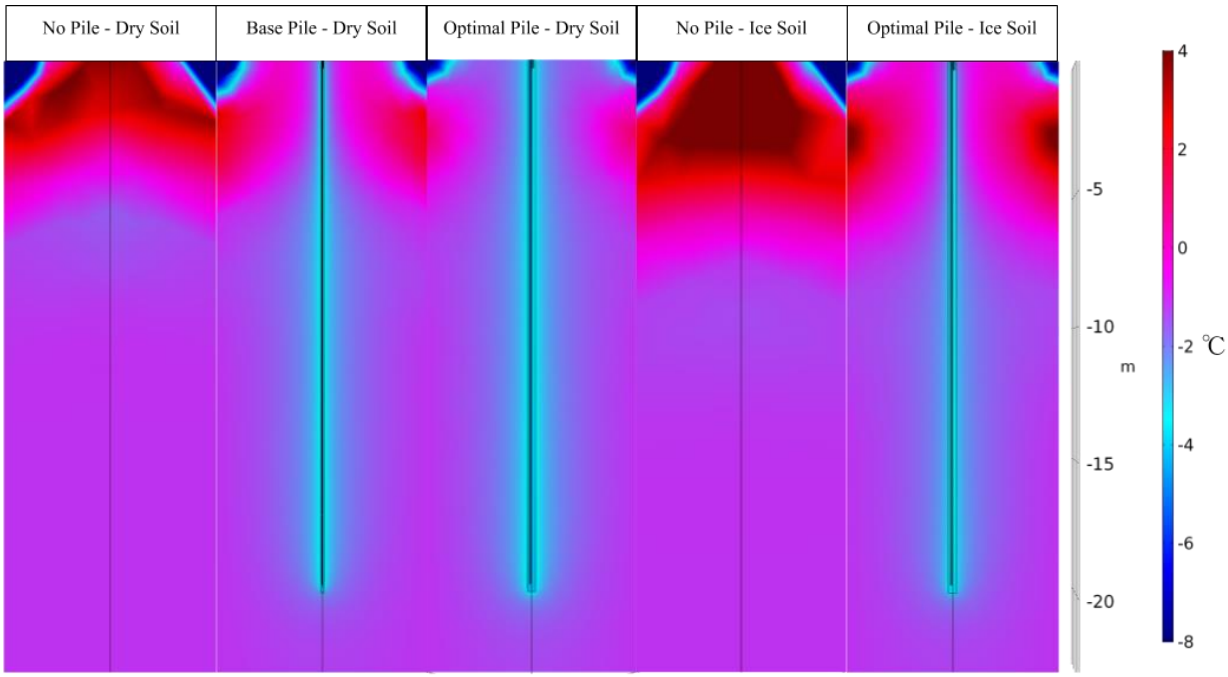

(b)

Figure 6.13. Temperature distributions (a) at the first time interval and (b) after 40 years of five operating conditions.

After 40 years, the majority of the soil domain for all cases has warmed up due to the increasing air temperature. As well, the active layers (shown as the dark blue sections of cold winter ground temperatures in Figure 6.13) have changed in shape and temperature after 40 years. The No-Pile

cases show that this active layer is above 0°C, and the depth of unfrozen ground has reached to around 5 m and 10 m depth for the dry and iced soil cases respectively. This shows that the permafrost regions saturated by solid ice may experience greater heat transmission from the ground surface into its depths, due to the increase thermal conductivity of a soil with ice. The presence of the piles in all pile cases maintained a volume of permafrost soil throughout the 40 years of simulation. This volume was largest in the Opt. Pile – Dry Soil. It is predicted that the high thermal conductivity of the ice reduces the thermal imbalance effects of overcooling the soil by applying the constant heating load. Whereas the dry soil case with lower thermal conductivity does not have as great an ability to conduct heat through its mass as the Ice Soil case – this serves as an advantage when competing with the effects of a warming ground surface. The increasing ambient air temperature from climate change is not conducted through the depths of the soil as effectively as in the case of the ice soil, and so the temperature effects of the heating load in the pile within this domain may have a greater impact on the dry soil case at these depths.

1.21 Thermal Energy from a Constant Heating Load Across the Permafrost Pile

The application of this constant heating load will yield usable heat for thermal applications in the supplied buildings. By fixing a constant inlet water temperature to the pile of -5°C, this heating load will vary across seasons and is defined by the desired ground temperature effects rather than the desired heating capacity output. In seasons when this heating load is not required (for summer conditions for example), several opportunities exist to exhaust excess heat. A network of heat exchangers may be installed to waste excess heat to the air, or it may be supplied to other applications such as a Domestic Hot Water (DHW) tank, industrial processes, or the preheating of gases or fluids in energy generation equipment.

To investigate the building energy load which might be supplied while delivering these permafrost temperature stabilization effects, a similar process outlined in Section 2.4.2 was followed. With an inlet water temperature of -5°C, Equation 7 yielded a heating COP of 2.6. Then, the building load energy ($Q_{building}$) was solved for using the ground heat exchanger thermal energy (Q_{GHE}) and the COP_H across time. This result was compared for the Opt. Pile – Dry Soil and Opt. Pile – Ice Soil in Figure 6.14, where the heating energy load is a negative value which is the numerical

representation of the direction of thermal energy exchange (heat leaving the GSHP). This figure also highlights the transient difference of the temperature in the ground at Point 2 (ΔT_{soil}) from the initial ground temperature at this depth. This value is calculated as the temperature of the Dry Soil and Ice Soil cases with the load applied minus the starting ground temperature at this depth. This starting ground temperature is -4.12°C and -3.98°C for the No Pile – Dry Soil and No Pile – Ice Soil cases respectively. By calculating this difference over time, how much the thermal load mitigates the climate change temperature effects can be visualized.

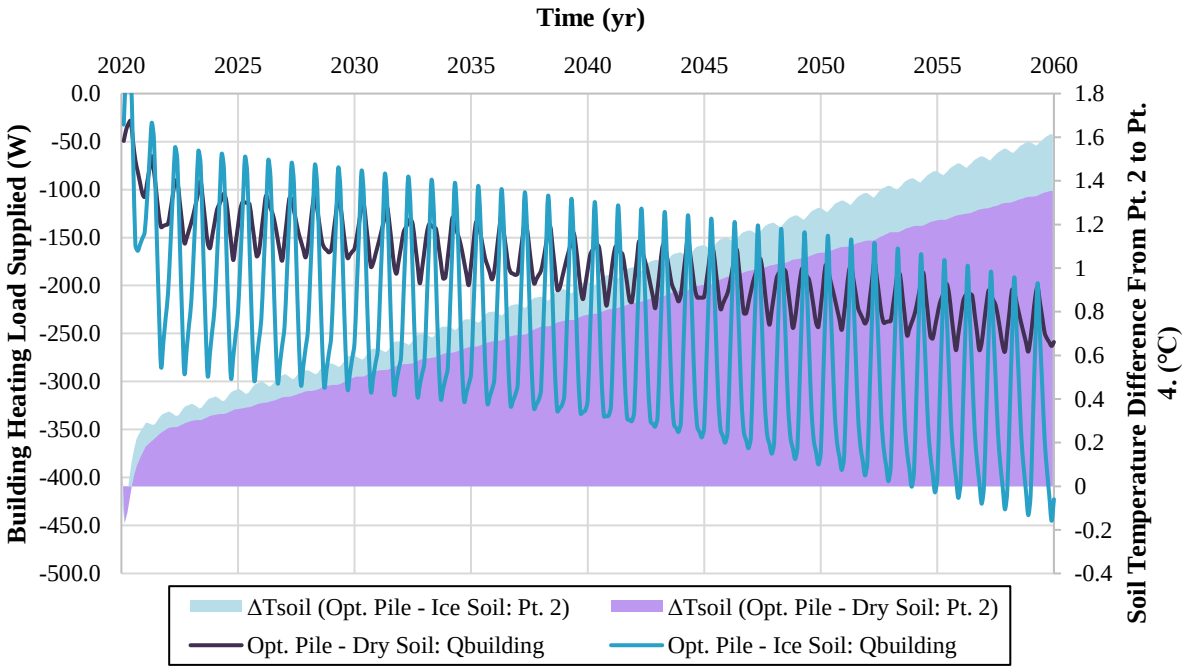

Figure 6.14. Building energy supplied ($Q_{building}$) and change in ground temperature at Point 2 across 40 years for the ice and dry soil optimized pile cases.

The change in temperature at Point 2 for both the Dry Soil and Ice Soil cases gradually increases over time (as the ambient air temperature increases due to climate change). The initial fluctuations in the curves are due to the transient effects of starting this heat exchange operation in previously undisturbed soil. After 40 years, the temperature at Point 2 is increased by 1.35°C and 1.61°C for the optimized piles in Dry Soil and Ice Soil conditions respectively. Compared to the No Pile simulations (which resulted in temperature increases at this point of 2.86°C and 3.00°C for the Dry Soil and Ice Soil cases), the use of this pile has reduced the projected increase in ground temperature due to climate change by 46-53%.

The ground temperature increase over time is slightly greater for the Ice Soil conductivity than the dry soil conductivity, however, the building energy load supplied from the Ice Soil case is greater than that of the Dry Soil case over time. The higher soil conductivity reduces the ground temperature effects but increases the thermal energy supplied to the working fluid. Both soil conditions produce less heating load during the period of the year at which the temperature difference between Point 2 and 4 is greatest (in the summer), and their maxima occur during the winter seasons, when the ground temperature difference is at a local minimum.

The average heating load needed to be supplied by the Opt. Pile – Dry Soil case across 40 years with a constant inlet water temperature of -5°C, a pile length of 20 m, and a corresponding COP_H of 2.6 is 177.0 W (0.05 tons), while the Opt. Pile – Ice Soil needs to supply an average of 251.6 W (0.07 tons) under the same operating conditions. Using only the heating season energy load, the average becomes 184.9 W and 280.5 W for the Opt. Pile – Dry Soil and Opt. Pile – Ice Soil cases respectively. Using this average heating season capacity to size a pile array for a 1-ton building heating load would require 19 (Dry Soil) and 13 (Ice Soil) 20 m piles. However, this energy load is not constant across time; as the soil domain increases in temperature due to the climate change warming of surrounding air, the heating energy load capacity also increases. More heating energy is available to be extracted from the soil for space conditioning at the end of the 40-year simulation than at the beginning, and this trend generally follows the linear increase in ambient air temperature.

Overall, the analysis has shown that local permafrost mitigation may be possible by applying a constant heating load through the GHE. This heating load can be used to supply thermal energy for space conditioning or other uses throughout the year, and this capacity increases with increasing ambient air temperature across time. The impact of the soil conditions on these two outputs have been shown through the temperature distributions and heat exchange results. Due to the higher thermal conductivity of the soil modelled with solid ice, the heat transmission from conduction occurring at the ground-air interface is greater than the lower thermal-conductivity dry soil. The thawing of the No Pile – Ice Soil case occurred to a greater depth than the No Pile – Dry Soil case, though both showed thawing across the 40 years of simulation. This higher thermal conductivity slightly reduced the thermal impact radius of the piles, wherein the Opt. Pile – Dry

Soil case had an impact on soil temperature gradients at farther distances than the other pile cases. However, the higher thermal conductivity of the ice soil resulted in greater heat exchange within the working fluid, which in turn supplied a higher capacity of heating load energy through the GSHP.

There is great potential to expand these findings through more research. While these initial results present a positive initial foundation for this application, there are yet many unanswered questions. For example, what is the effect of flow rate on the ground temperature distributions and heating capacity in permafrost? Are there unique seasonal load conditions which might further optimize the system? Will experimental field studies confirm these predictions?

It is clear that the conditions of the soil are important across GSHP research and design; improving this model to include the phase change of thawing ice, the flow of groundwater, properties that change with temperature, snow cover effects, and a porous heat transfer model that accounts for inter-particle transport is likely to yield further insights. As well, future research may improve the accuracy of this model by utilizing actual building loads from residences in the area of study, and by considering this GHE in a range of hybrid applications interlinking multiple renewable energy systems.

7. Summary and Conclusions

This research adds to the field of in-ground heat exchanger design for GSHPs by generating a validated numerical model of a novel helical steel pile in-ground heat exchanger. This shallow pile was simulated with multi-layered soil properties, and a variety of operating conditions to measure the heat exchange rate effects.

The first focus of this thesis was on developing a multi-layered soil model in various regions. This led to the generation of a dataset of soil conditions across 11 zones (defined by their soil type and climate conditions) covering the country of Canada (Section 3). Then, a single pile was optimized for its geometry within a single region (Section 4). The pile was then investigated for its expected thermal performance within a borehole array, supplying a building load (Section 5). This capacity investigation was performed as steady state studies across all 11 zones (Section 6.1), and as three transient studies of the performance of a pile within one zone – supplying three different types of building load demands (Section 5.2). Finally, the use of the pile as an intervention to permafrost thawing by climate change was simulated in a 40-year transient study in a semi-permafrost region (Sections 6.2 and 6.3). A summary of indications from these results is presented below.

The effect of a multilayered soil thermal conductivity model on GHE performance:

- Soil thermal conductivity varies by region (from an average of 0.69 W/m·K in dry soil from the southeastern Canadian region of Zone 10 to 1.69 W/m·K in iced soil from the northern-most Canadian region of Zone 1), and by saturation.
- Analytical methods can be used to calculate this conductivity by depth based on soil composition, but most databases are missing key variables and require correlations to be solved. The presented method results in conductivities that were slightly lower than expected values, but still contain variability by depth which better approximates soil properties than a constant soil model.
- Regions with high soil thermal conductivity (calculated in Section 3.1.1) coincide with regions predicted to experience permafrost melting most severely (shown in Figure 1.8, from Natural Resources Canada [19]).
- The optimal length of the outlet plastic pipe was shown to be affected by the soil layers and properties, and its length should be chosen to allow for the greatest water volume contact with soil layers of high thermal conductivity – a shallow outlet plastic pipe had higher thermal performance in the ground conditions of Section 4 as it allowed for greater conductive contact with the layers of higher conductive soil.

- Regions which were assumed to contain solid ice (soil temperatures below or at zero), had the greatest heat exchange rate by depth in the winter by zone, followed by the saturated soil conditions. Generally, the dry soil condition resulted in the lowest heating capacity, though for regions whose mean soil temperature were near the minimum inlet water temperature, this difference was minimal.
- Saturated soil conditions yielded an average of 6.94 W/m of heat exchange rate by depth greater than the dry soil conditions across the 11 zones.
- In both the summer and winter studies performed in Section 6.1, the higher conductivity of the saturated or ice soils yielded greater heat exchange rate by depth, but the magnitude of this heat exchange rate was heavily influenced by the inlet fluid temperature and mean soil temperature.
- More detail can be added to numerical models of soil by including variable soil properties by depth for heat capacity and density – as well as having all thermal properties as functions of soil temperature. Furthermore, soil models which account for groundwater flow, porosity, phase change of ice, and organisms and parasites can be studied for even greater depth of information. There is still much work to be done on the accurate modelling of the soil domain for GSHP research.

Effect of changing the geometry of GHE components on heat exchange performance:

- Increasing the fluid flow rate from 1 L/min to 2 L/min increases the heat exchange rate by the largest amount compared to any of the geometric changes investigated in Section 4. This is due to the increase in convective heat transfer that such a flowrate change has – in comparison, the range of geometric changes did not cause a change in thermal performance to the same magnitude as the fluid velocity change did.
- There exists an optimal peak combination of outer and inner pipe diameters: in the larger group of sizes (referred to as a double sized pile), the heat exchange rate by depth decreased as the steel pile and plastic pipe diameters were increased, whereas increasing the plastic pipe and steel pipe diameters for the smaller group of sizes (the normal sized pile) optimized the heat exchange rate. This indicates that there is a peak combination of water volume, and ratio of diameters at which the heat exchange rate is a maximum under laminar flow.
- Generally, the larger the geometric factor (*GF*), the larger the heat exchange rate, with a slightly parabolic trend with a maximum for each flow rate in the proposed pile design of Section 4 when *GF* is approximately 130 m^3.
- Changes to the pipe diameters more greatly affect the temperature of the fluid than the ground temperature distribution - and therefore a general rule-of-thumb distance between the piles in an array may be used across sizes, given appropriate spacing.
- The offset inner piping results in an offsetting of temperature distribution and heat flux along one edge of the steel pile, which may be used as an advantage in more customized pile array layouts and orientations. This offsetting also allowed for a high flowrate inlet

side (for convective heat transfer), with a larger volume, lower flowrate outlet side (for conductive heat transfer).

- Increasing the length of the inlet plastic pipe increases the heat exchange rate of the pile by approximately 21.7 W per meter of pipe length increase and is not significantly affected by variations in soil thermal conductivity by depth (as compared to the length of the outlet plastic pipe).
- If used for the dual purpose of structural support and heat exchange, the choice of HSP component sizes is likely to result from a combination of economic, manufacturing or installation, and structural requirements. Therefore, the geometric optimization should be done in coordination with other limitations on the pile geometry.

Predicting the ability of a HSP to supply building loads through a GSHP in various regions and building types:

- The steady state capacity of a single pile was found via a parametric sweep of inlet water temperature to measure the heat exchange capacity across a single pile - which was then converted to space conditioning capacity through an analytical method in Section 5.1.
- Above the mean ground temperature, the cooling capacity increases linearly with inlet water temperature. As the inlet water temperature decreases below the mean ground temperature, the heating capacity increases linearly (a negative building load value).
- The steady state capacity of the pile ranged from 19.5 W/m (dry soil Zone 10) to 31.6 W/m (saturated soil Zone 4) across regions for the summer cooling condition (chosen as noon on August 1). These capacities are based on the original pile design, not optimized for geometry.
- The steady state heating capacity of the pile ranged from zero heating ability (Zone 1) to 23.8 W/m (frozen wet soil from Zone 11, in the valley of the Rocky Mountains in southwestern Canada) across regions for the winter heating condition.
- The climate and soil conditions of Zone 1 (the northern-most region of Canada) made it unsuitable to provide heating energy with water as the working fluid. The working fluid must be mixed with an antifreeze which would allow for incoming water temperatures to be well below the mean ground temperature within this zone.
- Using a ¼ ton capacity per 20 ft pile (non-geometrically optimized) was able to supply three sets of building loads in Zone 9 (the southeastern region containing Toronto, Ontario) with their space conditioning needs over a year of operation, beginning January 1. These building load sets were chosen from the literature to represent the range of cooling dominant (Building 1, which spent 29% of the hours in a year heating), heating dominant (Building 2, which spent 76% of the year's hours in the heating mode), and balanced building (Building 3, with 55% of the year spend heating) types.
- Some initial investigations into the use of a turbulent 8 L/min flowrate show a decrease in heat exchange performance compared to the laminar 2 L/min flowrate by 71%. This is

predicted to be a result of the reduced residence time of the working fluid through the shallow pile while utilizing high flow. These initial findings indicate the important balance of prioritizing conductive and convective heat transfer effects within this system and should be further validated with turbulent experimental data when it becomes available.

- The heating dominant unbalanced load had lower GHE system temperatures (inlet fluid to the pile temperature, average soil volume temperature, and change in fluid temperatures across the pile) than the unbalanced load which was cooling dominant. The roughly balanced load resulted in system temperatures between the unbalanced load studies.
- Inlet fluid temperatures for all three building load types were within a reasonable range of -2.20℃ to 22.9℃, and can be improved by offsetting some of the unbalanced load in a hybrid system, or by staggering the start date of operation to warmer initial ground conditions. These initial results indicate that the ¼ ton capacity is not noticeably over stressing the system within the first year of operation. Further work can investigate various other capacities, flow rates, and operating cycles to achieve more optimal transient thermal performance.
- All three building load sets appeared to have minimum temperature disturbances at radial distances beyond 3 m from the centre of the pile (measured at a depth of 10 m below the surface of the ground and pile). This provides some initial guidelines for pile spacing, which can be further expanded in future research.

Climate change effects on ground temperature, and the potential to offset permafrost thawing with an unbalanced thermal load across the GHE:

- Analytical solutions for soil temperature by depth provide insight across seasons and vary widely by region.
- Applying an ambient air temperature increase of 2℃ in 40 years (applied uniformly as a 0.05℃ increase each year) to the soil temperature formula in Section 3.1.2 results in similar permafrost melting outcomes as those predicted by climate change researchers described in Section 1.2.3 [11] [18].
- Numerical simulations of the ground with this ambient air temperature increase show that the active layer depth gets larger and the temperature of the permafrost region warms to melting or near melting. This warming is more noticeable when the soil conductivity reflects that of solid ice soil than with the dry soil, however both conductivity conditions result in warming due to climate change.
- Adding a pile with a constant heating load applied annually (with the original pile geometry and the optimized geometry) reduces the amount of local ground warming experienced over time compared to the same soil simulated without a pile. The most significant impact on ground temperature distribution is seen in dry soil with a geometrically optimized pile. This pile reduced the predicted increase in ground temperature at a depth of 15 m by 15% compared to the No Pile case. The presence of ice in the soil conductivity model (with the

optimized pile) reduced the expected ground warming by less (46%) than the Dry Soil case, however, the Ice Soil case yielded greater building heating energy across time than in the Dry Soil case. In permafrost regions with dry conditions, the application of a constant load across the pile can have a greater impact on thawing mitigation, however, the usable heating energy generated from this soil condition may be less than a permafrost regions with frozen wet soil. This result is due to the increased thermal conductivity of soil with solid ice – which will more effectively conduct ambient air temperature rises through the depths of the soil, but will also more provide more efficient heat transfer with the working fluid for usable heat exchange across the pile.

- Mitigation of permafrost thawing occurs most significantly in the local area directly surrounding the pile, and gradually decays in impact until 3-4 m radially from the centre of the pile.
- At a 0.5 m radial distance from the centre of the pile, the application of the heating load through the GHE resulted in a reduction of predicted warming by around 2°C in 40 years. This results in a predicted delay of mean soil temperature reaching the melting point (0°C) by around 50 to 75 years for ice and dry soil conditions respectively, when compared to undisturbed soil.

While conventional in-ground heat exchangers tend to utilize turbulent fluid flow to take advantage of convective heat transfer across the significant depths of vertical boreholes, this research aims to provide a foundational case for laminar flow within larger volume shallow pile heat exchangers. While the overall heat transfer rates may not be equivalent to conventional borehole capacities, achieving a feasible performance at a reduced energy demand (from a laminar flow rate) and cost requirement means that these systems may become a reasonable option for small-scale installations, hybrid or Domestic Hot Water (DHW) systems, retrofits, and residential building types while avoiding costly oversizing.

This research aimed to investigate the potential climate and energy issues currently faced by northern and remote communities in Canada. The literature revealed that nearly 200,000 Canadians are currently relying on diesel energy for generation and heating – and that they are paying significantly more money for this energy than most other Canadians. This reliance on heavily emitting energy sources, and concerns over fuel supply, prices, and the maintenance of generators, all have significant economic, social, and environmental consequences for residents. Furthermore, these communities are among those in Canada who will experience the effects of

climate change the most. As ambient air temperature continues to rise, permafrost will continue to disappear – creating literal and figurative instability for communities and ecosystems.

While there are some thermal and non/thermal structures being implemented in new building construction in these areas, as yet they are cost inhibitive, and may only provide one or two functions (keep the ground frozen, and/or structural support). Furthermore, renewable energy generation is a source of government incentives, and there are exciting projects being funded across these regions – yet they still heavily focus on electricity, rather than thermal energy.

The potential to solve a combination of these issues lies in the use of Ground-Source Heat Pump (GSHP) technology paired with a novel helical steel pile Ground Heat Exchanger (GHE). In these regions this technology could significantly reduce energy requirements and offset diesel energy by the efficiency of the GSHP to space condition – having positive economic, and quality of life impacts on residences. Furthermore, the GHE can be used to provide structural support – as they utilize relatively common structural equipment (in this area), with installation practices and costs that are more feasible than other conventional GHE technologies. And finally, the thermal imbalance in the ground that can result from a GSHP's imbalanced heating or cooling demands can be used as a benefit to offset climate change effects. Essentially, the projected heat gained by the ground from climate change could be used as a heat source for buildings, domestic hot water, and other industrial/commercial purposes – while reducing the negative effects if left to thaw the soil. While it may not be feasible to install these systems across the entire area of Canada's permafrost, strategic implementation in areas most at risk – and locations with communities most in need, could provide a local positive feedback loop and slow the thawing of larger regions of permafrost. Simply offsetting or reducing the emissions from current diesel energy will provide environmental benefits globally.

A numerical simulation modelled this potential and showed that within a local volume around the steel pile, the ground temperature can remain near its current seasonal values in spite of a climate-change induced temperature increase across the next 40 years. The development of this model lead to methodologies for more closely representing the complexity of soil properties, an essential next step for GHE modelers and designers – one that can lead to further improvements and

customizations of the technology, especially in the regions of Canada characterized in this thesis. Further studies should include building simulations of actual construction in these areas to gain a better understanding of the annual thermal demands. Furthermore, the piles should be optimized for the purpose of improved range of "beneficial ground thermal imbalance" by considering geometric, operational, and pile arrangement changes which improve the impact and range of this technology.

This work has uncovered great potential for Canadians, which must closely involve traditionally underserved communities. With a majority of these areas belonging to First Nations, Inuit, and Métis groups, any implementation of novel energy technology should be developed in a genuine partnership with local landowners and leaders, respecting the diversity of values, regulations, and treaties in place. Furthermore, there is a requirement for Canadians as a whole to view their northern and remote neighbors as fellow citizens deserving of government funding, and large-scale improvement of energy systems. While most levels of government have voiced some commitment to these communities (and there are several funding programs already in place for this type of innovation), a collective Canadian purpose of providing better housing and energy stability to these groups is also important.

This thesis was written during the COVID-19 global pandemic, which highlighted further opportunities for improvements to living and working conditions globally. As many people have been required to self-isolate within their residences, working environments have drastically changed. While previously, the industry of renewable energy and high-performance building design has focused on commercial and industrial applications, now the residential sector has become an increasingly important area. What role can GSHPs play to improve the conditions within a home, and how might these improvements be best implemented through building retrofits or new developments in a volatile global economic situation, are now key issues. In this perspective, helical steel piles may yet be able to improve the stability of energy, housing, and employment by providing reliable thermal energy (which enables working from home to be more comfortable) while reducing the energy demand. There is also potential for community based, local, thermal energy generation from a shared pile array – reducing the need for travel and

maintenance personnel. Creating healthy, safe, and comfortable interior environments is an ever-present opportunity for designers in this field.

While there are a mix of economic incentives and challenges for commercialization of this technology, a wider cost perspective that includes the costs of recovering from the consequences of melted permafrost, aging and failing diesel generators, and fuel leakages and transportation – is likely to create a strong case for GSHP implementation. A full cost analysis of this system should follow demonstration projects, and optimization of the systems. For local and national technicians, this project has the potential to open up new employment opportunities as manufacturers, installers, and maintenance workers. Reducing the cost of electricity for these communities helps to remove a barrier to residents, local business owners, and entrepreneurs to have greater impact in Canada's economy, and having more reliable and affordable heating could improve the living conditions of individuals who currently face some of the harshest housing challenges in the country. Finally, creating connections with renewable energy generation projects and developers in these areas can support these off-grid communities moving closer to net-zero energy living, specifically with the potential for solar-GSHP hybrid systems. As a northern nation, all of Canada is connected to the stability of our permafrost, and the environmental cycles closely tied to it. Investing in the stability of this land is investing in the stability of Canada's future.

Appendix

Table 8.i presents the calculated soil thermal conductivities for the dry and saturated ("wet") soil conditions. The depth locations of each data point represent the location of the soil data collected from the Canadian Soil Information Service (CanSIS) [99]. For the locations chosen within each zone it is assumed that the conductivity remains the same as the previous value at depths where data is not present (represented by a dash). The soil conductivities shown here are still only approximate values and may be improved upon by experimental work to quantify key variables not represented in the CanSIS database. However, the variations of conductivity by depth and location aim to begin the process of categorizing the complexity of soil as a heat exchanging medium.

Table 8.i. Dry and saturated soil thermal conductivities by depth per location

	Zone 1 – Arctic													
	Depth (m)	0			-15			-30			-35		-60	
	Thermal Conductivity Dry/Wet (W/m·K)													
	Average	0.92/1.36			0.98/1.32			0.92/1.35			0.91/1.35		0.91/1.35	
Location	Tanquary	0.91/1.36			-			1.01/1.49			-		-	
	Omingmak	0.83/1.22			-			-			0.80/1.23		-	
	Kettle Lake	0.91/1.32			0.80/1.17			-			-		0.79/1.16	
	Cape Osborn	1.03/1.52			-			-			-		-	
	Zone 2 – Northwest Territories													
	Depth (m)	0			-15			-20			-32		-45	
	Thermal Conductivity Dry/Wet (W/m·K)													
	Average	0.89/1.30			0.91/1.33			0.87/1.30			0.93/1.38		0.92/1.35	
Locati	May Creek	0.82/1.24			0.88/1.31			-			-		-	
	McGill Bay	0.69/1.05			-			-			0.86/1.30		0.83/1.22	
	Snow Goose	1.14/1.62			-			1.04/1.53			-		-	
	Zone 3 – Yukon													
	Depth (m)	0	-1	-2	-4	-5	-7	-10	-15	-30	-36	-37	-49	-60	-93
	Thermal Conductivity Dry/Wet (W/m·K)													
	Average	1.50/ 1.88	0.93/ 1.32	0.88/ 1.29	0.82/ 1.24	0.80/ 1.22	0.80/ 1.22	0.81/ 1.24	0.81/ 1.24	0.80/ 1.23	0.82/ 1.26	0.82/ 1.26	0.81/ 1.25	0.81/ 1.25	0.83/ 1.28

Location	Whitehorse	3.24/ 3.61	0.95/ 1.40	-	-	-	-	0.98/ 1.45	-	-	1.06/ 1.56	-	-	1.05/ 1.56	-
	Champagne	0.70/ 0.98	-	0.49/ 0.84	-	-	-	-	-	0.46/ 0.83	-	-	-	-	-
	Morley Bay	1.08/ 1.46	-	-	0.83/ 1.25	-	0.83/ 1.25	-	-	0.82/ 1.24	-	-	0.79/ 1.22	-	-
	Carcross	0.99/ 1.45	-	-	-	0.94/ 1.40	-	-	0.94/ 1.41	-	-	0.93/ 1.40	-	-	1.01/ 1.50
	Zone 4 - Pacific														
	Depth (m)	0	-4	-11	-12	-17	-23	-30	-34	-35	-40	-45	-50	-73	-75	-101
	Thermal Conductivity Dry/Wet (W/m·K)														
	Average	0.91/ 1.34	0.85/ 1.27	0.85/ 1.27	0.84/ 1.27	0.82/ 1.25	0.78/ 1.20	0.80/ 1.22	0.75/ 1.16	0.73/ 1.15	0.73/ 1.15	0.62/ 1.01	0.67/ 1.06	0.67/ 1.07	0.65/ 1.04	0.65/ 1.05
Location	Keefer	0.92/ 1.32	0.83/ 1.24	-	-	0.76/ 1.16	-	-	-	0.71/ 1.12	-	-	-	0.72/ 1.13	-	-
	Telegraph	0.84/ 1.28	0.69/ 1.08	-	0.67/ 1.06	-	-	0.76/ 1.18	-	-	0.75/ 1.17	-	-	-	-	-
	Thunder Mt.	0.85/ 1.29	-	0.85/ 1.28	-	-	0.68/ 1.07	-	0.45/ 0.83	-	-	-	0.65/ 1.04	-	-	0.67/ 1.07
	Parksville	1.01/ 1.49	-	-	-	-	-	-	-	-	-	0.56/ 0.93	-	-	0.46/ 0.83	-

	Zone 5 – Prairies												
	Depth (m)	0	-15	-19	-20	-22	-30	-35	-46	-47	-50	-58	-80
	Thermal Conductivity Dry/Wet (W/m·K)												
	Average	0.79/1.24	0.78/1.23	0.75/1.19	0.73/1.18	0.69/1.14	0.68/1.12	0.67/1.12	0.69/1.14	0.70/1.16	0.70/1.16	0.67/1.17	0.67/1.18
Location	Lethbridge	0.72/1.10	0.67/1.07	-	0.65/1.04	-	0.58/0.97	-	0.64/1.04	-	-	-	0.64/1.05
	Wainwright	0.97/1.42	-	-	0.94/1.40	-	-	0.93/1.41	-	-	0.94/1.42	-	-
	Yorkton	0.82/1.21	-	-	-	0.66/1.05	-	-	-	0.71/1.12	-	-	-
	Melfort	0.65/1.21	-	0.52/1.05	-	-	-	-	-	-	-	0.38/1.12	-
	Zone 6 – Atlantic												
	Depth (m)	0	-2	-10	-15	-18	-25	-26	-28	-30	-36	-45	-61	-71
	Thermal Conductivity Dry/Wet (W/m·K)													

	Average	0.78/ 1.16	0.79/ 1.17	0.80/ 1.17	0.79/ 1.16	0.76/ 1.15	0.78/ 1.18	0.76/ 1.17	0.76/ 1.16	0.74/ 1.15	0.75/ 1.16	0.76/ 1.17	0.74/ 1.15	0.73/ 1.14
Location	Gander	0.67/ 1.06	0.73/ 1.10	-	0.73/ 1.13	-	-	-	0.71/ 1.11	-	-	-	-	-
	Deer Lake	0.96/ 1.38	-	0.98/ 1.39	-	0.90/ 1.31	-	-	-	-	0.93/ 1.35	-	0.83/ 1.26	-
	Juniper	0.77/ 1.08	-	-	-	0.72/ 1.11	0.81/ 1.23	-	-	-	-	0.83/ 1.26	-	-
	Stony Brook	0.75/ 1.15	-	-	0.70/ 1.10	-	-	-	-	0.64/ 1.04	-	-	-	0.60/ 0.99
	Mahone	0.76/ 1.12	-	-	-	-	-	0.67/ 1.07	-	-	-	0.68/ 1.09	-	-

	Zone 7 – Northwestern Forest													
	Depth (m)	0	-3	-5	-6	-13	-20	-21	-26	-30	-45	-56	-81	-100
	Thermal Conductivity Dry/Wet (W/m·K)													
	Average	0.77/ 1.16	0.78/ 1.19	0.76/ 1.17	0.74/ 1.16	0.73/ 1.14	0.69/ 1.10	0.70/ 1.11	0.67/ 1.09	0.69/ 1.11	0.70/ 1.12	0.69/ 1.11	0.74/ 1.17	0.75/ 1.18
Location	Newbrook	0.66/ 1.04	-	0.61/ 1.00	-	-	0.48/ 0.86	-	-	0.54/ 0.93	-	-	-	0.58/ 0.97
	Pitchimi	0.73/ 1.11	-	-	0.67/ 1.06	-	-	0.69/ 1.10	-	-	0.70/ 1.12	-	-	-
	Pinehurst	0.91/ 1.34	0.95/ 1.41	-	-	0.92/ 1.38	-	-	0.85/ 1.30	-	-	0.82/ 1.27	0.98/ 1.46	-
	Zone 8 –Northeastern Forest													
	Depth (m)	0	-10		-12	-15	-18		-23	-28	-30	-43		-74
	Thermal Conductivity Dry/Wet (W/m·K)													
	Average	0.99/1.43	0.95/1.40		0.96/1.40	1.03/1.46	0.95/1.39		0.95/1.41	0.94/1.39	0.94/1.39	0.94/1.39		0.94/1.39
Locati	Coffin	1.01/1.50	-		1.03/1.48	-	-		1.05/1.52	-	-	-		-
	Dolbeau	0.89/1.25	0.76/1.16		-	0.97/1.32	0.73/1.11		-	0.69/1.07	-	-		-
	Ivry	1.08/1.56	-		-	1.08/1.58	-		-	-	1.07/1.57	1.07/1.57		1.07/1.57
	Zone 9 –Southwestern Great Lakes													
	Depth (m)	0	-15		-17	-20	-27		-30	-36	-37	-38		-56
	Thermal Conductivity Dry/Wet (W/m·K)													

	Average	0.84/1.27	0.78/1.22	0.77/1.21	0.78/1.23	0.72/1.16	0.74/1.20	0.73/1.18	0.73/1.19	0.74/1.20	0.74/1.20
Locati	Brighton	1.20/1.64	1.03/1.51	-	-	-	-	-	-	1.04/1.54	1.05/1.55
	Brantford	0.67/1.06	-	0.62/1.02	-	0.44/0.81	-	-	0.46/0.83	-	-
	London	0.65/1.10	-	-	0.67/1.16	-	0.74/1.28	0.70/1.23	-	-	-

	Zone 10 – Northeastern Great Lakes												
	Depth (m)	0	-12	-15	-18	-28	-30	-35	-38	-47	-51	-53	-67
	Thermal Conductivity Dry/Wet (W/m·K)												
	Average	0.75/1.14	0.78/1.17	0.76/1.16	0.74/1.14	0.66/1.07	0.65/1.06	0.62/1.02	0.66/1.07	0.60/1.01	0.67/1.08	0.70/1.12	0.73/1.16
Location	Laval	0.78/1.17	-	0.71/1.12	-	-	0.68/1.08	-	-	-	-	0.78/1.19	-
	Richmond	0.97/1.42	1.08/1.51	-	-	0.86/1.30	-	0.80/1.23	0.92/1.38	0.76/1.19	0.95/1.42	-	1.04/1.53
	Gananoque	0.49/0.84	-	-	0.42/0.79	-	-	0.37/0.75	-	-	-	0.38/0.76	-

	Zone 11 – B.C. Valley													
	Depth (m)	0	-5	-6	-10	-14	-22	-25	-28	-32	-48	-56	-70	-71	-76
	Thermal Conductivity Dry/Wet (W/m·K)														
	Average	0.94/1.36	0.92/1.34	0.97/1.41	0.93/1.38	0.95/1.41	0.99/1.41	0.99/1.45	0.91/1.45	0.90/1.35	0.90/1.35	0.89/1.35	0.89/1.35	0.89/1.35	0.91/1.37
Location	Kernaghan	0.85/1.26	-	0.99/1.45	-	-	-	-	0.76/1.15	-	-	0.73/1.15	-	-	0.79/1.21
	Soda Creek	0.91/1.28	-	-	0.78/1.18	0.85/1.28	0.94/1.41	-	-	0.93/1.40	-	-	0.93/1.40	-	-
	Mapes	1.06/1.53	1.01/1.49	-	1.02/1.50	-	-	1.02/1.50	-	-	1.01/1.50	-	-	1.01/1.50	-

References

[1] Natural Resources Canada, “Energy Fact Book 2018-2019,” 2018.

[2] Aboriginal Affairs and Northern Development Canada; Natural Resources Canada, *Status of Remote / Off-Grid Communities in Canada - August 2011*, no. August. 2011.

[3] National Energy Board, “Energy Facts - Energy Use in Canada’s North,” 2011.

[4] L. Mortensen, A. M. Hansen, and A. Shestakov, “How three key factors are driving and challenging implementation of renewable energy systems in remote Arctic communities,” *Polar Geogr.*, vol. 40, no. 3, pp. 163–185, 2017.

[5] Government of Canada, “Climate change in Indigenous and Northern communities,” *Government of Canada*, 2019. [Online]. Available: https://www.aadnc-aandc.gc.ca/eng/1100100034249/1100100034253?utm_source=climate&utm_medium=url.

[6] Gwich’in Council International, “Diverging From Diesel,” 2017.

[7] M. Arriaga, C. A. Canizares, and M. Kazerani, “Renewable energy alternatives for remote communities in Northern Ontario, Canada,” *IEEE Trans. Sustain. Energy*, vol. 4, no. 3, pp. 661–670, 2013.

[8] Toronto Hydro, “Residential electricity rates,” 2019.

[9] Government of Canada, “Reconciliation - Support For Distinctions-Based Housing Strategies,” 2018. [Online]. Available: https://www.budget.gc.ca/2018/docs/plan/chap-03-en.html#Support-for-Distinctions-Based-Housing-Strategies.

[10] Standing Senate Committee on Energy the Environment and Natural Resources, “Powering Canada’s Territories,” p. 58, 2014.

[11] S. L. Smith, J. Throop, and A. G. Lewkowicz, “Recent changes in climate and permafrost temperatures at forested and polar desert sites in northern Canada,” *Can. J. Earth Sci.*, no. 49, pp. 914–924, 2012.

[12] T. E. Osterkamp, “Characteristics of the recent warming permafrost in Alaska,” *J. Geophys. Res. Earth Surf.*, vol. 112, no. 2, pp. 1–10, 2007.

[13] Y. Zhang, W. Chen, and D. W. Riseborough, “Transient projections of permafrost distribution in Canada during the 21st century under scenarios of climate change,” *Glob. Planet. Change*, vol. 60, no. 3–4, pp. 443–456, 2008.

[14] S. V Kokelj, B. Zajdlik, and M. S. Thompson, “The Impacts of Thawing Permafrost on the Chemistry of Lakes across the Subarctic Boreal-Tundra Transition, Mackenzie Delta Region, Canada,” *Permafr. Periglac. Process.*, vol. 20, no. February, pp. 185–199, 2009.

[15] T. R. Christensen *et al.*, “Thawing sub-arctic permafrost: Effects on vegetation and methane emissions,” *Geophys. Res. Lett.*, vol. 31, no. 4, 2004.

[16] J. M. S. Jacques and D. J. Sauchyn, “Increasing winter baseflow and mean annual streamflow from possible permafrost thawing in the Northwest Territories, Canada,” *Geophys. Res. Lett.*, vol. 36, no. 1, pp. 1–6, 2009.

[17] M. Braverman and W. L. Quinton, “Hydrological impacts of seismic lines in the wetland-dominated zone of thawing, discontinuous permafrost, Northwest Territories, Canada,” *Hydrol. Process.*, vol. 30, no. 15, pp. 2617–2627, 2016.

[18] S. Nishimura, C. J. Martin, R. J. Jardine, and C. H. Fenton, “A new approach for assessing geothermal response to climate change in permafrost regions,” *Geotechnique*, vol. 59, no. 3, pp. 213–227, 2009.

[19] Natural Resources Canada, “Implications of Changing Climate for the Arctic Environment,” *Government of Canada*, 2019.

[20] O. A. Carpino, A. A. Berg, W. L. Quinton, and J. R. Adams, “Climate change and permafrost thaw-induced boreal forest loss in northwestern Canada,” *Environ. Res. Lett.*, vol. 13, no. 8, p. 84018, 2018.

[21] S. Brown, “Thawing permafrost sinks buildings , hikes costs in North,” The Canadian Broadcasting Corportation, 2011.

[22] R. M. Deconto *et al.*, “Past extreme warming events linked to massive carbon release from thawing permafrost,” *Nature*, vol. 484, no. 7392, pp. 87–91, 2012.

[23] Y. A. Kronik and M. V. Rabinovich, “Calculation of the Thermal Stress-Strain State of Permafrost and Thawing Bases of Buildings in the Presence of Accidental Leaks from Utility Lines,” *Soil Mech. Found. Eng.*, vol. 56, no. 2, pp. 136–141, 2019.

[24] H. R. Thomas, P. Cleall, Y. C. Li, C. Harris, and M. Kern-Luetschg, “Modelling of cryogenic processes in permafrost and seasonally frozen soils,” *Geotechnique*, vol. 59, no. 3, pp. 173–184, 2009.

[25] Environment and Climate Change Canada, “Canadian Centre for Climate Modeling and Analysis (CCCma) (University of Victoria),” *Government of Canada*.

[26] D. Scott-thomas, “Labrador ’ s melting landscape : Cultural centre offers lesson on how to build on thawing permafrost Climate change is melting permafrost and raising sea levels , and already , growing communities such as Nain are feeling the effects . But even without re,” pp. 1–10, 2019.

[27] V. Paramonov, I. Sakharov, and S. Kudriavtcev, “Forecast the Processes of Thawing of Permafrost Soils under the Building with the Large Heat Emission,” *MATEC Web Conf.*, vol. 73, 2016.

[28] S. V. Obydenkova and J. M. Pearce, “Technical viability of mobile solar photovoltaic systems for indigenous nomadic communities in northern latitudes,” *Renew. Energy*, vol. 89, pp. 253–267, 2016.

[29] Canada Weather Stats, “Sunlight - Monthly data,” 2019.

[30] J. D. Stephen *et al.*, “Biomass for residential and commercial heating in a remote Canadian aboriginal community,” *Renew. Energy*, vol. 86, pp. 563–575, 2016.

[31] C. Yan, D. Rousse, and M. Glaus, “Multi-criteria decision analysis ranking alternative heating systems for remote communities in Nunavik,” *J. Clean. Prod.*, vol. 208, pp. 1488–1497, 2019.

[32] Natural Resources Canada, “Energy Innovation Program,” *Government of Canada,* 2019. .

[33] Natural Resources Canada, “Hybrid smart-grid solar PV and battery demonstration project,” *Government of Canada*, 2019.

[34] Natural Resources Canada, “Destruction Bay Renewable Hybrid-Diesel Project,” *Government of Canada,* 2019.

[35] Natural Resources Canada, “Gull Bay First Nation Diesel Offset Micro Grid Project,” *Government of Canada,* 2019.

[36] Natural Resources Canada, “Mary’s Harbour Renewables,” *Government of Canada,* 2019.

[37] Indigenous and Northern Affairs Canada, “Northern REACHE Program,” *Government of Canada,* 2019.

[38] Natural Resources Canada, “Government of Canada Promotes Renewable Energy Innovation in Mining,” *Government of Canada,* 2019.

[39] J. Schnieders, W. Feist, and L. Rongen, “Passive Houses for different climate zones,” *Energy Build.*, vol. 105, pp. 71–87, 2015.

[40] J. Straube, “BSD-200: Low-Energy Commercial and Institutional Buildings: Top Ten Smart Things to Do for Cold Climates,” *Building Science Corporation,* 2014.

[41] W. Net and Z. Solutions, “Challenges and Solutions for Building Passive House & Net Zero Energy Ready Housing in Northern Canada Overarching Research Question,” pp. 1–56, 2019.

[42] P. A. Kew and D. A. Reay, “Heat pipes: theory, design and applications .” Butterworth-Heinemann , GB , 2006.

[43] ArcticFoundations, “Two-Phase Thermosyphons,” 2019. [Online]. Available: https://arcticfoundations.com/two-phase-thermosyphons/.

[44] Arctic Foundations of Canada, “Thermopiles,” 2018.

[45] M. Schreiber, “The Race to Save Arctic Cities As Permafrost Melts,” *CityLab*, 2018. .

[46] S. Karytsas and I. Choropanitis, “Barriers against and actions towards renewable energy technologies diffusion: A Principal Component Analysis for residential ground source heat pump (GSHP) systems,” *Renew. Sustain. Energy Rev.*, vol. 78, no. April, pp. 252–271, 2017.

[47] I. W. Johnston, G. A. Narsilio, and S. Colls, “Emerging geothermal energy technologies,” *KSCE J. Civ. Eng.*, vol. 15, no. 4, pp. 643–653, 2011.

[48] M. A. Rosen and S. Koohi-Fayegh, *Geothermal Energy: Sustainable Heating and Cooling Using the Ground*, First. John Wiley & Sons, Ltd., 2017.

[49] P. J. Hughes, *Geothermal (ground-source) heat pumps: Market status, barriers to adoption, and actions to overcome barriers*, vol. 33, no. December. 2009.

[50] C. K. Lee and H. N. Lam, “A simplified model of energy pile for ground-source heat pump systems,” *Energy*, vol. 55, pp. 838–845, 2013.

[51] A. Mustafa Omer, “Ground-source heat pumps systems and applications,” *Renew. Sustain. Energy Rev.*, vol. 12, no. 2, pp. 344–371, 2008.

[52] H. Yang, P. Cui, and Z. Fang, “Vertical-borehole ground-coupled heat pumps: A review of models and systems,” *Appl. Energy*, vol. 87, no. 1, pp. 16–27, 2010.

[53] Q. Lu, G. A. Narsilio, G. R. Aditya, and I. W. Johnston, “Economic analysis of vertical ground source heat pump systems in Melbourne,” *Energy*, vol. 125, pp. 107–117, 2017.

[54] A. K. Sani, R. M. Singh, T. Amis, and I. Cavarretta, “A review on the performance of geothermal energy pile foundation, its design process and applications,” *Renew. Sustain. Energy Rev.*, vol. 106, pp. 54–78, May 2019.

[55] S. Li, W. Yang, and X. Zhang, “Soil temperature distribution around a U-tube heat exchanger in a multi-function ground source heat pump system,” *Appl. Therm. Eng.*, vol. 29, no. 17–18, pp. 3679–3686, 2009.

[56] B. Sanner, C. Karytsas, D. Mendrinos, and L. Rybach, “Current status of ground source heat pumps and underground thermal energy storage in Europe,” *Geothermics*, vol. 32, no. 4, pp. 579–588, 2003.

[57] P. Christodoulides, L. Aresti, and G. Florides, “Air-conditioning of a typical house in moderate climates with Ground Source Heat Pumps and cost comparison with Air Source Heat Pumps,” *Appl. Therm. Eng.*, vol. 158, no. January, p. 113772, 2019.

[58] Y. L. E. Law and S. B. Dworkin, “Characterization of the effects of borehole configuration and interference with long term ground temperature modelling of ground source heat pumps,” *Appl. Energy*, vol. 179, pp. 1032–1047, Oct. 2016.

[59] H. V. Nguyen, Y. L. E. Law, M. Alavy, P. R. Walsh, W. H. Leong, and S. B. Dworkin, “An analysis of the factors affecting hybrid ground-source heat pump installation potential in North America,” *Appl. Energy*, vol. 125, pp. 28–38, 2014.

[60] A. Zarrella, G. Emmi, and M. De Carli, “Analysis of operating modes of a ground source heat pump with short helical heat exchangers,” *Energy Convers. Manag.*, vol. 97, pp. 351–361, Jun. 2015.

[61] Energy Saving Trust, “Domestic Ground Source Heat Pumps: Design and installation of closed-loop systems – A guide for specifiers, their advisors and potential users,” p. 22, 2007.

[62] Jalaluddin, A. Miyara, K. Tsubaki, S. Inoue, and K. Yoshida, “Experimental study of several types of ground heat exchanger using a steel pile foundation,” *Renew. Energy*, vol. 36, no. 2, pp. 764–771, 2011.

[63] Jalaluddin and A. Miyara, “Thermal performance investigation of several types of vertical ground heat exchangers with different operation mode,” *Appl. Therm. Eng.*, vol. 33–34, pp. 167–174, 2012.

[64] C. E. Moon and J. M. Choi, “Heating performance characteristics of the ground source heat pump system with energy-piles and energy-slabs,” *Energy*, vol. 81, pp. 27–32, 2015.

[65] M. J. Kim, S. R. Lee, S. Yoon, and J. S. Jeon, “Evaluation of geometric factors influencing thermal performance of horizontal spiral-coil ground heat exchangers,” *Appl. Therm. Eng.*, vol. 144, no. August, pp. 788–796, 2018.

[66] T. Sivasakthivel, K. Murugesan, and P. K. Sahoo, “Optimization of ground heat exchanger parameters of ground source heat pump system for space heating applications,” *Energy*, vol. 78, pp. 573–586, 2014.

[67] P. M. Congedo, G. Colangelo, and G. Starace, “CFD simulations of horizontal ground heat exchangers: A comparison among different configurations,” *Appl. Therm. Eng.*, vol. 33–34, no. 1, pp. 24–32, 2012.

[68] C. Li, J. Mao, H. Zhang, Z. Xing, Y. Li, and J. Zhou, “Numerical simulation of horizontal spiral-coil ground source heat pump system: Sensitivity analysis and operation characteristics,” *Appl. Therm. Eng.*, vol. 110, pp. 424–435, 2017.

[69] B. Bouhacina, R. Saim, and H. F. Oztop, “Numerical investigation of a novel tube design for the geothermal borehole heat exchanger,” *Appl. Therm. Eng.*, vol. 79, pp. 153–162, 2015.

[70] T. Mimouni and L. Laloui, “Towards a secure basis for the design of geothermal piles,” *Acta Geotech.*, vol. 9, no. 3, pp. 355–366, 2014.

[71] M. De Moel, P. M. Bach, A. Bouazza, R. M. Singh, and J. O. Sun, “Technological advances and applications of geothermal energy pile foundations and their feasibility in Australia,” *Renew. Sustain. Energy Rev.*, vol. 14, no. 9, pp. 2683–2696, 2010.

[72] F. Tang and H. Nowamooz, “Long-term performance of a shallow borehole heat exchanger installed in a geothermal field of Alsace region,” *Renew. Energy*, vol. 128, pp. 210–222, 2018.

[73] H. Brandl, “Energy foundations and other thermo-active ground structures,” *Geotechnique*, vol. 56, no. 2, pp. 81–122, 2006.

[74] D. Adam and R. Markiewicz, “Energy from earth-coupled structures, foundations, tunnels and sewers,” *Geotechnique*, vol. 59, no. 3, pp. 229–236, 2009.

[75] K. Morino and T. Oka, “Study on heat exchanged in soil by circulating water in a steel pile,” *Energy Build.*, vol. 21, no. 1, pp. 65–78, 1994.

[76] D. Marcotte and P. Pasquier, “On the estimation of thermal resistance in borehole thermal conductivity test,” *Renew. Energy*, vol. 33, no. 11, pp. 2407–2415, Nov. 2008.

[77] O. Ghasemi-Fare and P. Basu, “Predictive assessment of heat exchange performance of geothermal piles,” *Renew. Energy*, vol. 86, pp. 1178–1196, 2016.

[78] W. Zhang, H. Yang, L. Lu, and Z. Fang, “The analysis on solid cylindrical heat source model of foundation pile ground heat exchangers with groundwater flow,” *Energy*, vol. 55, pp. 417–425, 2013.

[79] Y. Wang, Y. Liu, Y. Cui, W. Guo, and J. Lv, “Numerical simulation of soil freezing and associated pipe deformation in ground heat exchangers,” *Geothermics*, vol. 74, no. 266, pp. 112–120, 2018.

[80] R. A. McBride, R. L. Slessor, and P. J. Joosse, “Estimating the particle density of clayrich soils with diverse mineralogy,” *Soil Sci. Soc. Am. J.*, vol. 76, no. 2, pp. 569–574, 2012.

[81] Z. Tian, Y. Lu, R. Horton, and T. Ren, “A simplified de Vries-based model to estimate thermal conductivity of unfrozen and frozen soil,” *Eur. J. Soil Sci.*, vol. 67, no. 5, pp. 564–572, 2016.

[82] Y. Nam, R. Ooka, and S. Hwang, “Development of a numerical model to predict heat exchange rates for a ground-source heat pump system,” *Energy Build.*, vol. 40, no. 12, pp. 2133–2140, 2008.

[83] K. D. Murphy and J. S. McCartney, “Seasonal Response of Energy Foundations During Building Operation,” *Geotech. Geol. Eng.*, vol. 33, no. 2, pp. 343–356, 2015.

[84] H. Park, S. R. Lee, S. Yoon, H. Shin, and D. S. Lee, “Case study of heat transfer behavior of helical ground heat exchanger,” *Energy Build.*, vol. 53, pp. 137–144, 2012.

[85] M. Wizard and G. Definitions, “Introduction to COMSOL Multiphysics by example,” pp. 1–6, 2014.

[86] Government of Canada, “Historical Data,” 2019. [Online]. Available: https://climate.weather.gc.ca/historical_data/search_historic_data_e.html.

[87] Olaf Schenk and K. Gaerter, “PARDISO, User Guide Version 6.0.0,” vol. 0, pp. 0–67, 2018.

[88] S. Profile, “RECORD OF BOREHOLE No . BH-01,” vol. 127.

[89] APE HD ™ PILING, “Helical Piles Brochure.”

[90] PEXUniverse.com, “PEX Tubing Technical Specifications.” [Online]. Available: https://www.pexuniverse.com/pex-tubing-technical-specs.

[91] M. Alavy, H. V. Nguyen, W. H. Leong, and S. B. Dworkin, “A methodology and computerized approach for optimizing hybrid ground source heat pump system design,” *Renew. Energy*, vol. 57, pp. 404–412, 2013.

[92] “Installation Instructions: Ground Coupled Loop System Design Manual (Ground Source GS System),” Bryan, Ohio, 2007.

[93] O. Johansen, “Thermal conductivity of soils,” *Int. J. Rock Mech. Min. Sci. Geomech. Abstr.*, vol. 15, no. 5, p. A99, 1978.

[94] K. Frob, “Measuring and modeling of soil thermal properties and ground heat flux at two different sites at Lena Delta, Siberia,” no. June, p. 99, 2011.

[95] D. de Vries, *Heat transfer in soils*. Eindhoven University of Technology, 1975.

[96] D. Barry-Macaulay, A. Bouazza, B. Wang, and R. M. Singh, “Evaluation of soil thermal conductivity models,” *Can. Geotech. J.*, vol. 52, no. 11, pp. 1892–1900, 2015.

[97] V. R. Tarnawski, M. L. McCombie, W. H. Leong, P. Coppa, S. Corasaniti, and G. Bovesecchi, “Canadian Field Soils IV: Modeling Thermal Conductivity at Dryness and Saturation,” *Int. J. Thermophys.*, vol. 39, no. 3, p. 35, 2018.

[98] Bo & Associates Inc., “Record of Borehole No. BH-01,” Mississauga, 2018.

[99] Canadian Soil Information Service, “Soil name and layer data for Canada,” *Government of Canada*, 2013.

[100] J. Luo *et al.*, “Investigation of shallow geothermal potentials for different types of ground source heat pump systems (GSHP) of Wuhan city in China,” *Renew. Energy*, vol. 118, pp. 230–244, Apr. 2018.

[101] W. Pei, W. Yu, S. Li, and J. Zhou, “A new method to model the thermal conductivity of soil-rock media in cold regions: An example from permafrost regions tunnel,” *Cold Reg. Sci. Technol.*, vol. 95, pp. 11–18, 2013.

[102] Z. M. Subin, C. D. Koven, W. J. Riley, M. S. Torn, D. M. Lawrence, and S. C. Swenson, “Effects of soil moisture on the responses of soil temperatures to climate change in cold regions,” *J. Clim.*, vol. 26, no. 10, pp. 3139–3158, 2013.

[103] M. Alavy, H. V. Nguyen, W. H. Leong, and S. B. Dworkin, “A methodology and computerized approach for optimizing hybrid ground source heat pump system design,” *Renew. Energy*, vol. 57, pp. 404–412, 2013.